NASA TECHNICAL MEMORANDUM

NASA TM X-1498

NASA TM X-1498

WIND-TUNNEL INVESTIGATION OF THREE PROPOSED LAUNCH VEHICLES AT MACH NUMBERS FROM 2.30 TO 4.63

by A. B. Blair, Jr., and Melvin M. Carmel

Langley Research Center
Langley Station, Hampton, Va.

NATIONAL AERONAUTICS AND SPACE ADMINISTRATION • WASHINGTON, D. C. • FEBRUARY 1968

NASA TM X-1498

WIND-TUNNEL INVESTIGATION OF THREE PROPOSED LAUNCH VEHICLES AT MACH NUMBERS FROM 2.30 TO 4.63

By A. B. Blair, Jr., and Melvin M. Carmel

Langley Research Center
Langley Station, Hampton, Va.

NATIONAL AERONAUTICS AND SPACE ADMINISTRATION

For sale by the Clearinghouse for Federal Scientific and Technical Information
Springfield, Virginia 22151 – CFSTI price $3.00

WIND-TUNNEL INVESTIGATION OF THREE PROPOSED LAUNCH VEHICLES AT MACH NUMBERS FROM 2.30 TO 4.63

By A. B. Blair, Jr., and Melvin M. Carmel
Langley Research Center

SUMMARY

An investigation has been made in the Langley Unitary Plan wind tunnel to determine the aerodynamic characteristics of three 1/12.4-scale models of proposed multistage launch vehicles. Tests of the second stage alone were made for one of the models. The investigation included tests of models both with and without fins and auxiliary boosters.

The results of the investigation indicated approximately linear variations of the aerodynamic coefficients with angle of attack and sideslip over the range of the tests. The first-stage fins were effective in providing stabilizing increments of pitching and yawing moment although the increments decreased with increasing Mach number. The rolling moment due to sideslip appeared to be reasonably small over the range of the tests.

INTRODUCTION

The National Aeronautics and Space Administration is currently conducting flight-test programs in which various payloads are launched to high altitudes by means of multistaged boosters. In order to assure maximum success for such flights, it is important to know the aerodynamic characteristics of the entire launch system. Three launch systems have recently been proposed by the Langley Research Center for use in a high-altitude decelerator study; because of the unusual shape of these vehicles, it seemed desirable to predetermine their aerodynamic characteristics by means of a wind-tunnel investigation.

Accordingly, tests have been performed on 1/12.4-scale models of the three launch vehicles in the Langley Unitary Plan wind tunnel at Mach numbers from 2.30 to 4.63, and the results of these tests are herein presented. The tests were performed through an angle-of-attack range from about -4° to 8°, through an angle-of-sideslip range from about -4° to 6°, and at a Reynolds number per foot (per 30.5 cm) of 3.0×10^{6}. In addition, for the final stage of one of the vehicles, the angle-of-attack range was extended to about 20°.

SYMBOLS

The coefficients of forces and moments are referred to the body axis system. The moments are presented about the moment centers of each test configuration. (See fig. 1.) The symbols are defined as follows:

A cross-sectional area of first stage of models 1, 2, and 3

C_A axial-force coefficient, $\frac{\text{Axial force}}{qA}$

$C_{A,c}$ chamber axial-force coefficient, $\frac{\text{Chamber axial force}}{qA}$

$C_{A,o}$ axial-force coefficient at 0^o angle of attack

C_l rolling-moment coefficient, $\frac{\text{Rolling moment}}{qAd}$

$C_{l_\beta} = \frac{\Delta C_l}{\Delta \beta}$ at $\beta = 0^o, 2^o$

C_m pitching-moment coefficient, $\frac{\text{Pitching moment}}{qAd}$

C_{m_α} slope of pitching-moment curve at $\alpha = 0^o$

C_N normal-force coefficient, $\frac{\text{Normal force}}{qA}$

C_{N_α} slope of normal-force curve at $\alpha = 0^o$

C_n yawing-moment coefficient, $\frac{\text{Yawing moment}}{qAd}$

$C_{n_\beta} = \frac{\Delta C_n}{\Delta \beta}$ at $\beta = 0^o, 2^o$

C_Y side-force coefficient, $\frac{\text{Side force}}{qA}$

$C_{Y_\beta} = \frac{\Delta C_Y}{\Delta \beta}$ at $\beta = 0^o, 2^o$

d diameter of first stage of models 1, 2, and 3

M	free-stream Mach number
q	free-stream dynamic pressure
r	radius of forebody nose
x_{ac}	aerodynamic-center location aft of nose in percent of body length
α	angle of attack of model center line, deg
β	angle of sideslip of model center line, deg

Fin designations:

F_1	fins for first stage of models 1, 2, and 3
F_2	fins for second stage of model 3 and for model 4

APPARATUS AND METHODS

Tunnel

Tests were conducted in the high Mach number test section of the Langley Unitary Plan wind tunnel which is a variable-pressure, continuous-flow facility. The test section is approximately 7 feet (2.14 m) long and 4 feet (1.22 m) square. The nozzle leading to the test section is of the asymmetric sliding-block type, which permits a continuous variation in Mach number from about 2.30 to 4.65.

Models

Dimensional details of the 1/12.4-scale test models are presented in figure 1, and photographs of the models are presented in figure 2. The launch-vehicle models, hereinafter referred to as models 1, 2, and 3, incorporated a common afterbody, aft cruciform fins, and two auxiliary rockets; and all had forebodies with greater maximum diameters than for the afterbody. Model 1 differed from model 2 in that model 2 had a reduced maximum diameter and boattail angle of the forebody. Model 3 had a different forebody shape which incorporated cruciform fins, and had the same boattail section as model 2. The nose half-angle of model 3 was 15° whereas the nose half-angles of models 1 and 2 were 10°. Model 4 was the isolated forebody of model 3. All fins used were of trapezoidal planform and had hexagonal sections with sharp leading and trailing edges.

Test Conditions

The test conditions for the investigation were as follows:

Mach number	Stagnation temperature		Stagnation pressure		Reynolds number	
	^{o}F	^{o}K	lb/sq ft abs	N/m^2	per foot	per meter
2.3	150	338.67	2298	110 028	3.0×10^6	9.84×10^6
2.96	150	338.67	3253	155 754	3.0	9.84
3.95	175	352.56	5794	277 417	3.0	9.84
4.63	175	352.56	7913	378 874	3.0	9.84

Models 1, 2, and 3 were tested with the fins and auxiliary rockets both on and off through an angle-of-attack range from about -4^{o} to 8^{o} and an angle-of-sideslip range from about -4^{o} to 6^{o}. Model 4 was tested at angles of attack from -4^{o} to 20^{o} and an angle-of-sideslip range approximately the same as that for the other models. The stagnation dewpoint was maintained below -30^{o} F (238.70^{o} K) in order to avoid any significant tunnel condensation effects.

A 1/16-inch (0.1587 cm) wide strip of 0.0108 (nominal)-inch (0.0274 cm) diameter carborundum grains was affixed around each model 1.2 inches (3.048 cm) aft of the nose and on each fin 0.4 inch (1.016 cm) aft of the leading edge in a streamwise direction.

Measurements and Corrections

Aerodynamic forces and moments were measured by means of a six-component, electrical strain-gage balance housed within the models. The balance, in turn, was rigidly fastened by means of an aft-sting support to the tunnel support system. The balance-chamber pressure was measured for each model and test condition.

Angles of attack were corrected for tunnel-flow angularity and angles of attack and sideslip were corrected for deflection of the sting and balance combinations caused by aerodynamic loading. The axial-force data were adjusted to correspond to free-stream static conditions in the balance chamber. Typical values of chamber axial-force coefficient are presented in figure 3.

RESULTS AND DISCUSSION

The longitudinal aerodynamic characteristics at Mach numbers from 2.30 to 4.63 for the four test models are presented in figures 4 to 7 for both the complete models and

the models with the fins and auxiliary boosters removed. The normal-force and pitching-moment coefficient data are generally linear in the low angle-of-attack range of these tests; however, at the higher angles of attack the normal-force slope increases with increasing α. The increase in normal-force slope leads to a slight decrease in stability level. The first-stage fins are effective in providing a stabilizing increment of pitching moment although the increment decreases with increasing Mach number. A summary of these results is presented in figures 8 and 9. It should be reiterated that the moment data presented are about arbitrary points on each model; thus any comparison of stability levels is invalid.

With the fins and boosters on, the familiar decrease in C_{N_α} with increase in Mach number is apparent for all the models. Model 3 develops the greatest C_{N_α} because of the two sets of fins. There are large destabilizing trends with increase in Mach number for models 1 and 2, considerably less change in C_{m_α} occurring for models 3 and 4. There are only small changes in C_{m_α} and C_{N_α} with increase in Mach number for any of the test models without fins and auxiliary boosters.

Model 2 has the least value of $C_{A,o}$ throughout the Mach number range because of its generally more slender shape and smaller wetted area. The aerodynamic-center variations with Mach number for the test models are presented in figure 9. For the three complete launch vehicles, the aerodynamic center for model 3 is the farthest forward throughout the Mach number range. With increasing Mach number for this speed region, there is a general forward shift in the aerodynamic-center location. With the fins and auxiliary boosters removed from the models, there is generally little change in aerodynamic center except for model 1 which, because of its longer conical nose section, produces an aft movement of aerodynamic center with increasing Mach number.

The variations of the lateral coefficients with sideslip angle are presented in figures 10 to 13. These results indicate generally linear variations with β. The sideslip parameters (figs. 14 to 17) indicate no large changes with increase in angle of attack. The first-stage fins are effective in producing side force and providing a positive increment in directional stability for each model although the increment decreases with increasing Mach number. The rolling moments due to sideslip appear to be reasonably small over the angle-of-attack range of the investigation. The effect of Mach number on the lateral stability parameters (fig. 18), as would be expected, is about the same as the Mach number effect on the longitudinal stability; that is, models 1 and 2 have large decreases in C_{n_β} with increase in Mach number, whereas the decrease in C_{n_β} for model 3 is somewhat less.

CONCLUDING REMARKS

Tests of three multistage launch-vehicle models at Mach numbers from 2.30 to 4.63 indicated approximately linear variations of the aerodynamic coefficients with angle of attack and sideslip over the range of the tests. The first-stage fins were effective in providing stabilizing increments of pitching and yawing moment although the increments decreased with increasing Mach number. The rolling moment due to sideslip appeared to be reasonably small over the range of the tests.

Langley Research Center,
National Aeronautics and Space Administration,
Langley Station, Hampton, Va., August 17, 1967,
709-10-00-01-23.

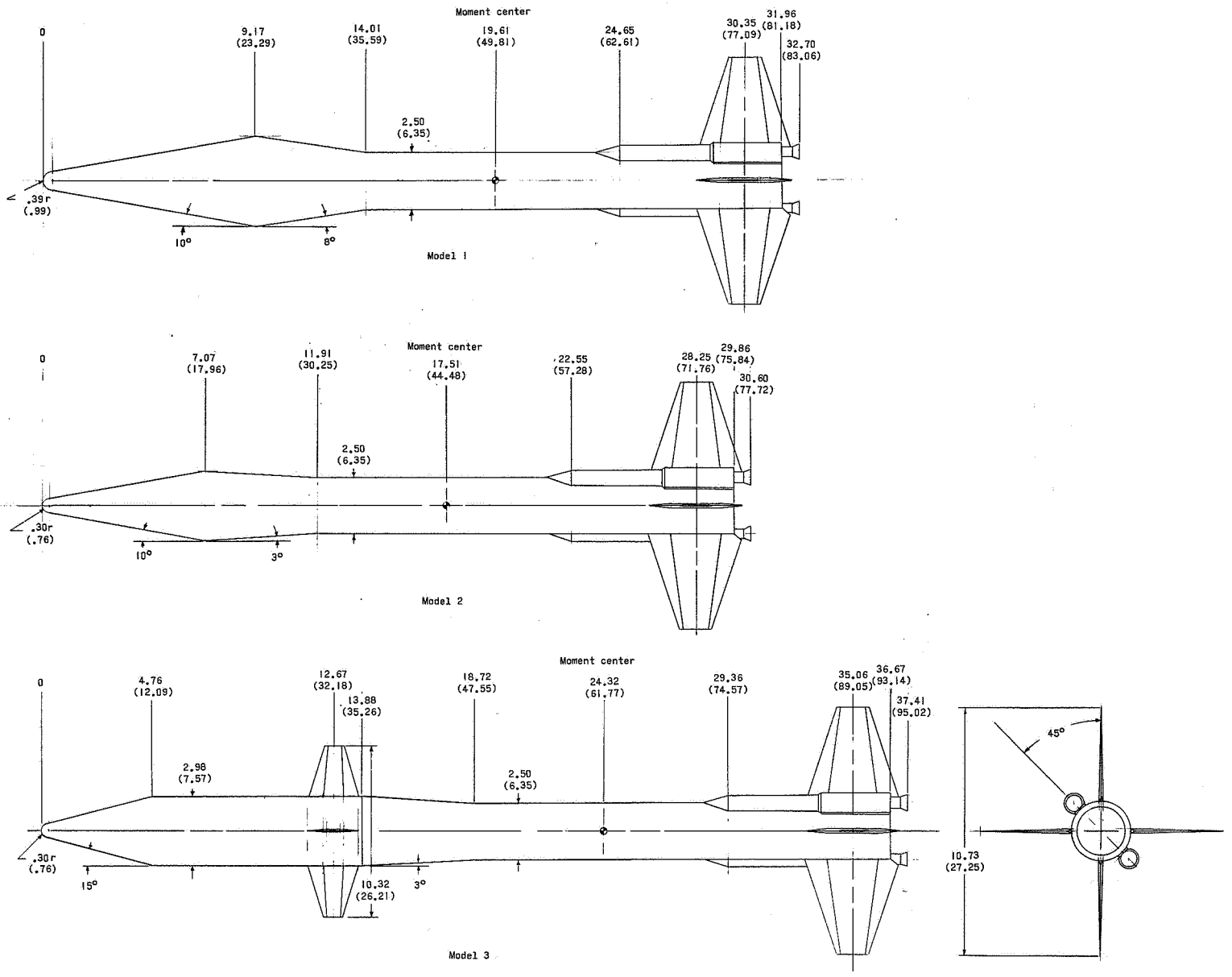

Figure 1.- Dimensional details of models used in the investigation. All dimensions are given in inches and parenthetically in centimeters.

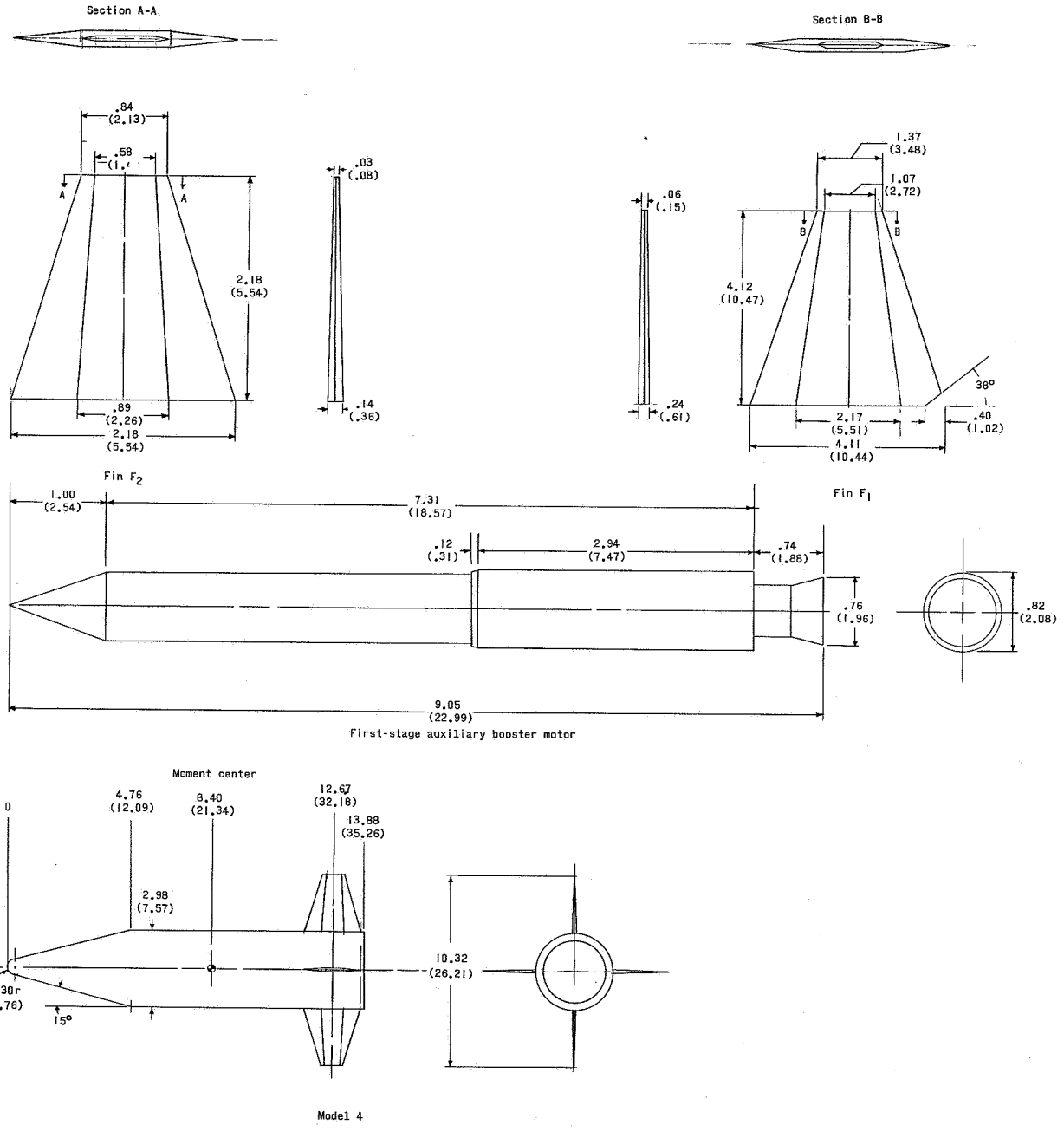

Figure 1.- Concluded.

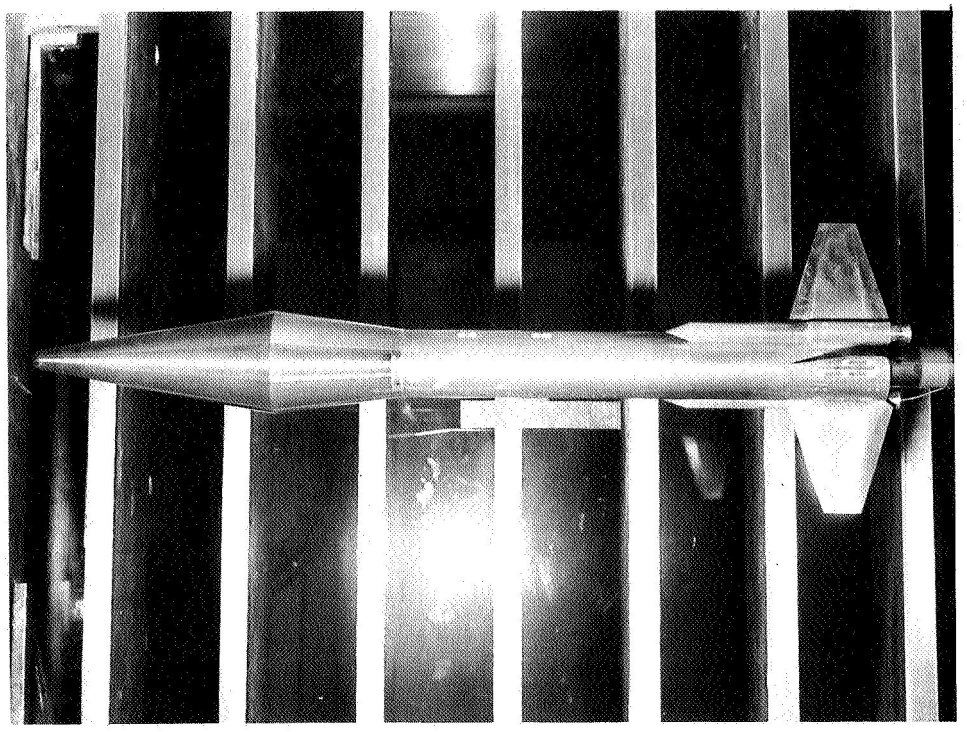

(a) Model 1. L-66-7942

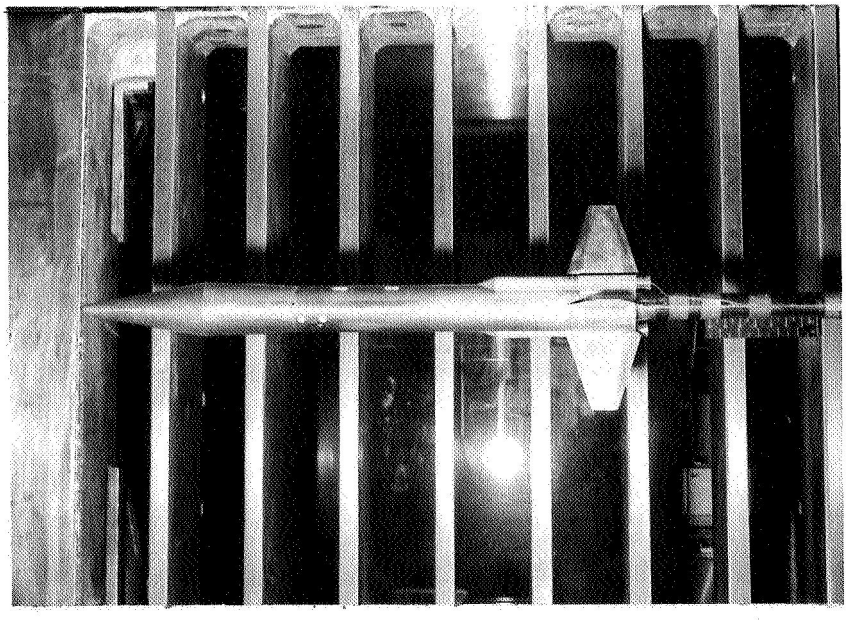

(b) Model 2. L-66-8197

Figure 2.- Models used in the investigation.

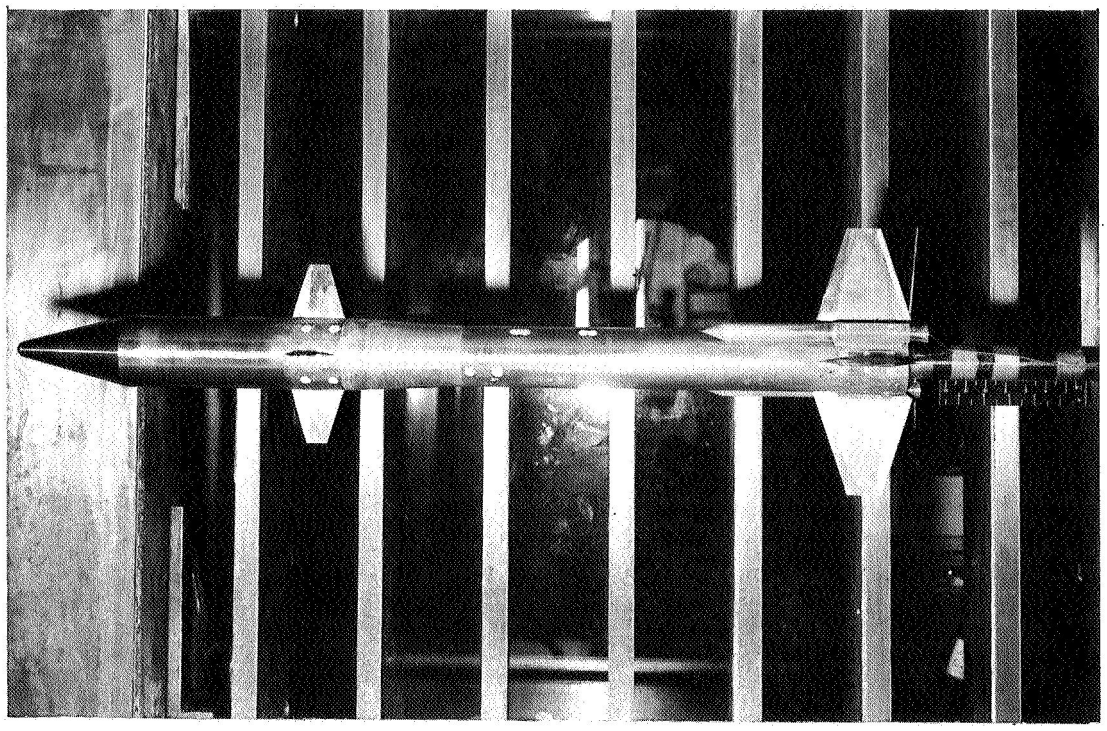

(c) Model 3. L-66-7950

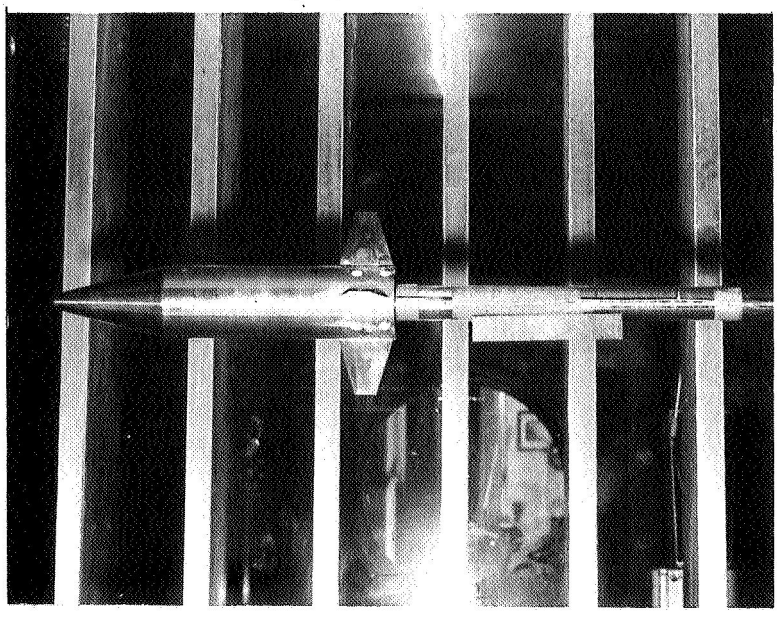

(d) Model 4. L-66-7951

Figure 2.- Concluded.

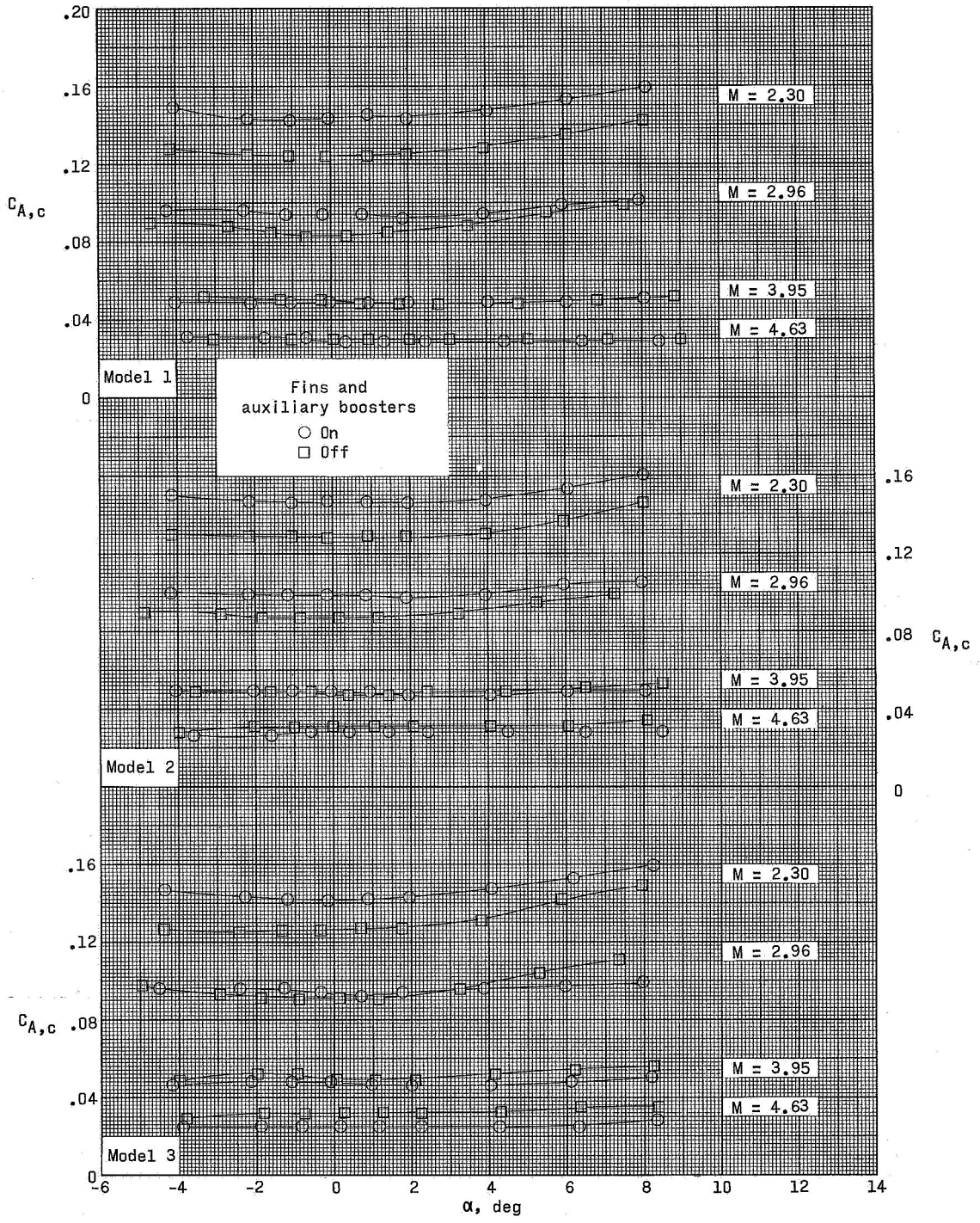

(a) Models 1, 2, and 3.

Figure 3.- Typical values of chamber axial-force coefficients.

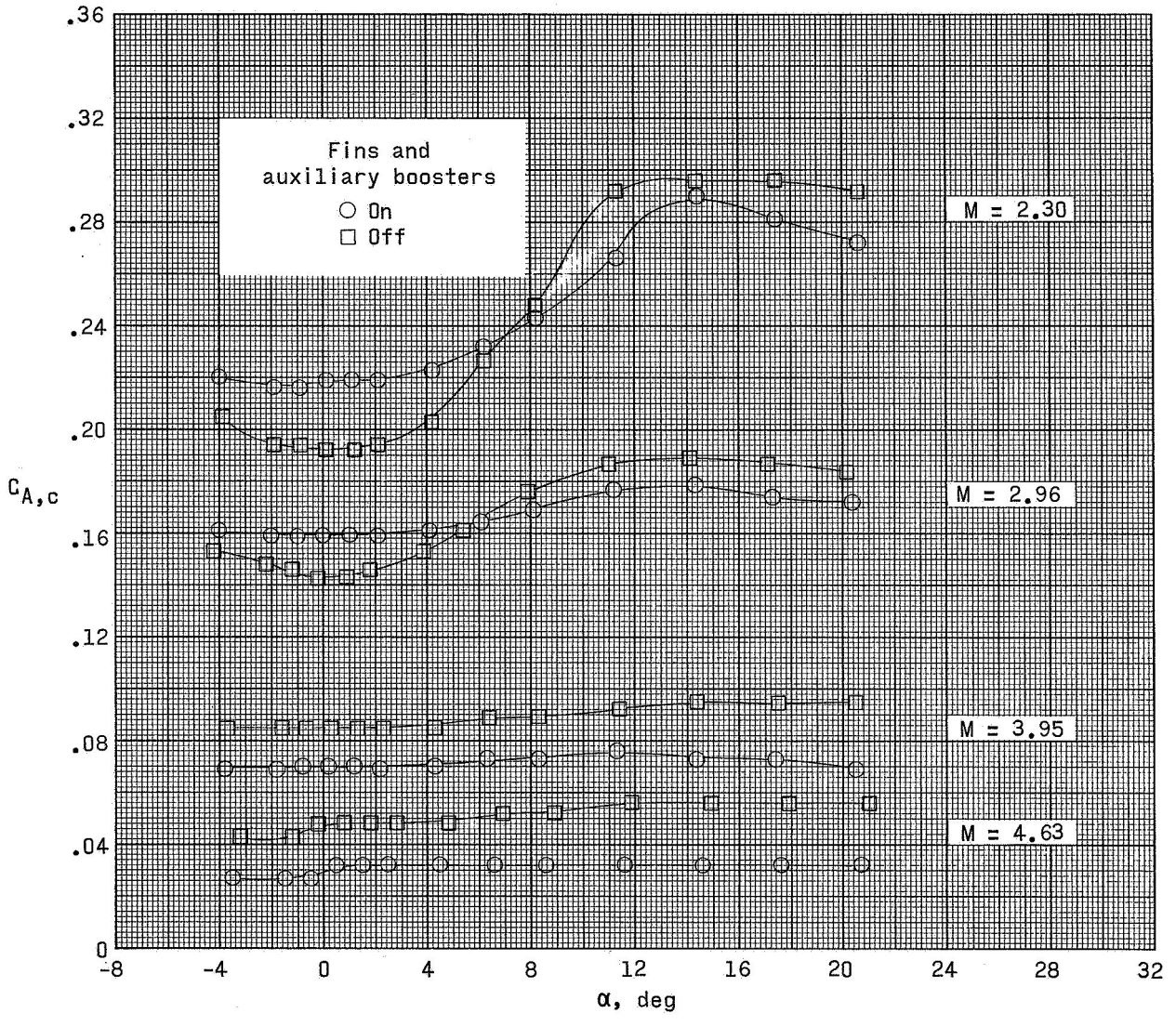

(b) Model 4.

Figure 3.- Concluded.

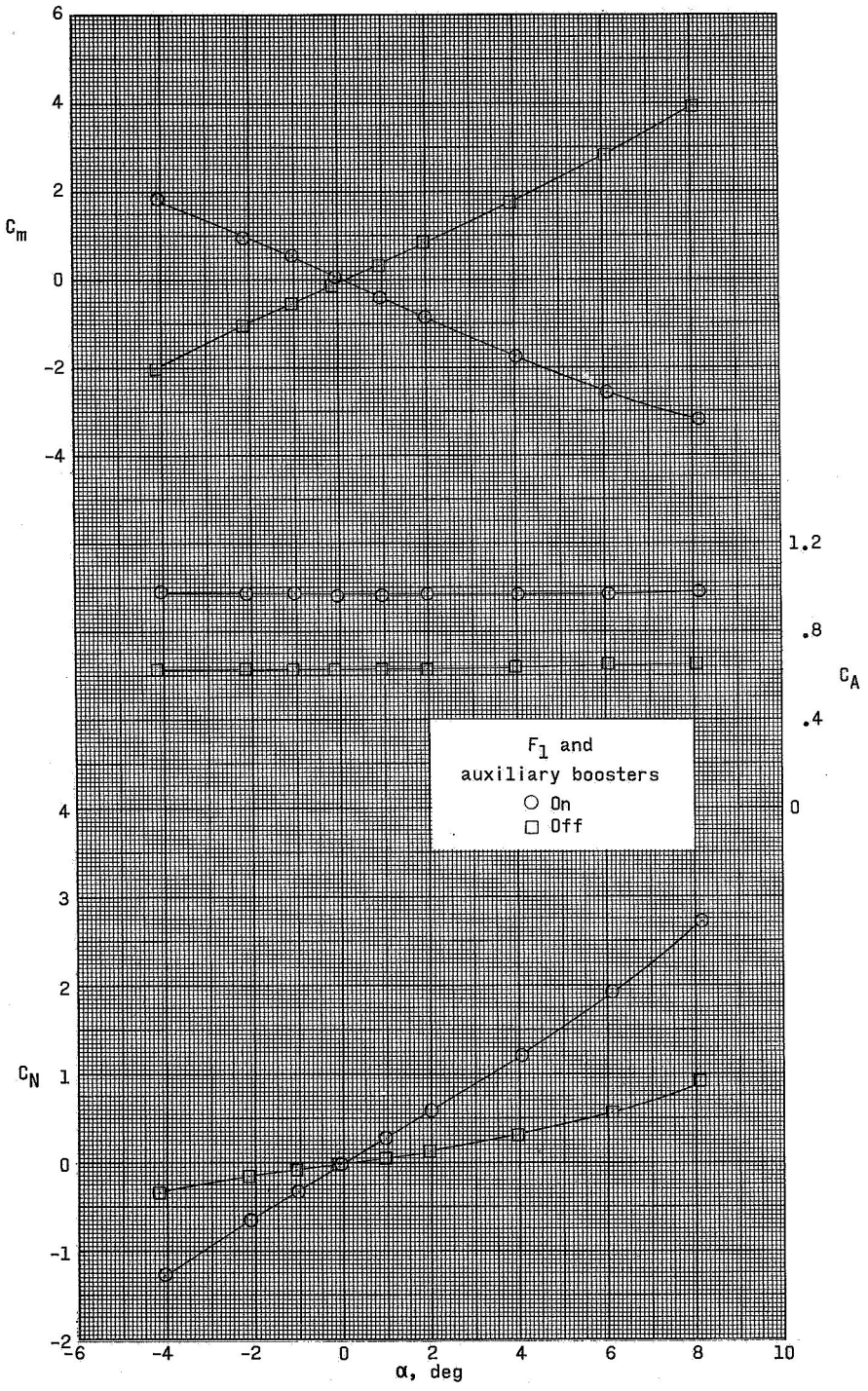

(a) M = 2.30.

Figure 4.- Longitudinal aerodynamic characteristics of model 1.

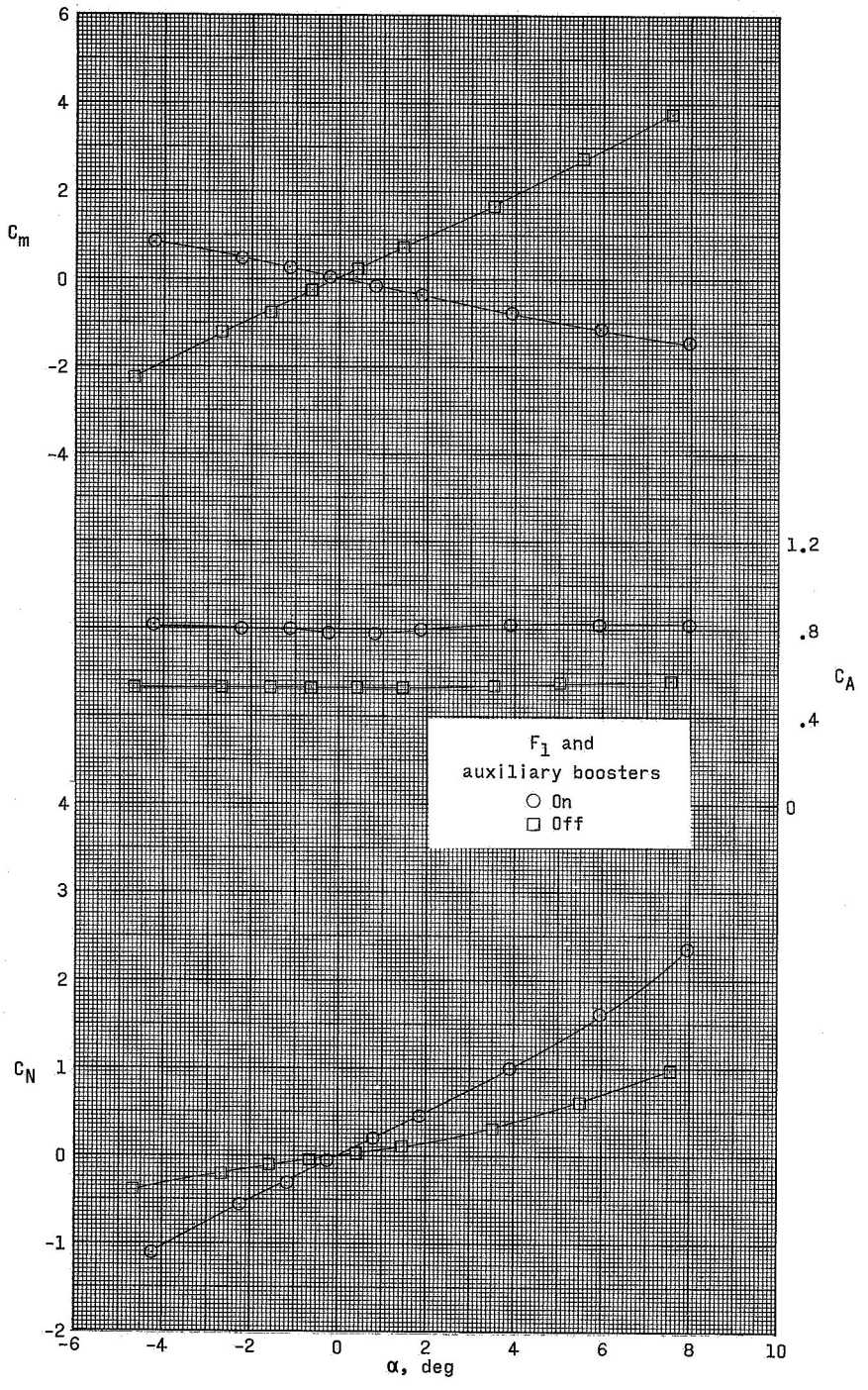

(b) M = 2.96.

Figure 4.- Continued.

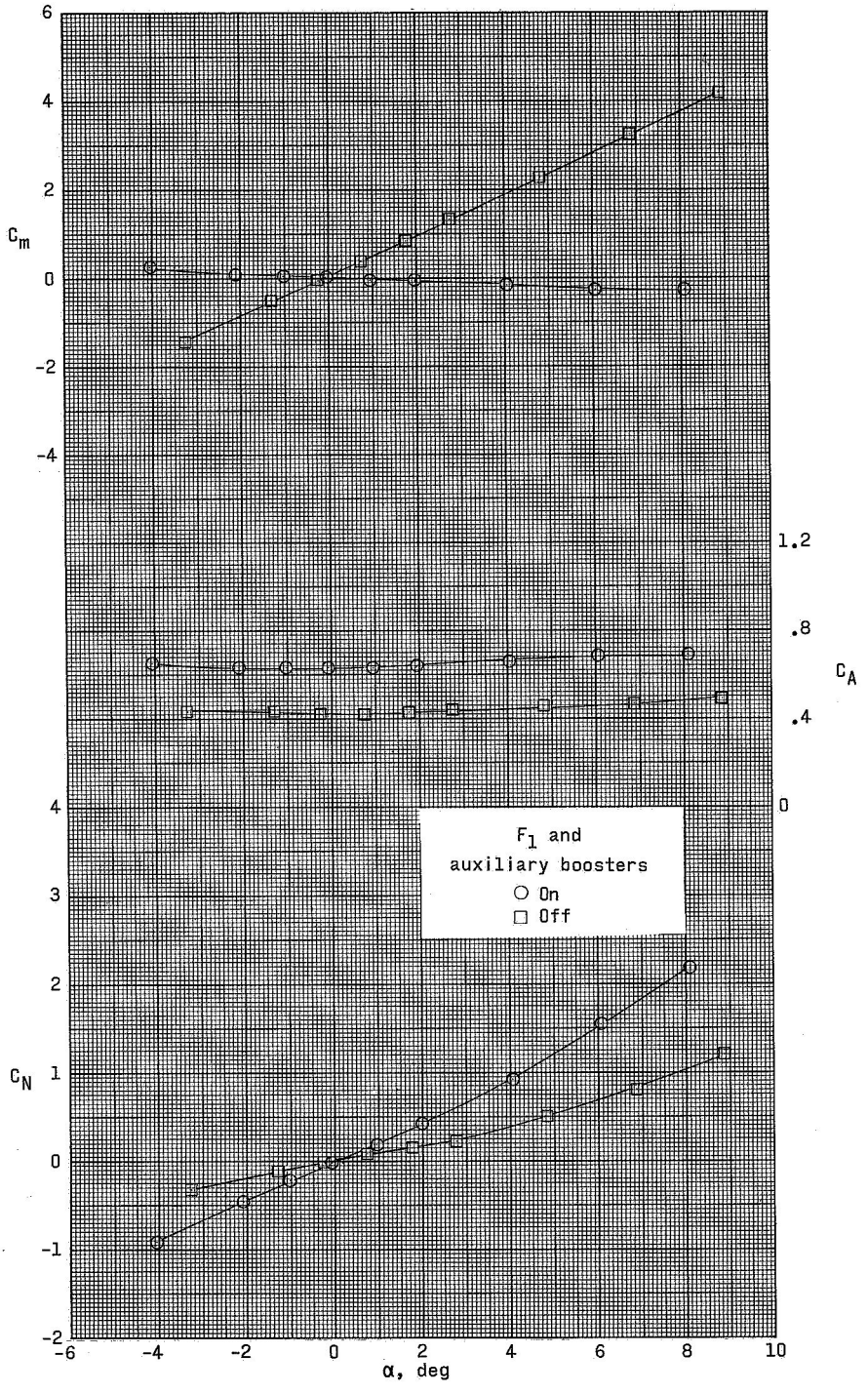

(c) M = 3.95.

Figure 4.- Continued.

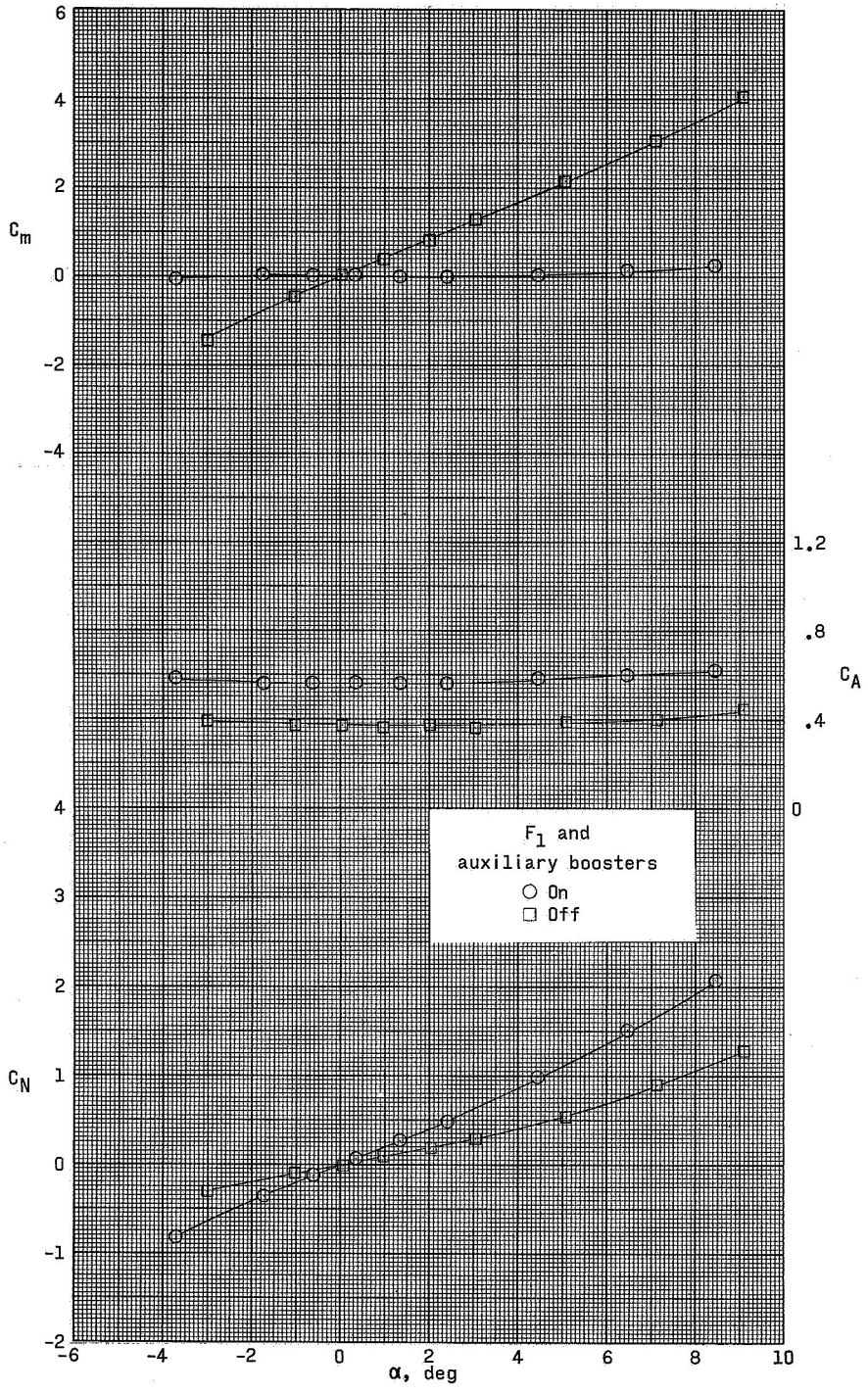

(d) M = 4.63.

Figure 4.- Concluded.

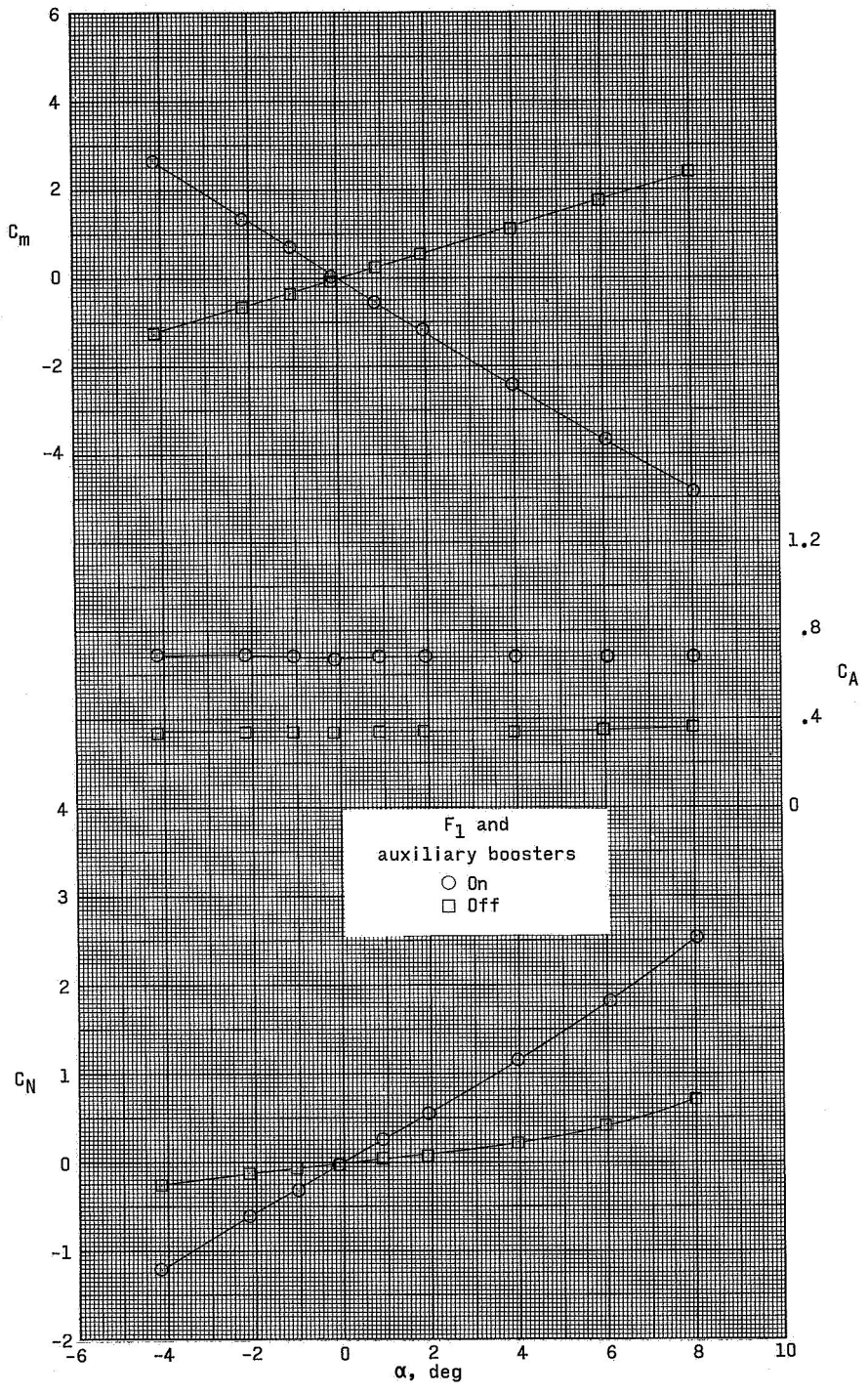

(a) M = 2.30.

Figure 5.- Longitudinal aerodynamic characteristics of model 2.

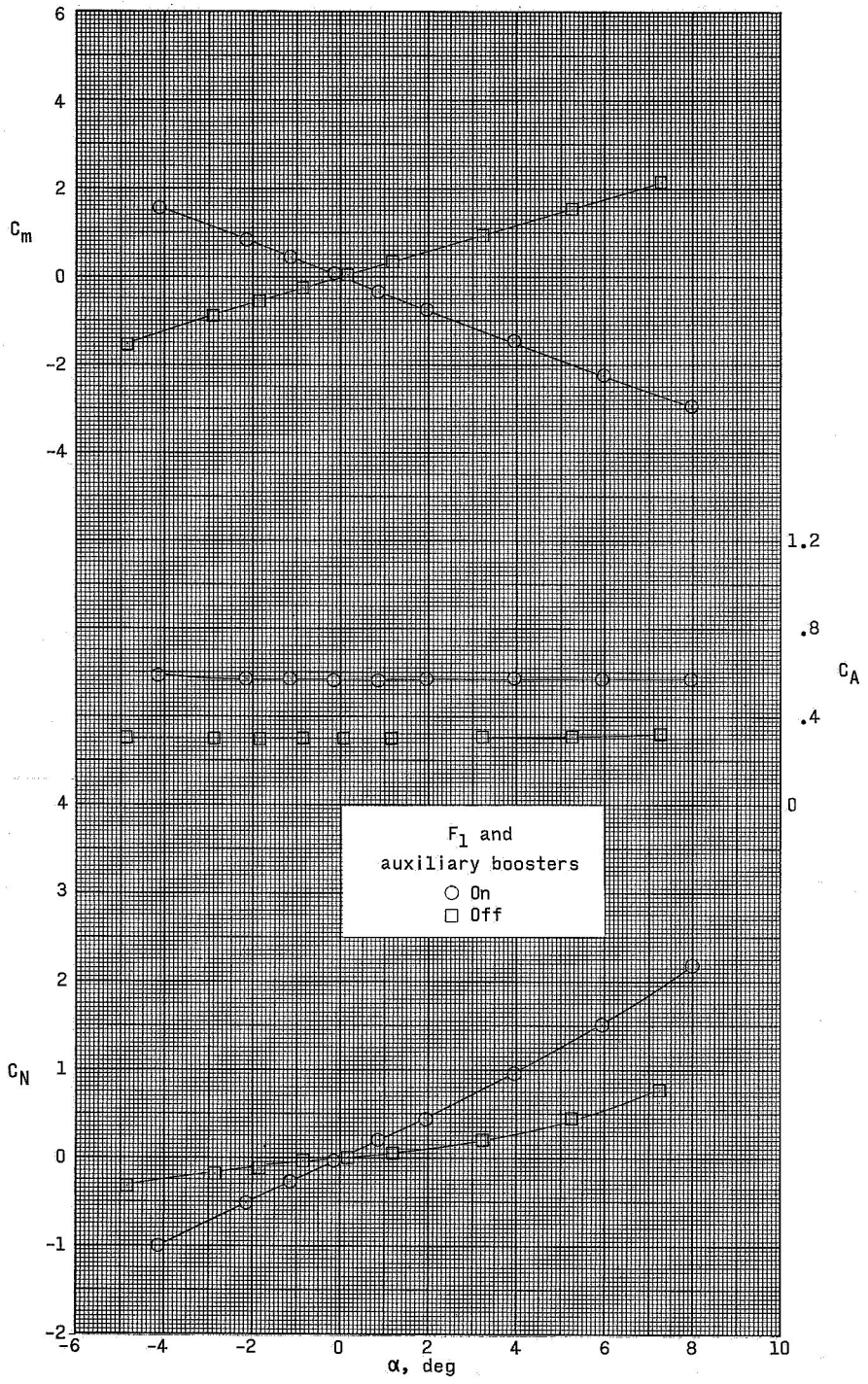

(b) M = 2.96.

Figure 5.- Continued.

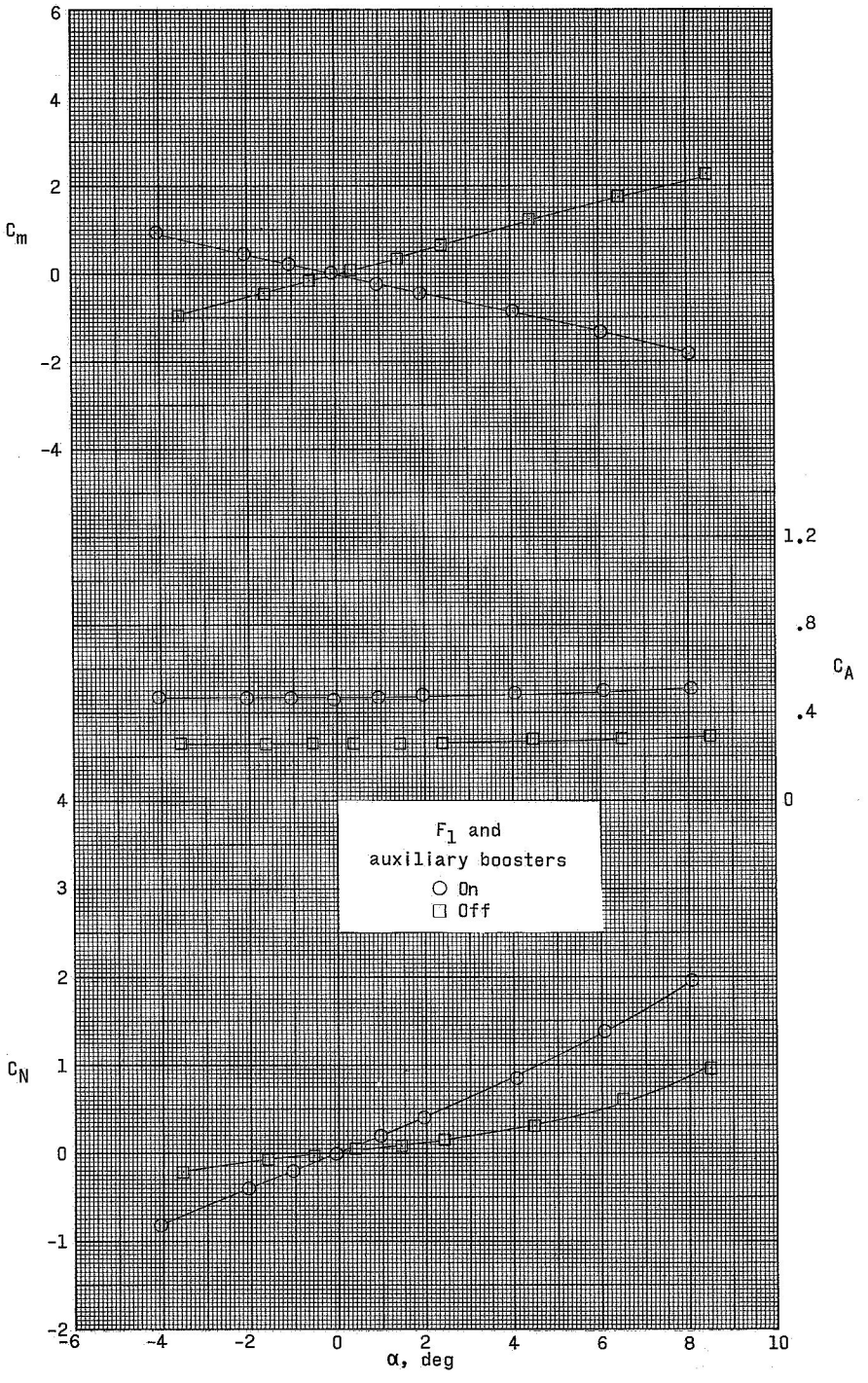

(c) M = 3.95.

Figure 5.- Continued.

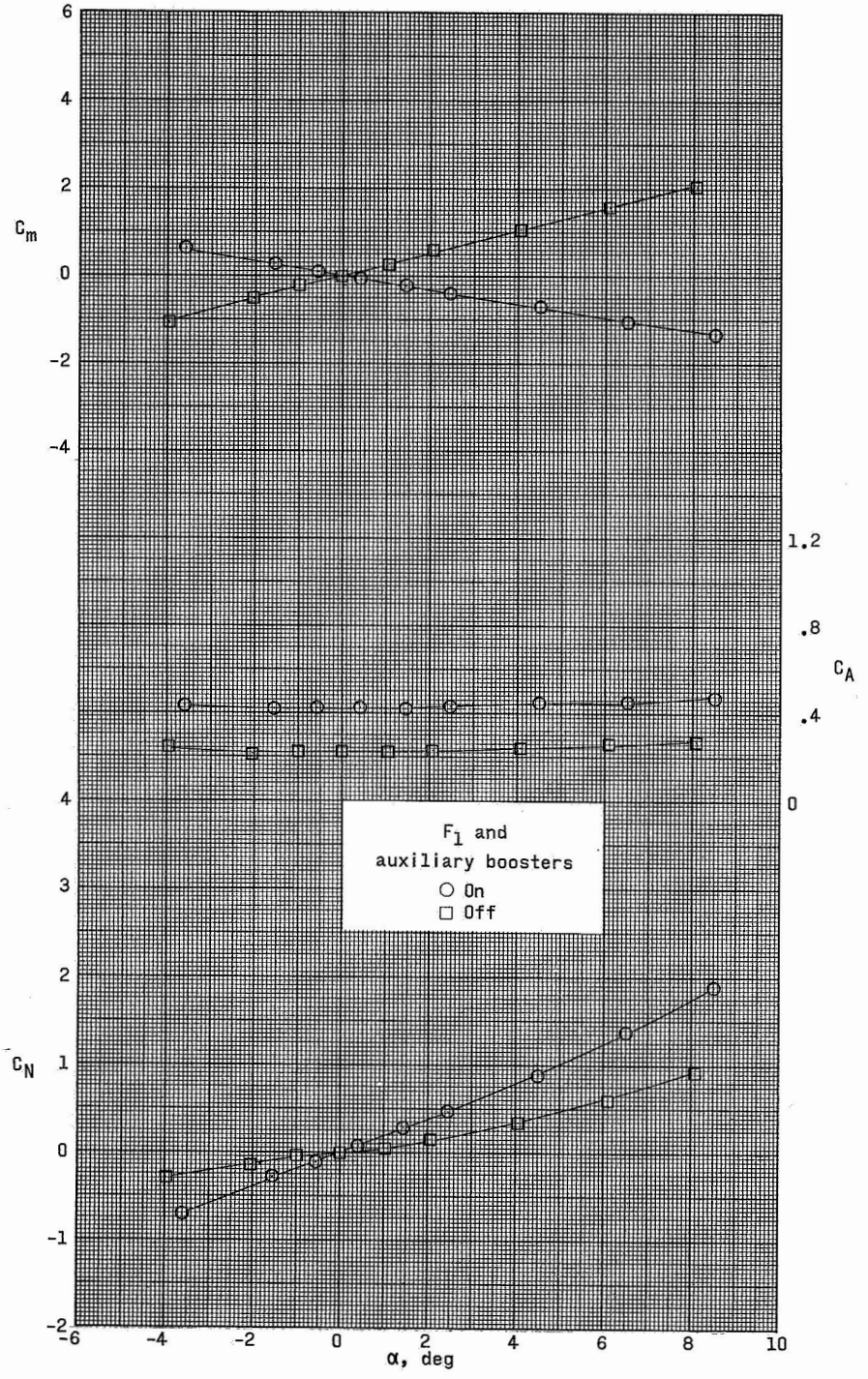

(d) M = 4.63.

Figure 5.- Concluded.

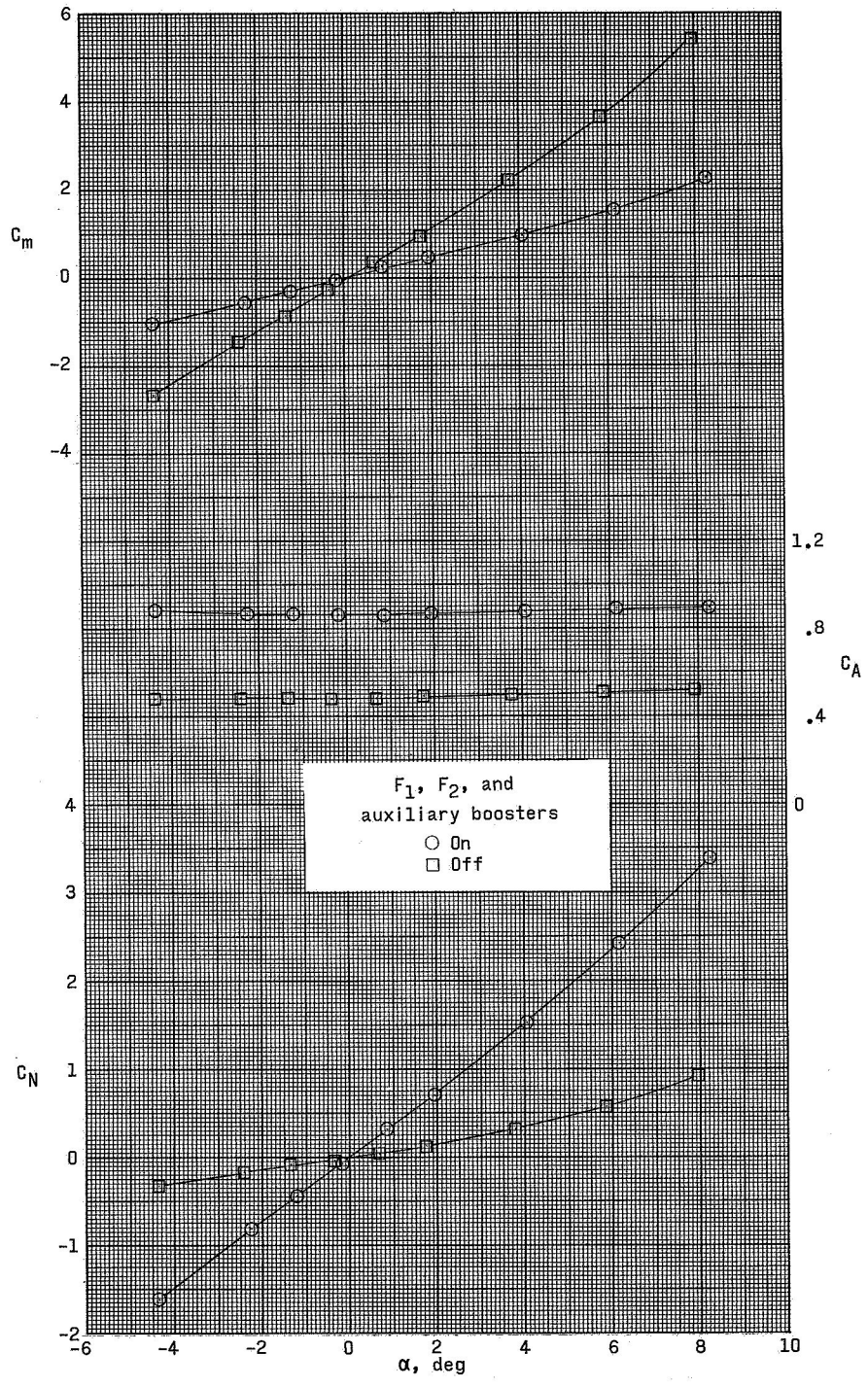

(a) M = 2.30.

Figure 6.- Longitudinal aerodynamic characteristics of model 3.

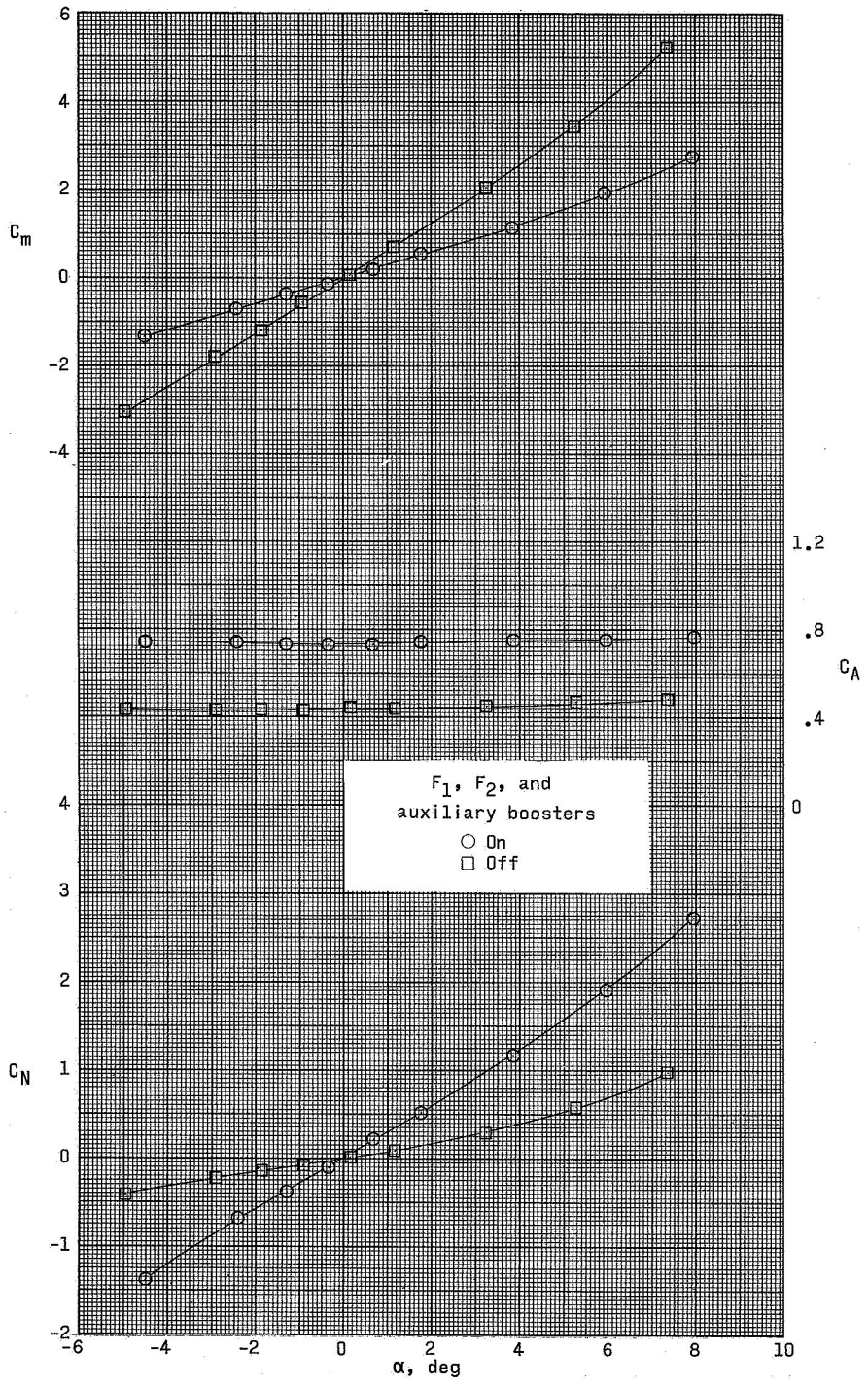

(b) M = 2.96.

Figure 6.- Continued.

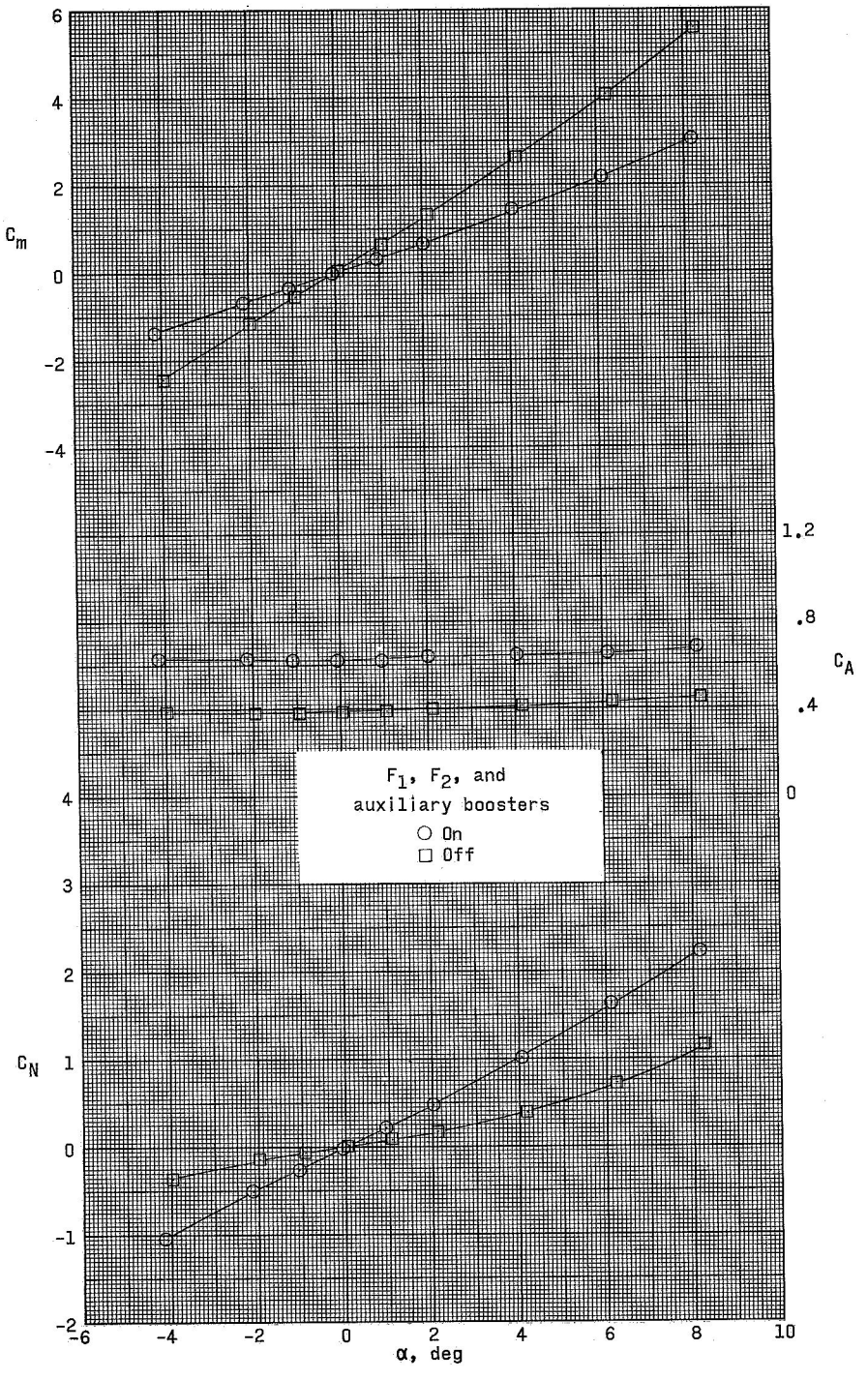

(c) M = 3.95.

Figure 6.- Continued.

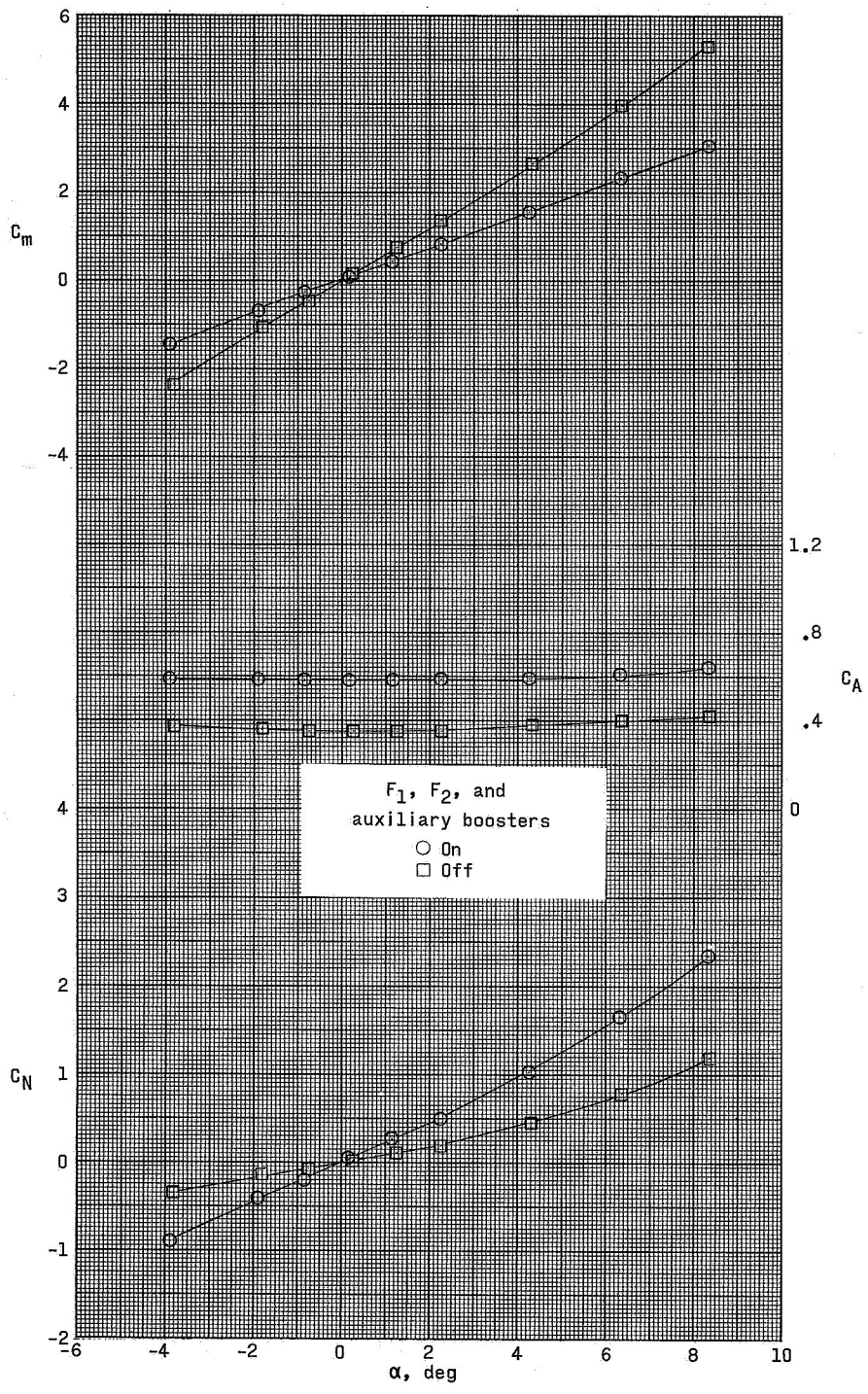

(d) M = 4.63.

Figure 6.- Concluded.

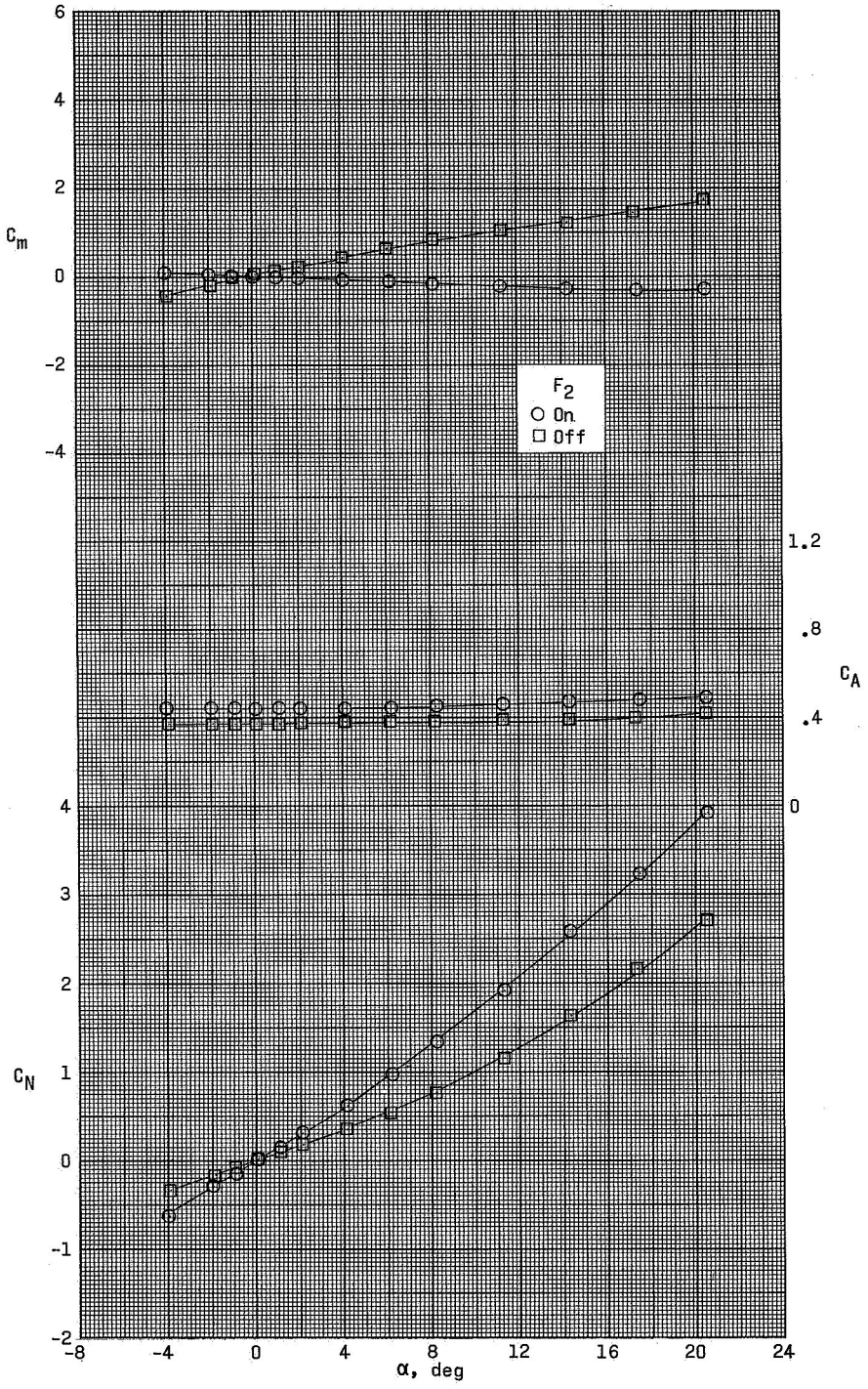

(a) M = 2.30.

Figure 7.- Longitudinal aerodynamic characteristics of model 4.

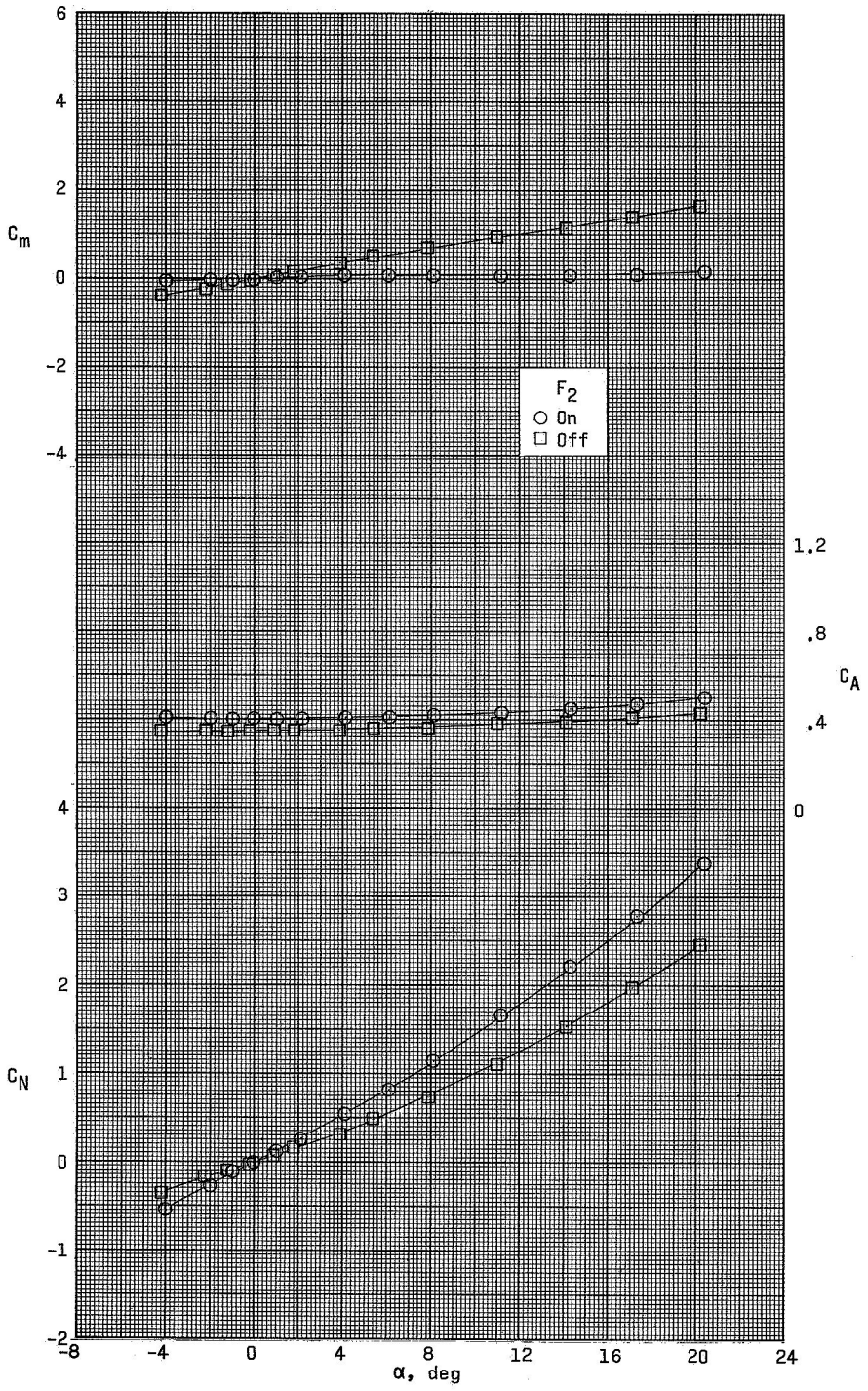

(b) M = 2.96.

Figure 7.- Continued.

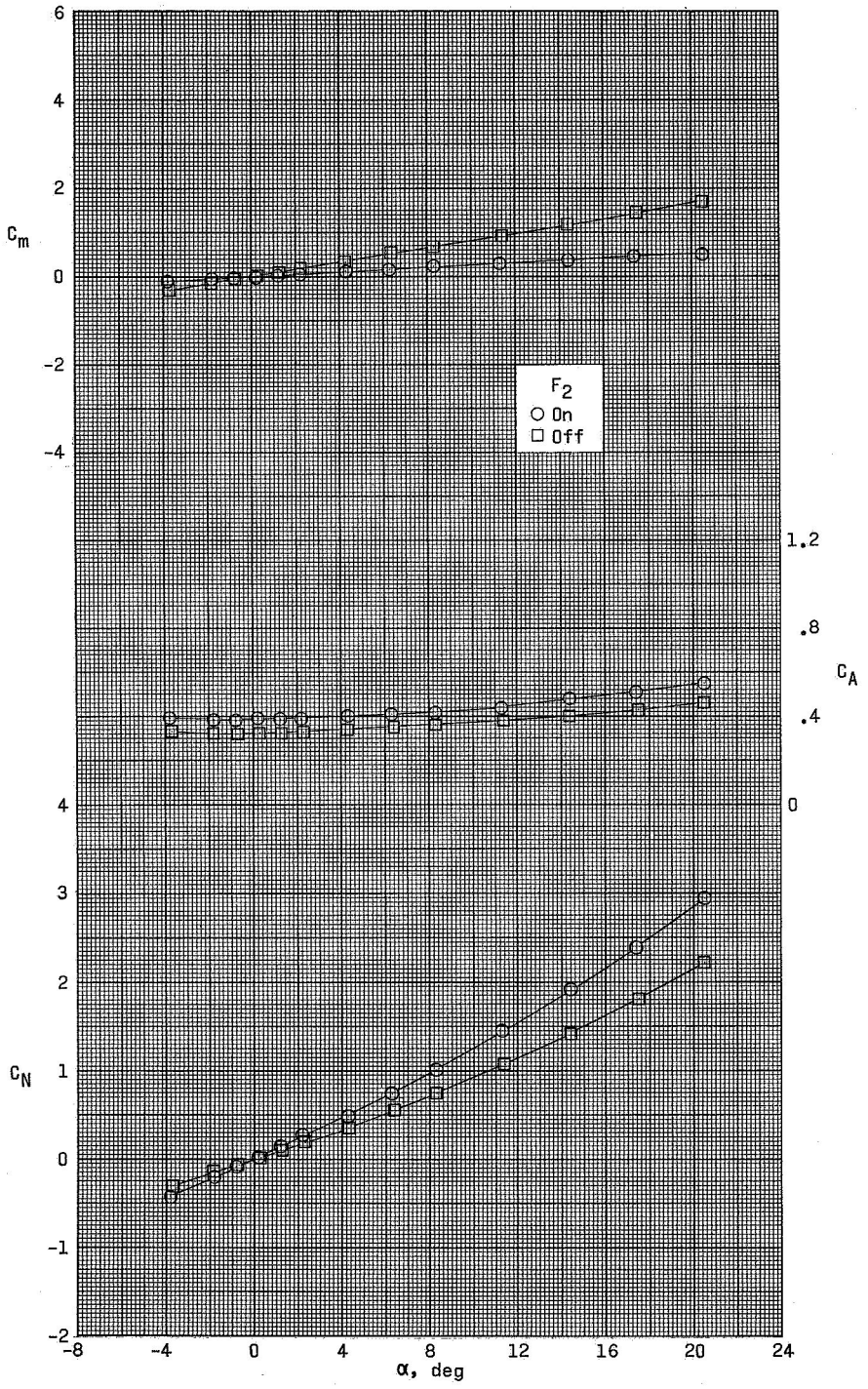

(c) M = 3.95.

Figure 7.- Continued.

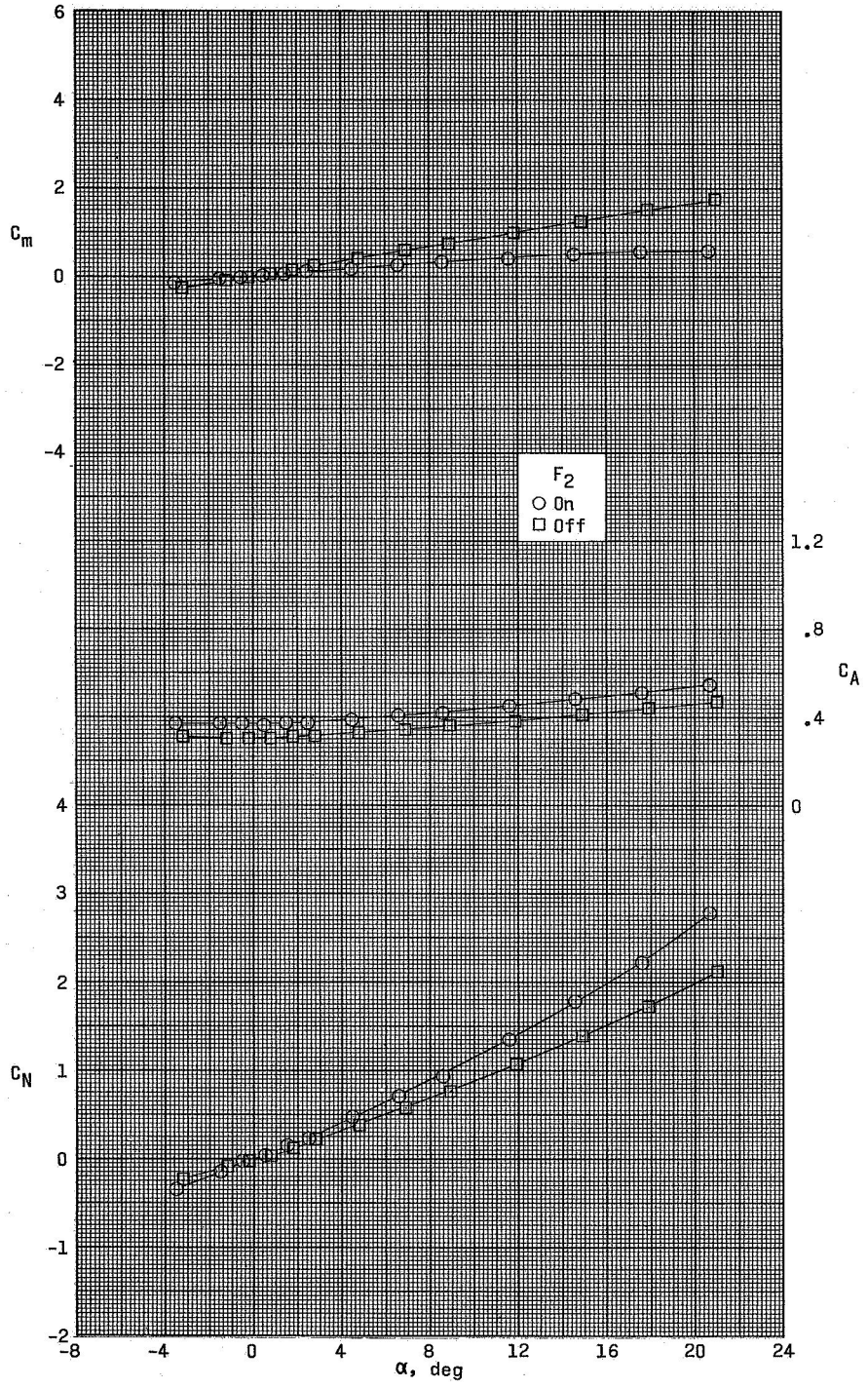

(d) M = 4.63.

Figure 7.- Concluded.

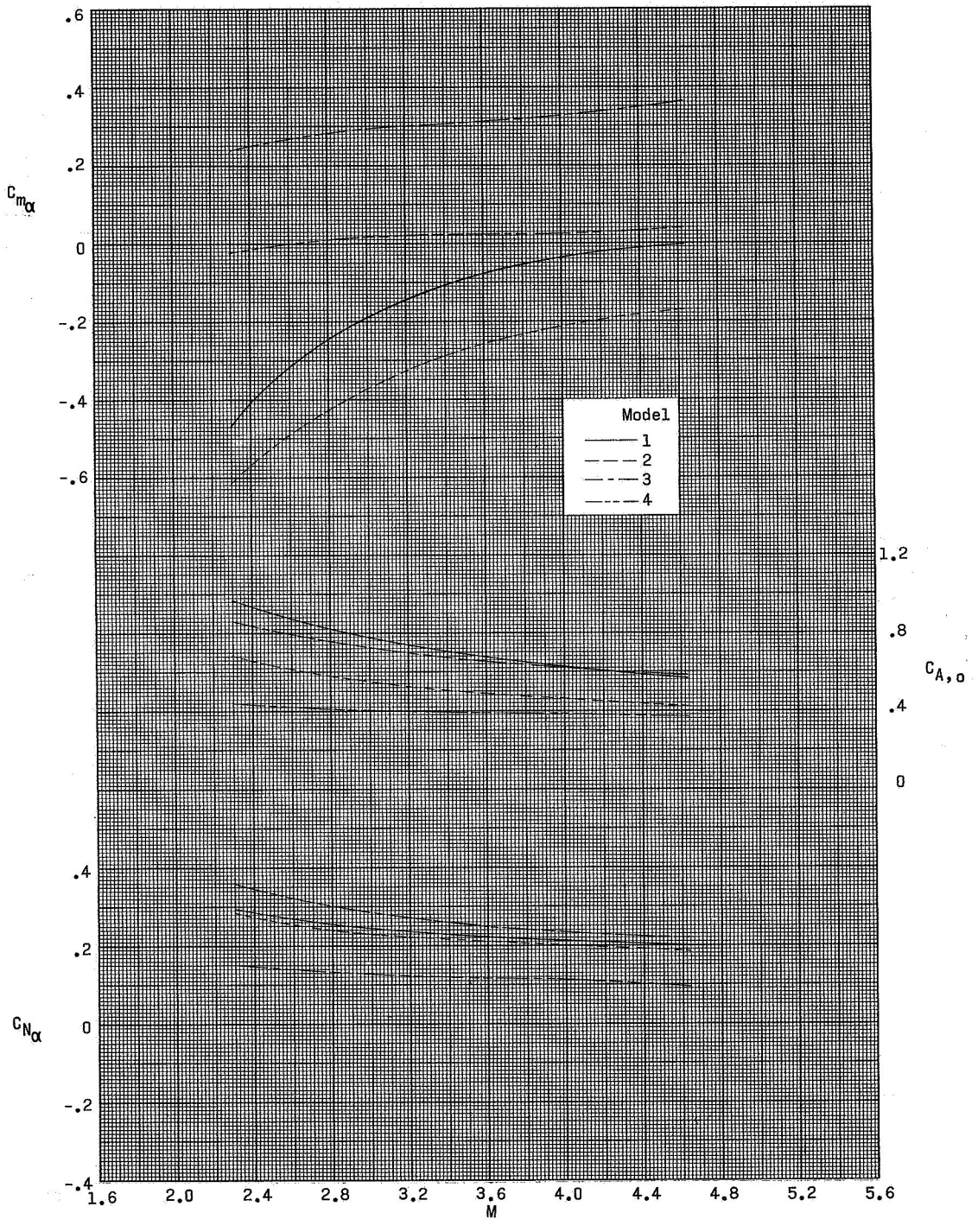

(a) Fins and auxiliary boosters on.

Figure 8.- Variation of longitudinal aerodynamic parameters with Mach number.

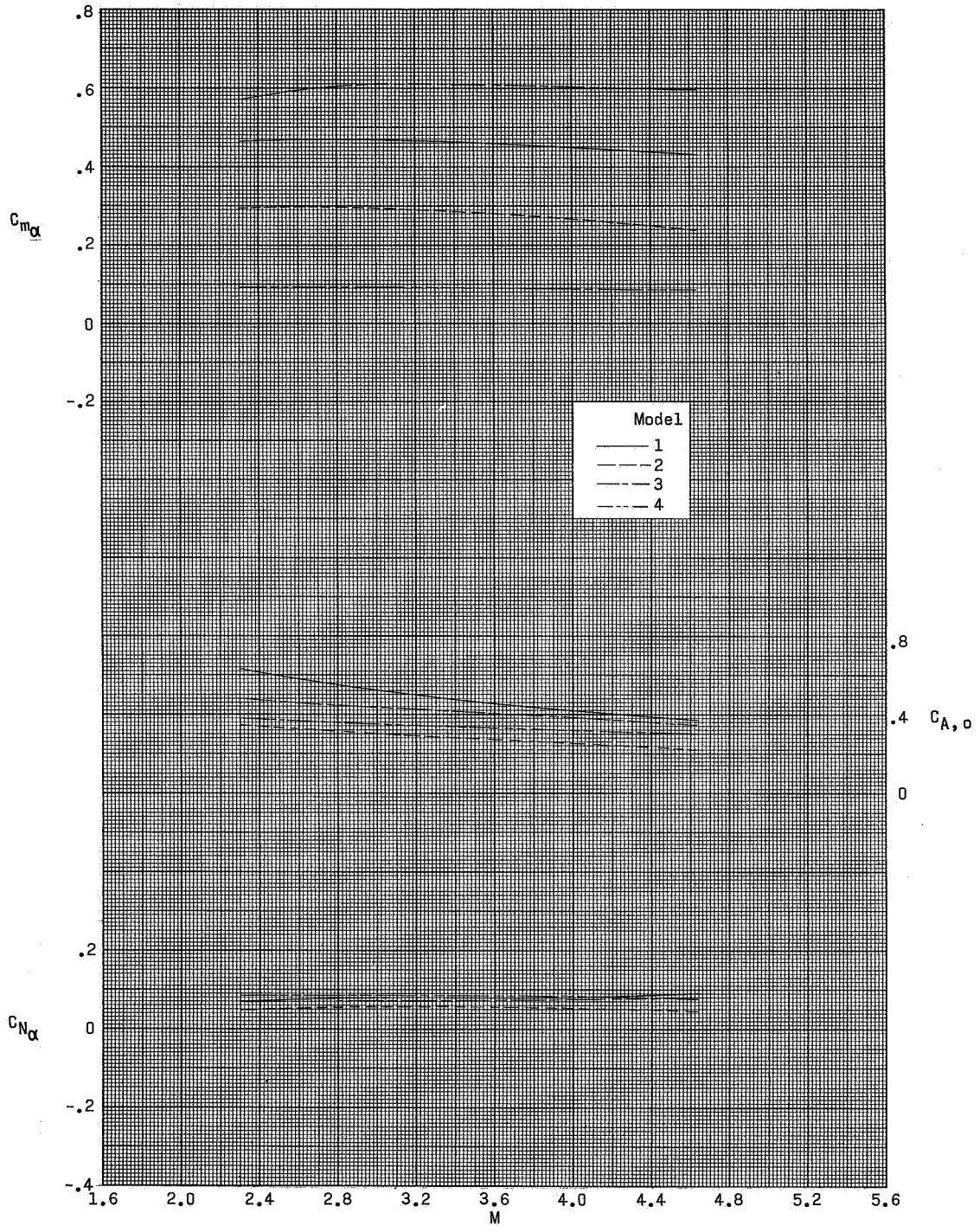

(b) Fins and auxiliary boosters off.

Figure 8.- Concluded.

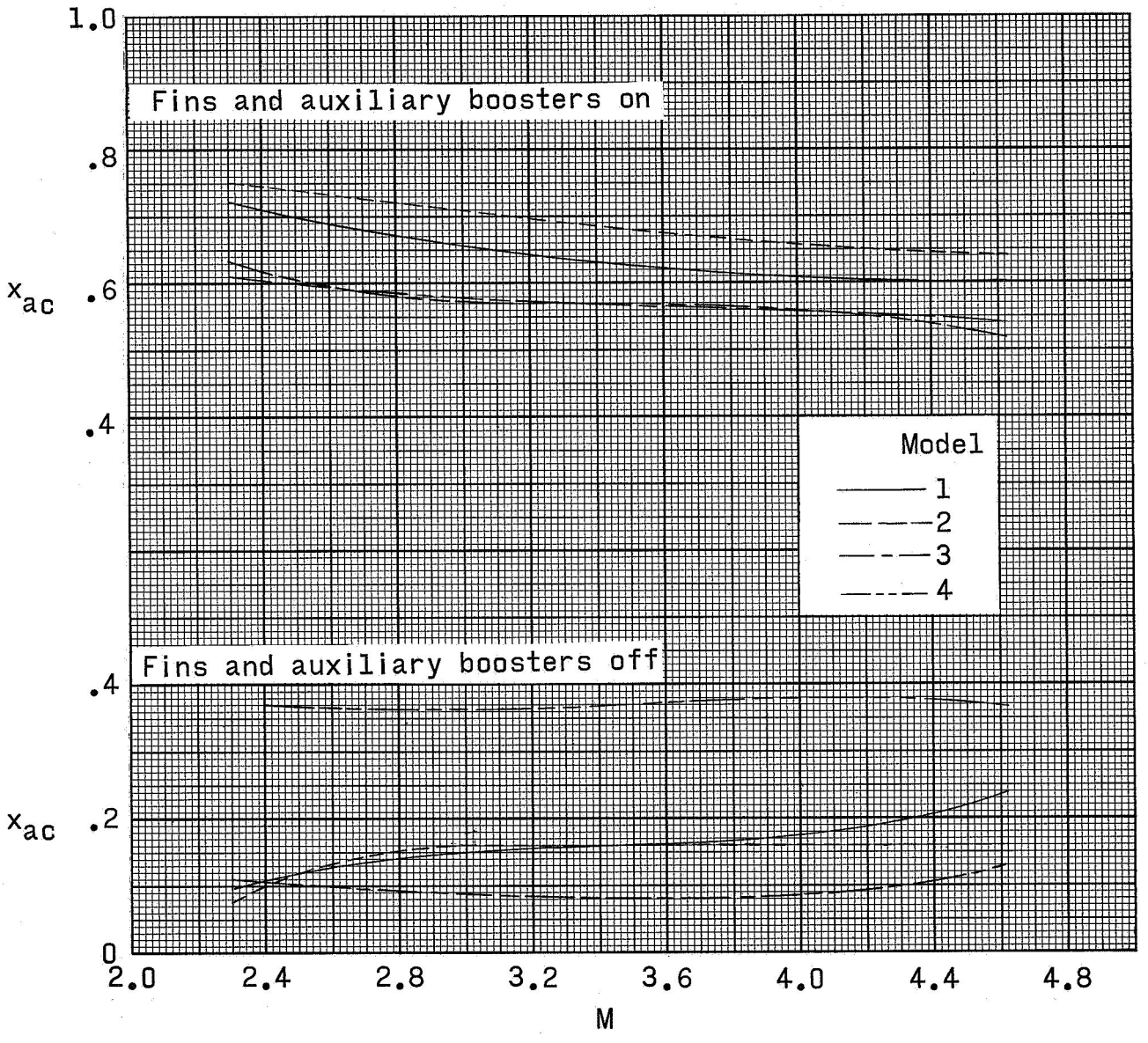

Figure 9.- Variation of x_{ac} with Mach number.

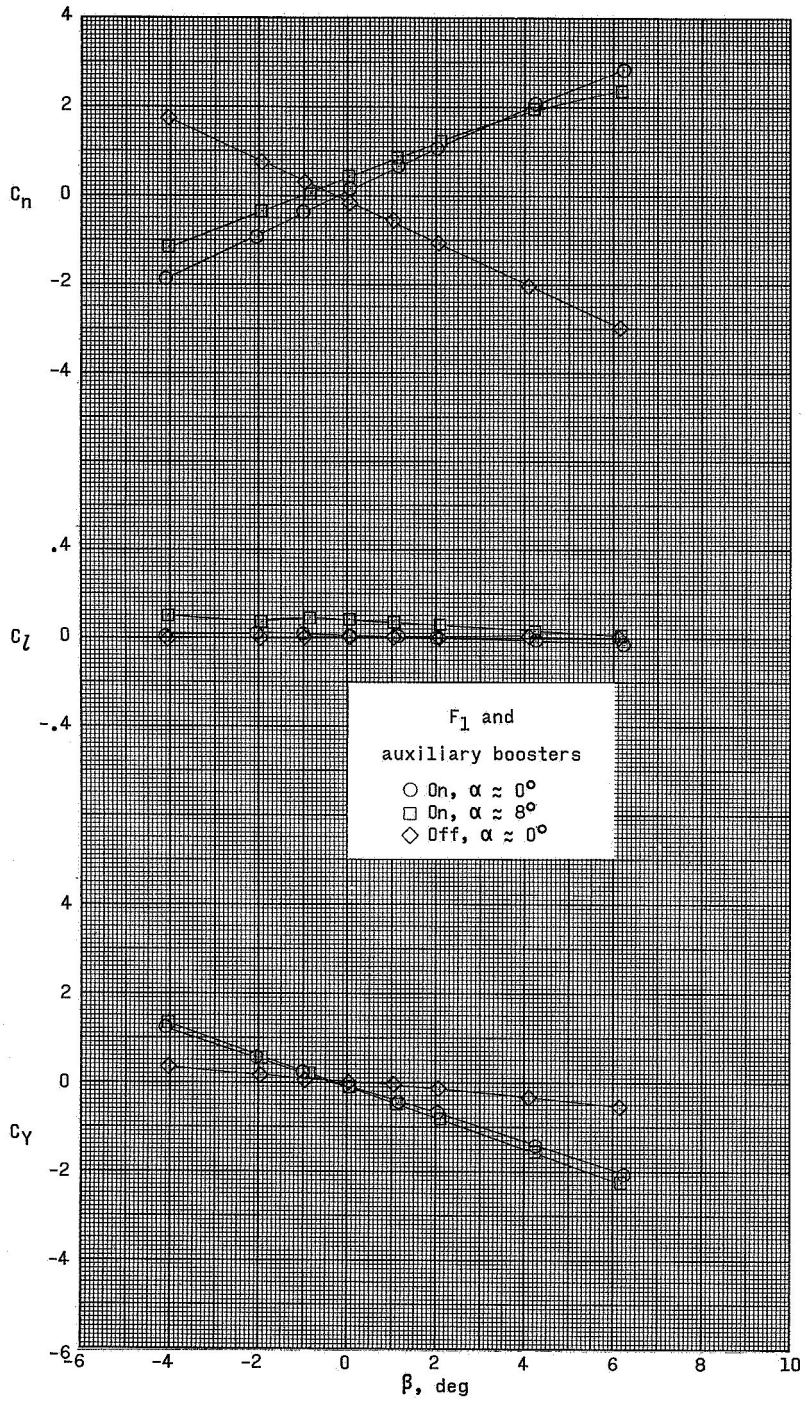

(a) M = 2.30.

Figure 10.- Lateral aerodynamic characteristics of model 1.

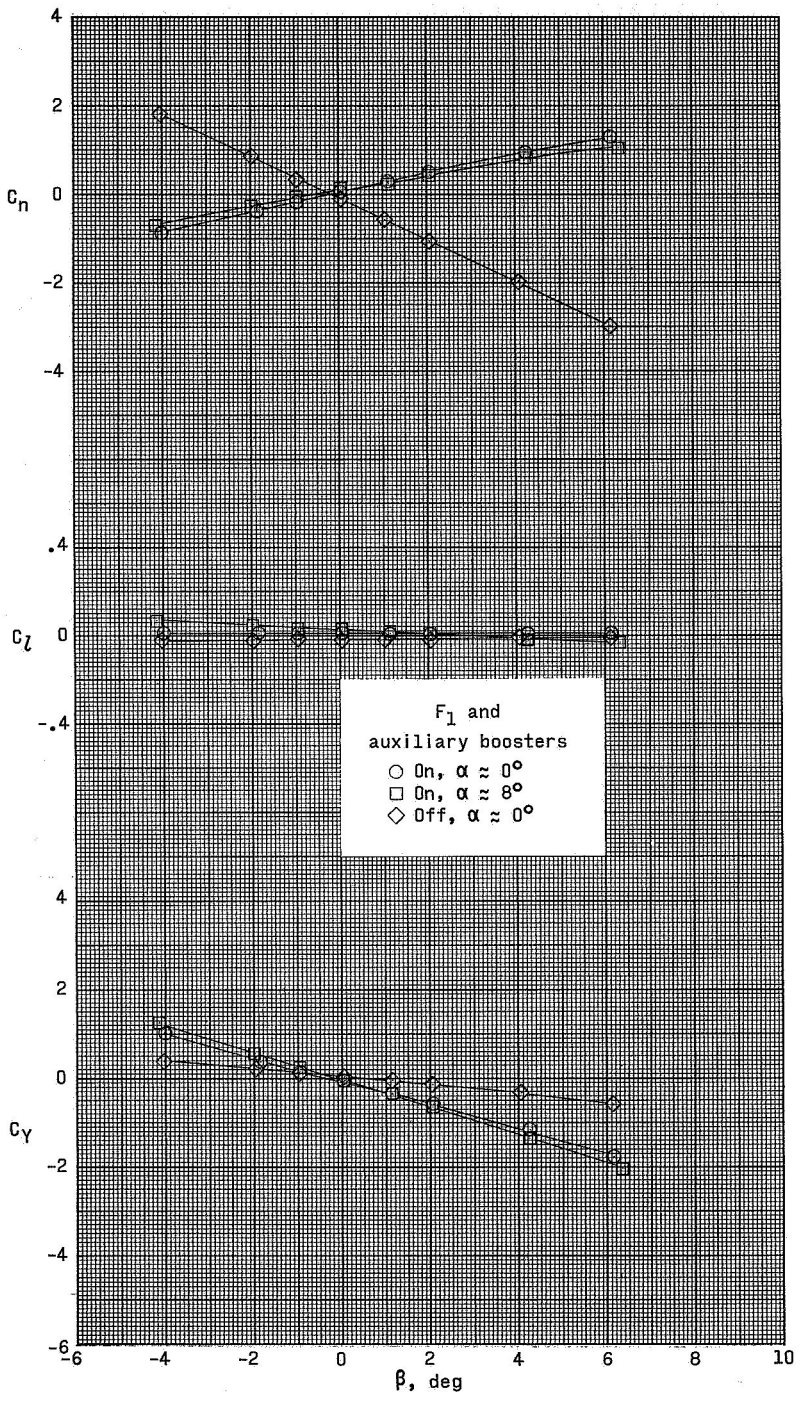

(b) M = 2.96.

Figure 10.- Continued.

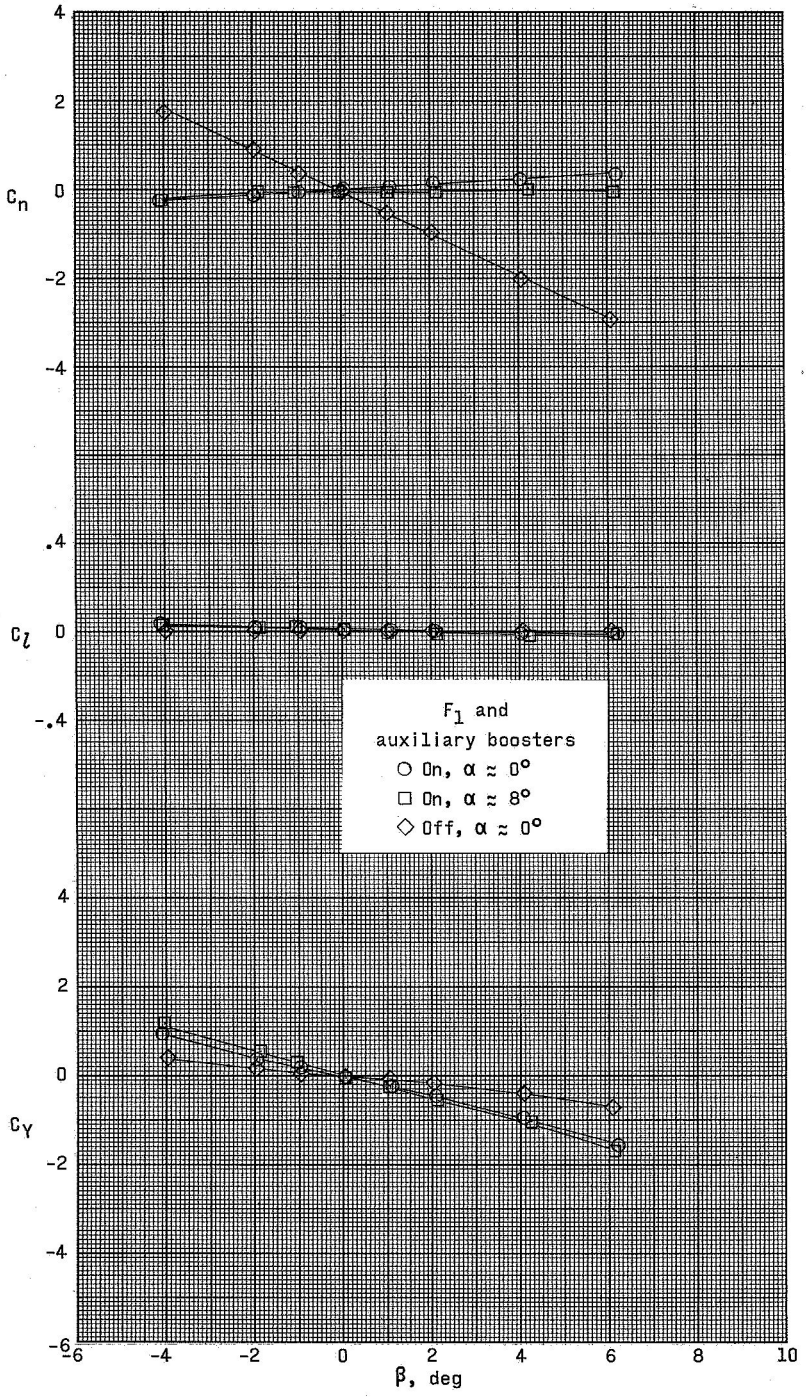

(c) M = 3.95.

Figure 10.- Continued.

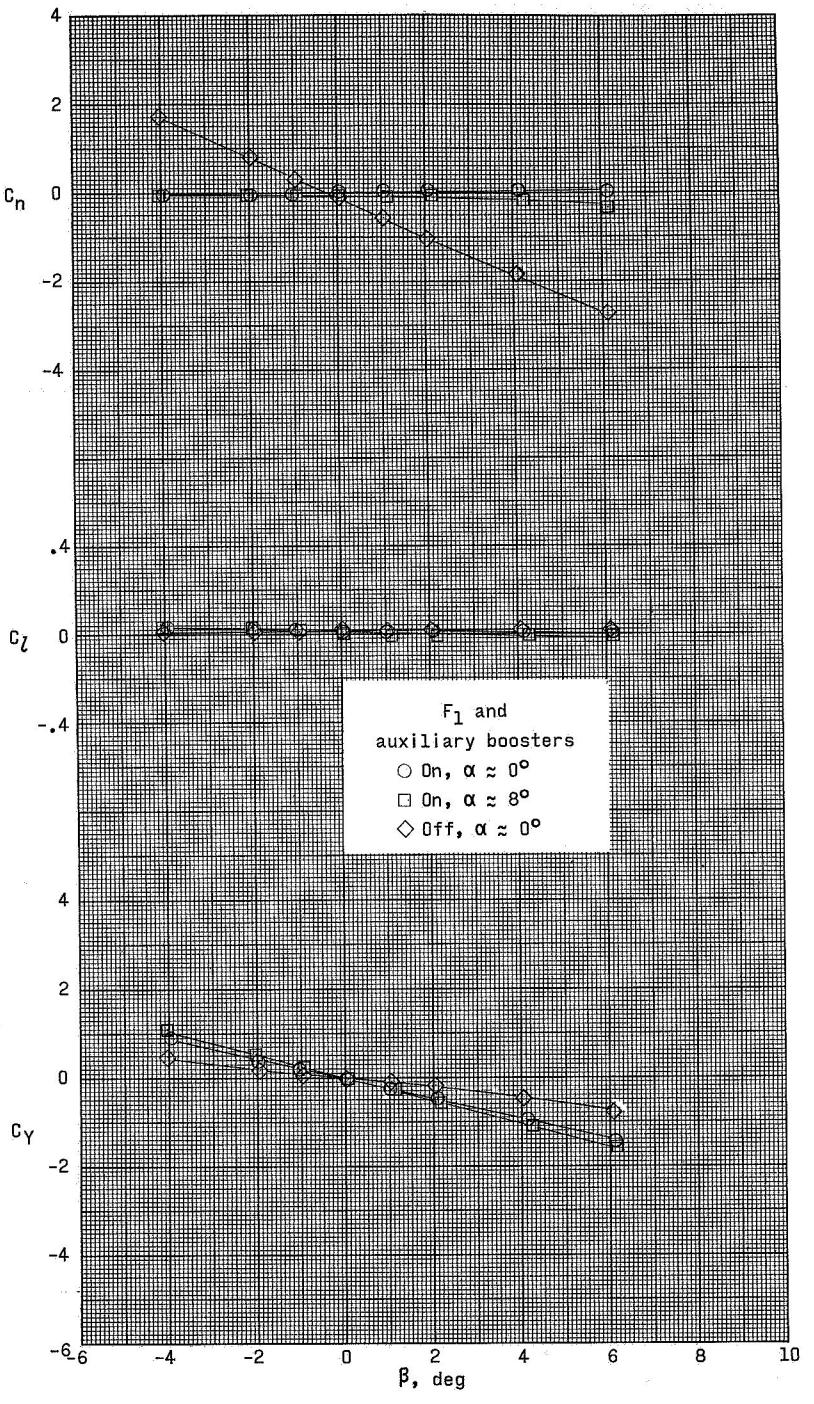

(d) M = 4.63.

Figure 10.- Concluded.

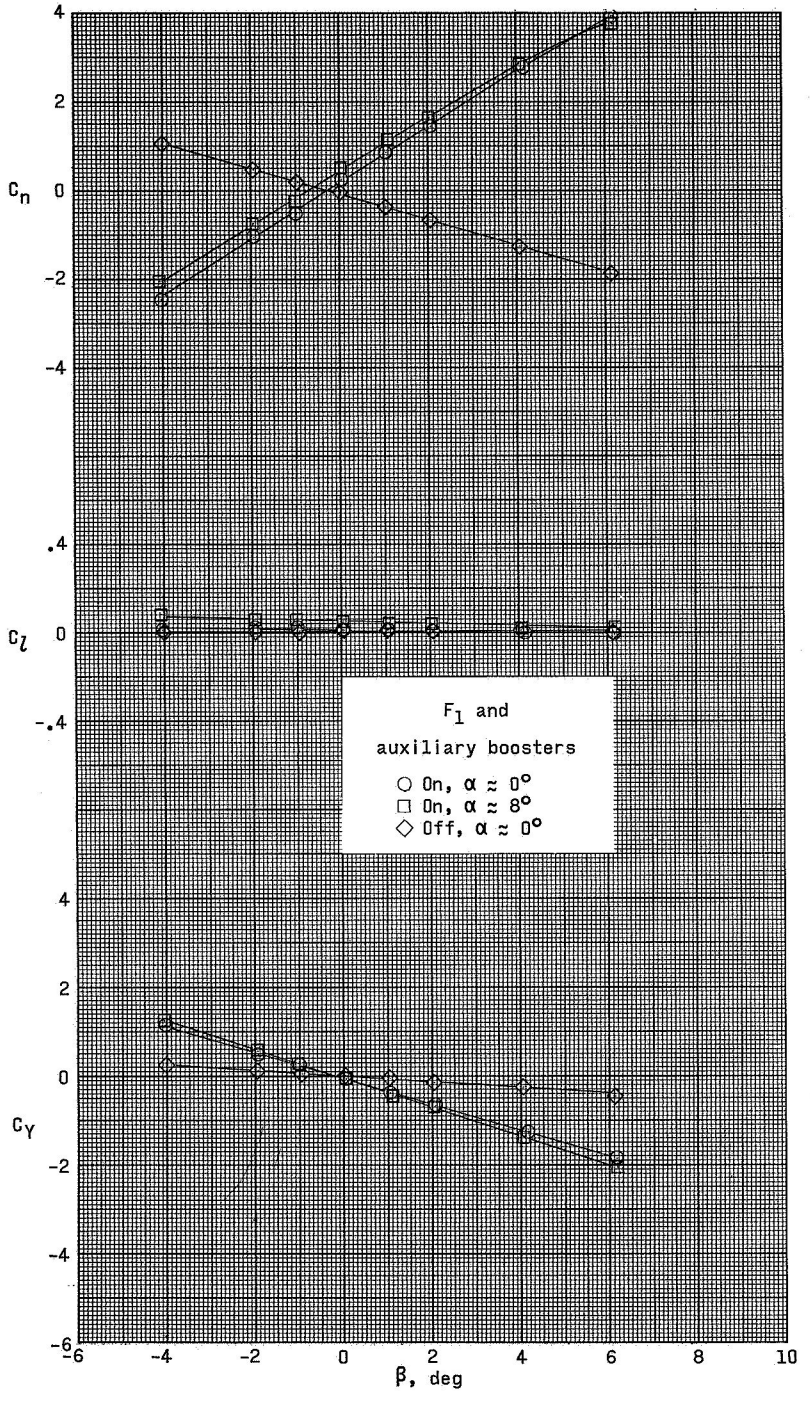

(a) M = 2.30.

Figure 11.- Lateral aerodynamic characteristics of model 2.

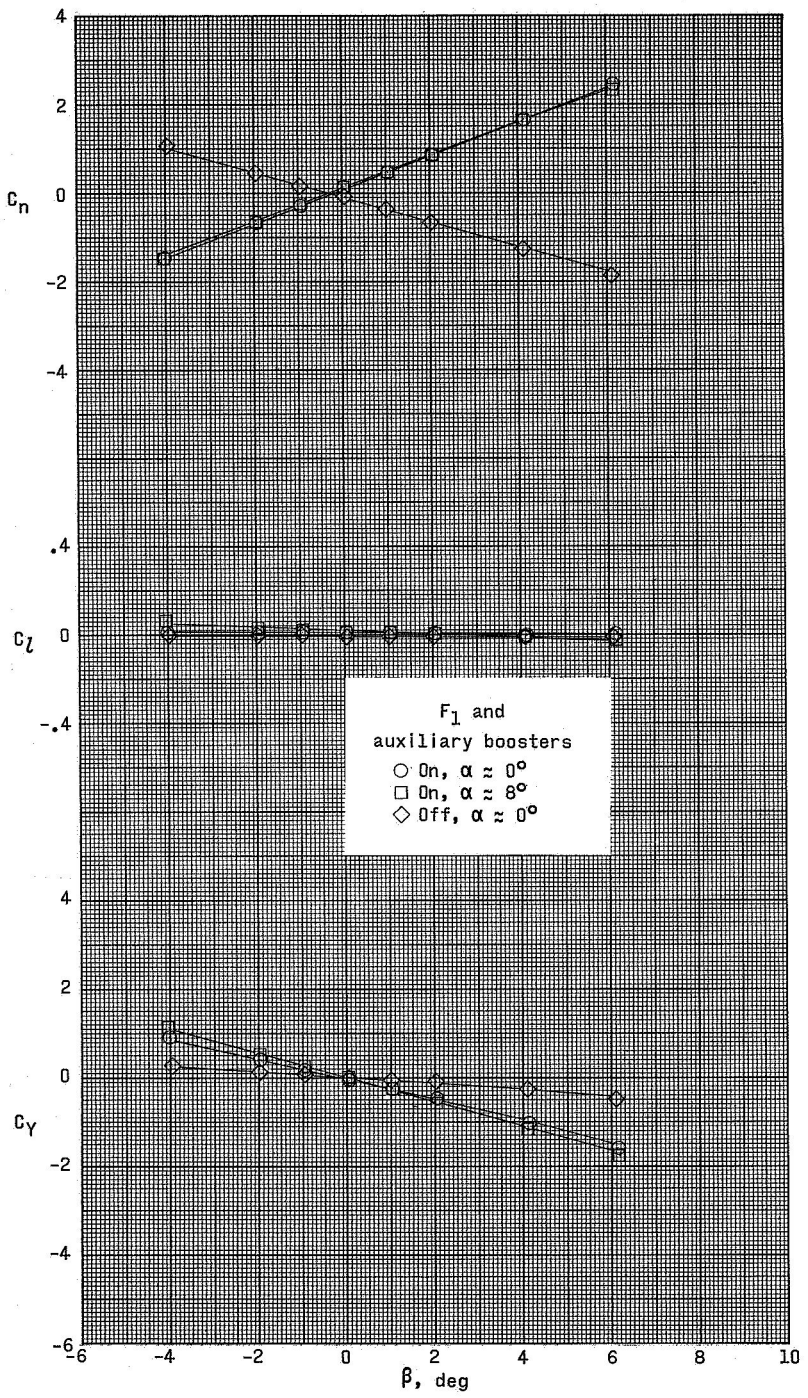

(b) M = 2.96.

Figure 11.- Continued.

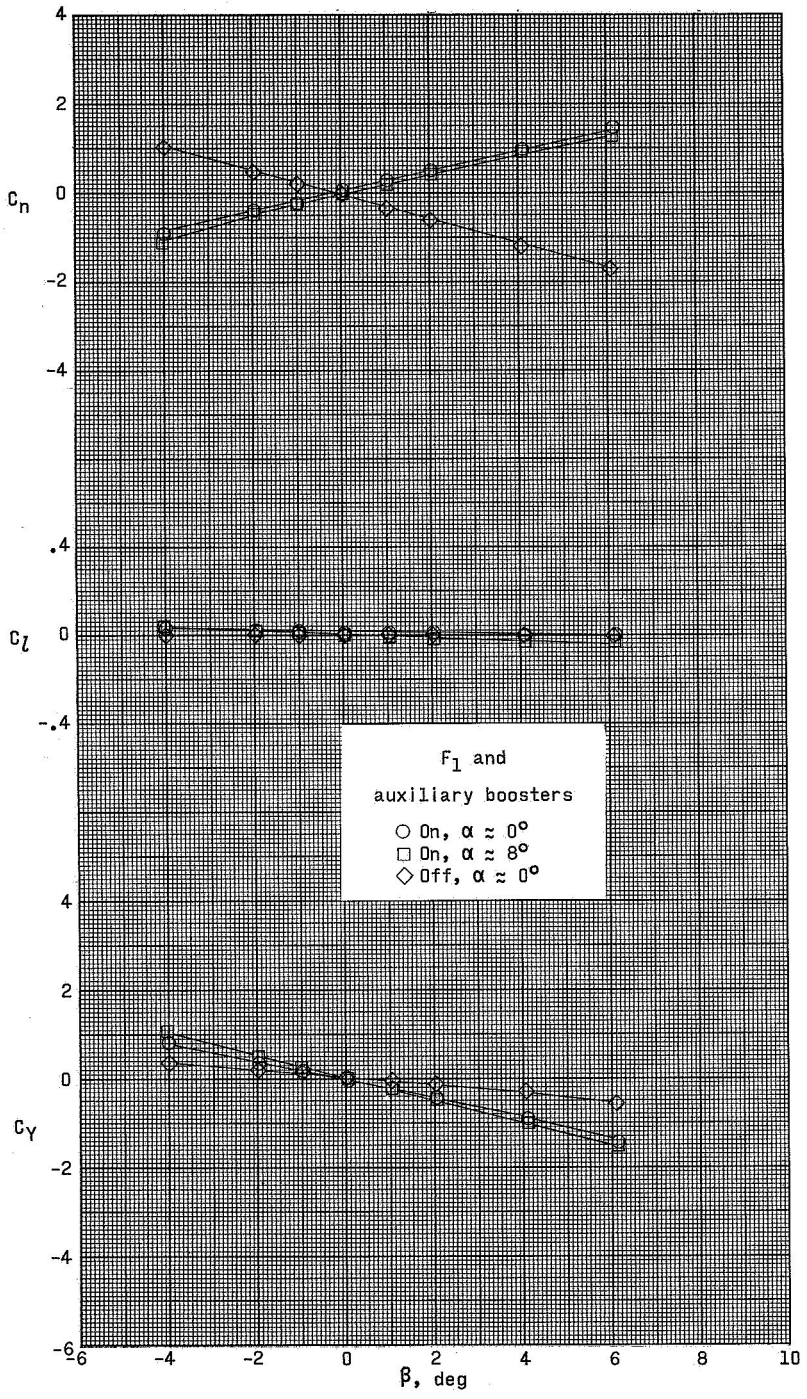

(c) M = 3.95.

Figure 11.- Continued.

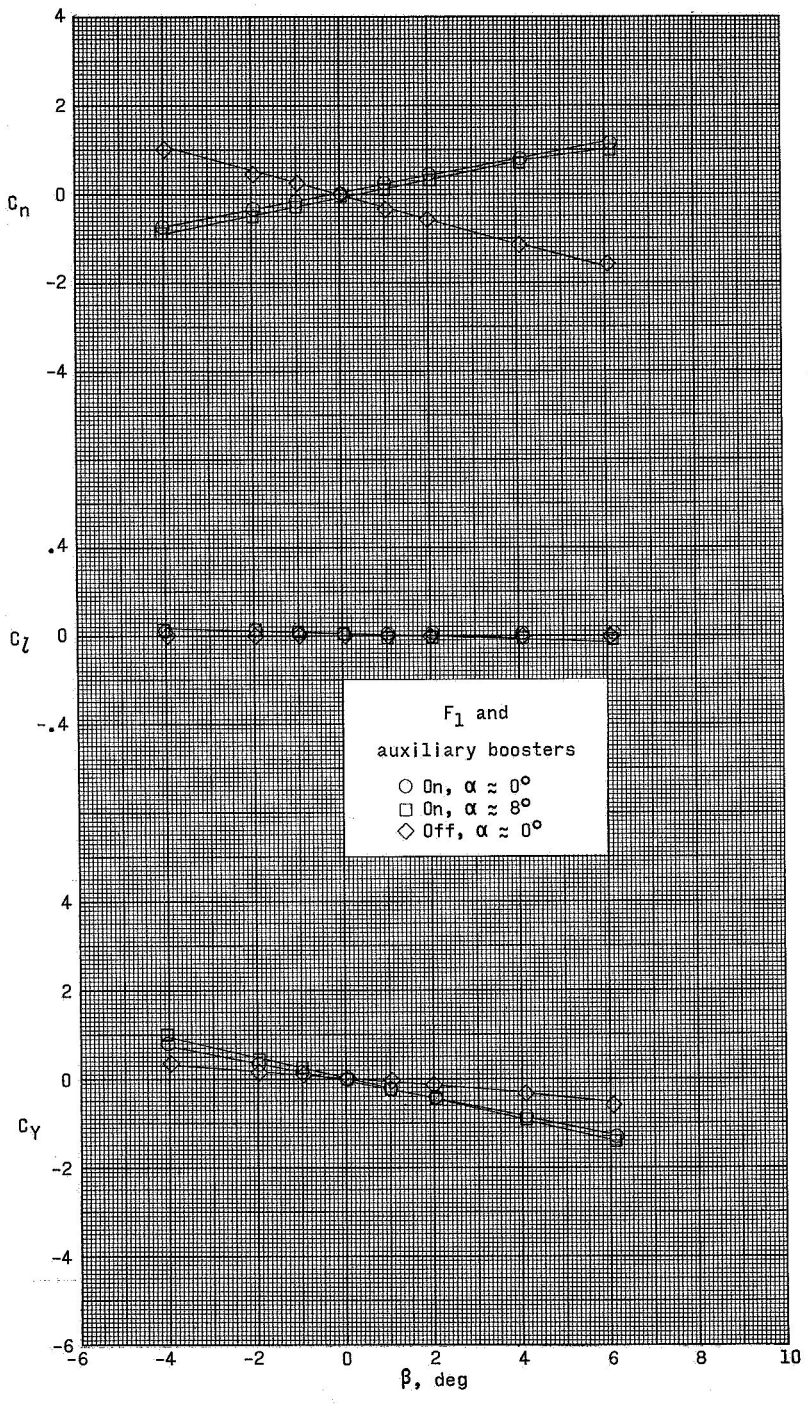

(d) M = 4.63.

Figure 11.- Concluded.

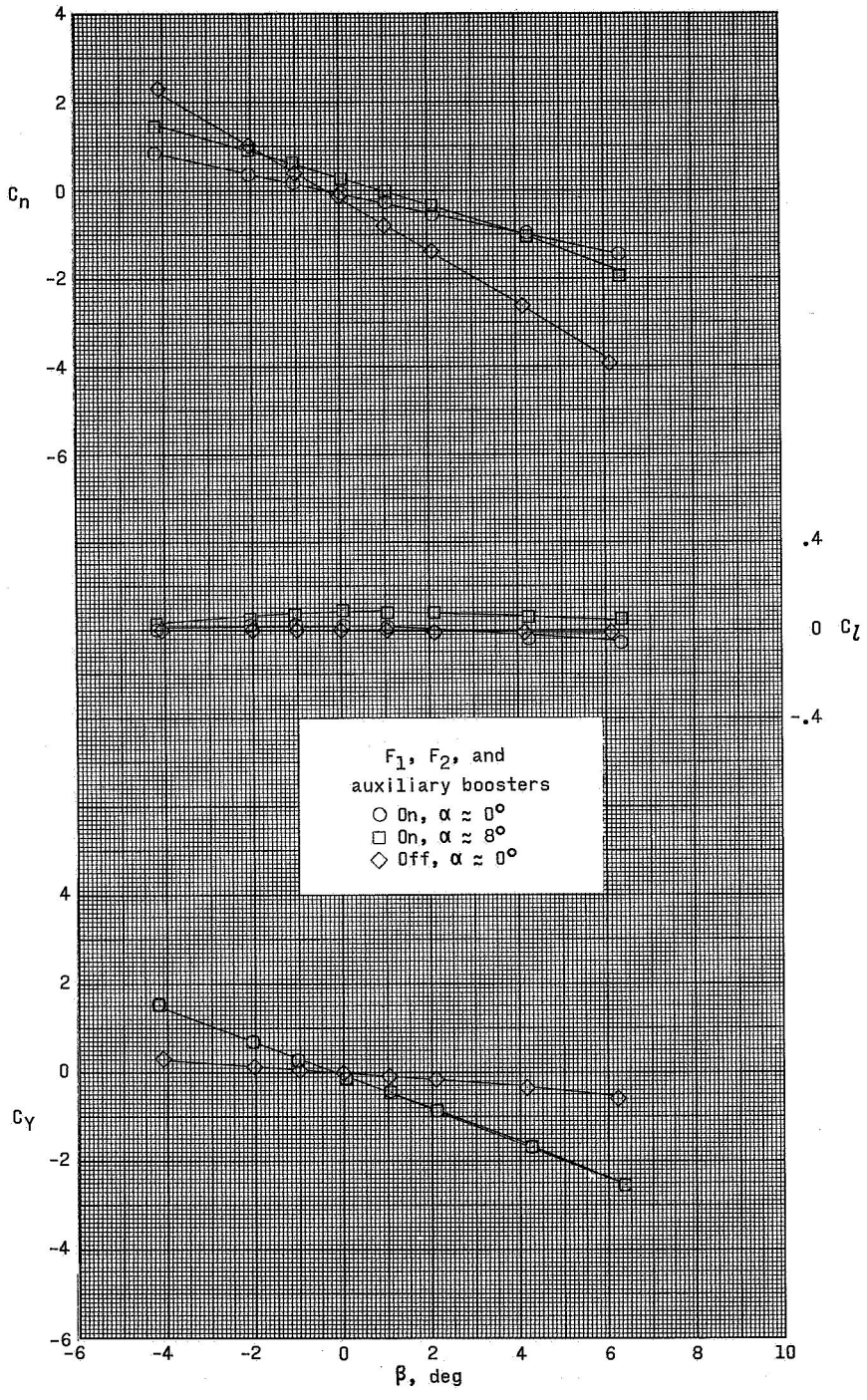

(a) M = 2.30.

Figure 12.- Lateral aerodynamic characteristics of model 3.

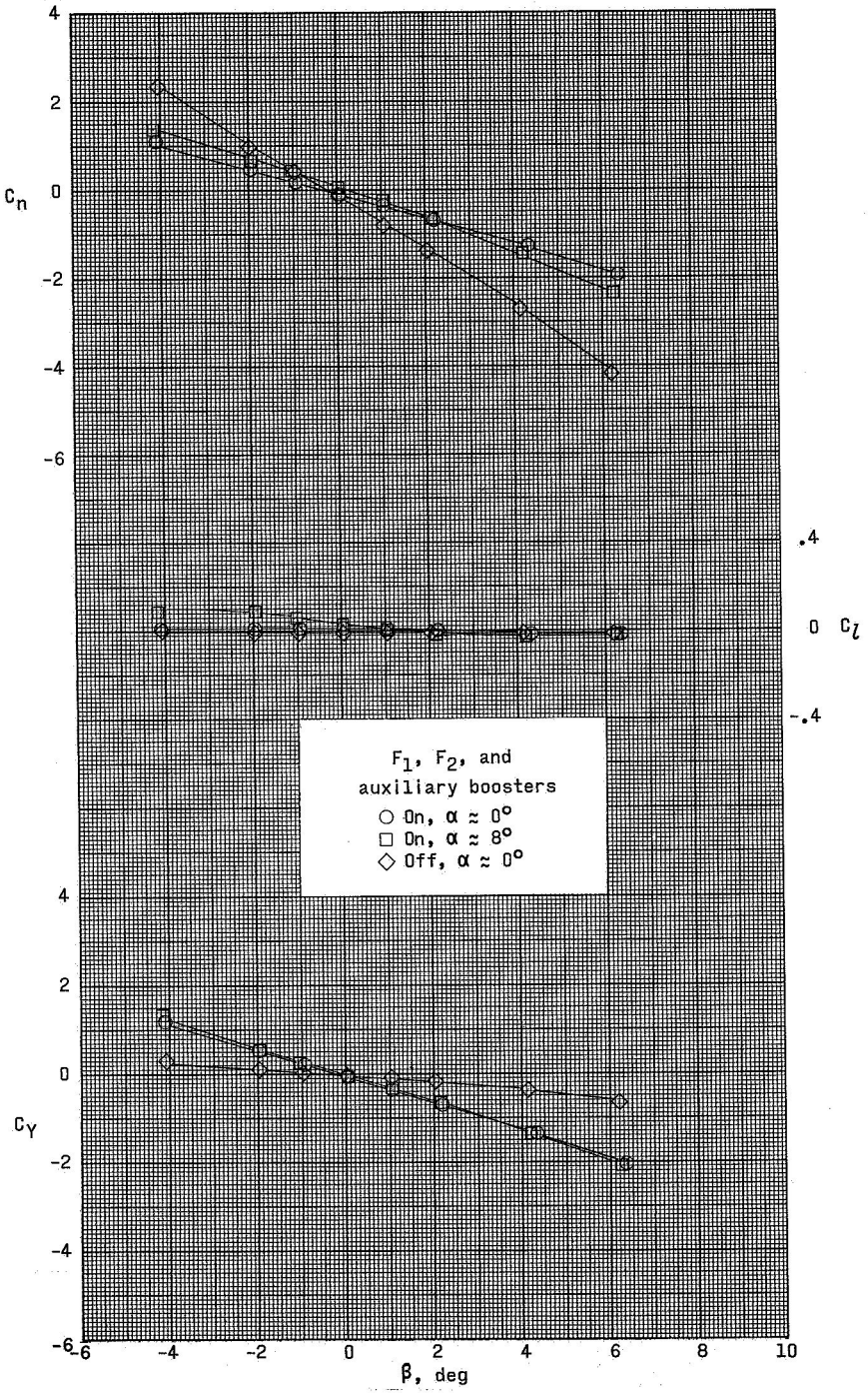

(b) M = 2.96.

Figure 12.- Continued.

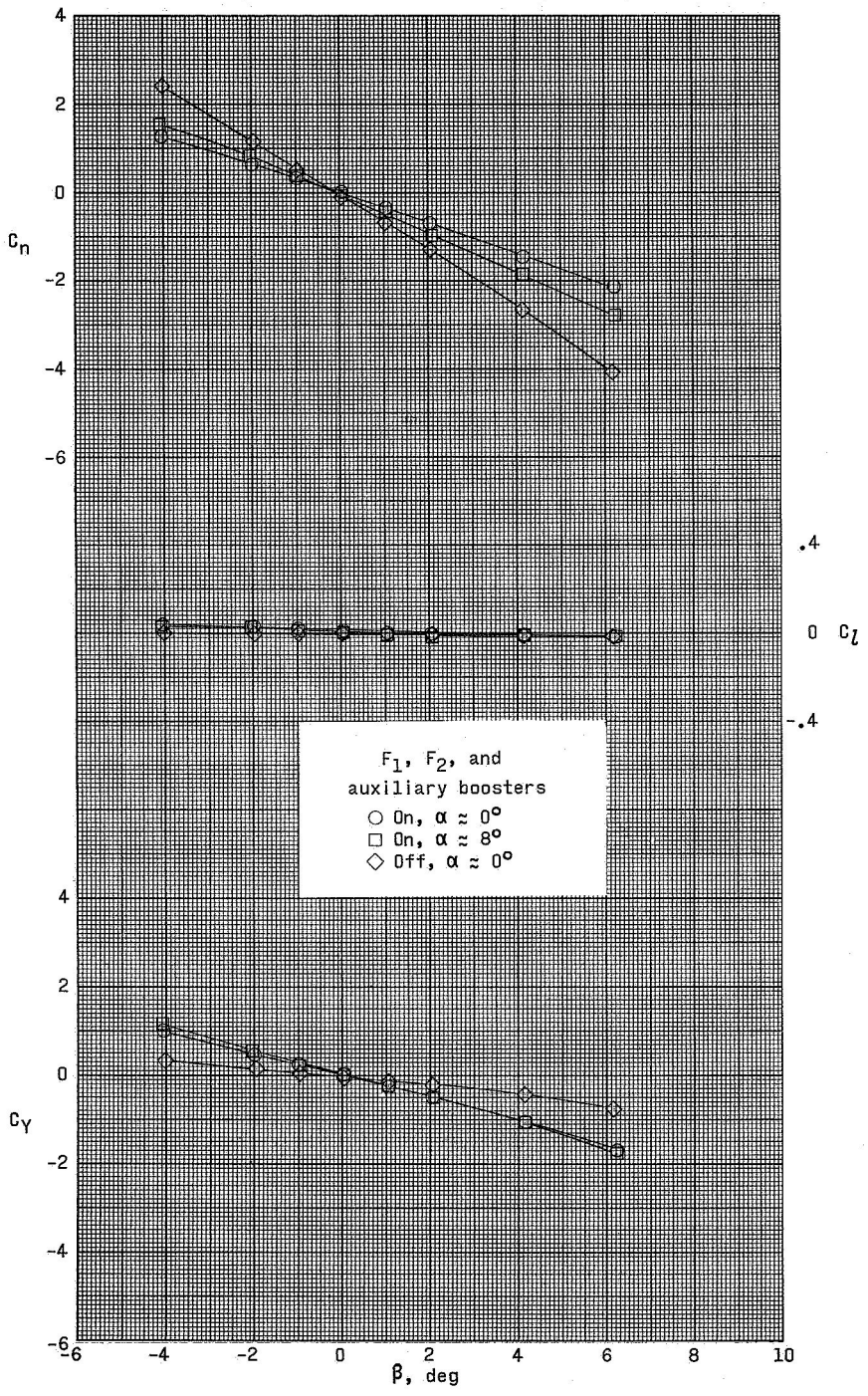

(c) M = 3.95.

Figure 12.- Continued.

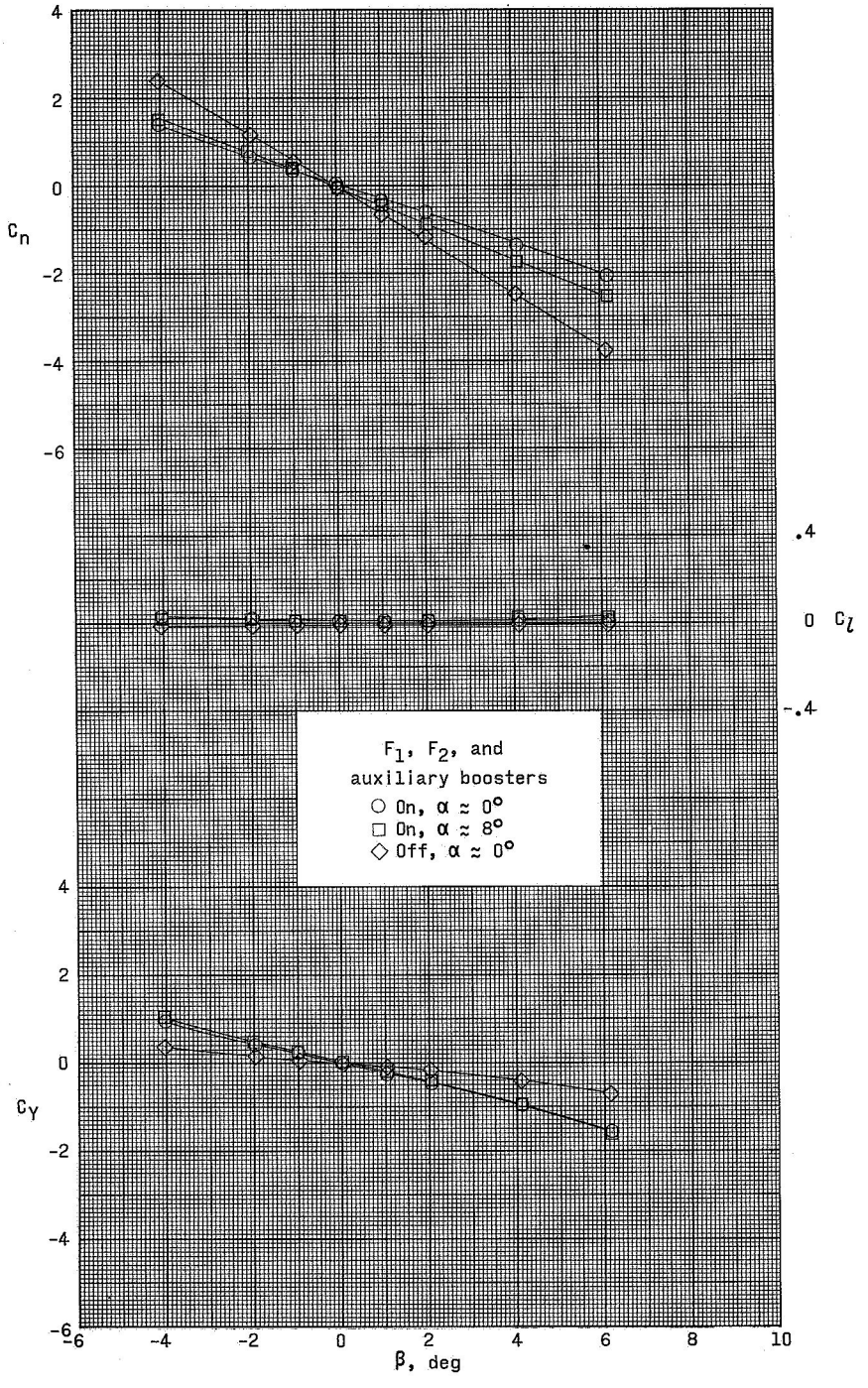

(d) M = 4.63.

Figure 12.- Concluded.

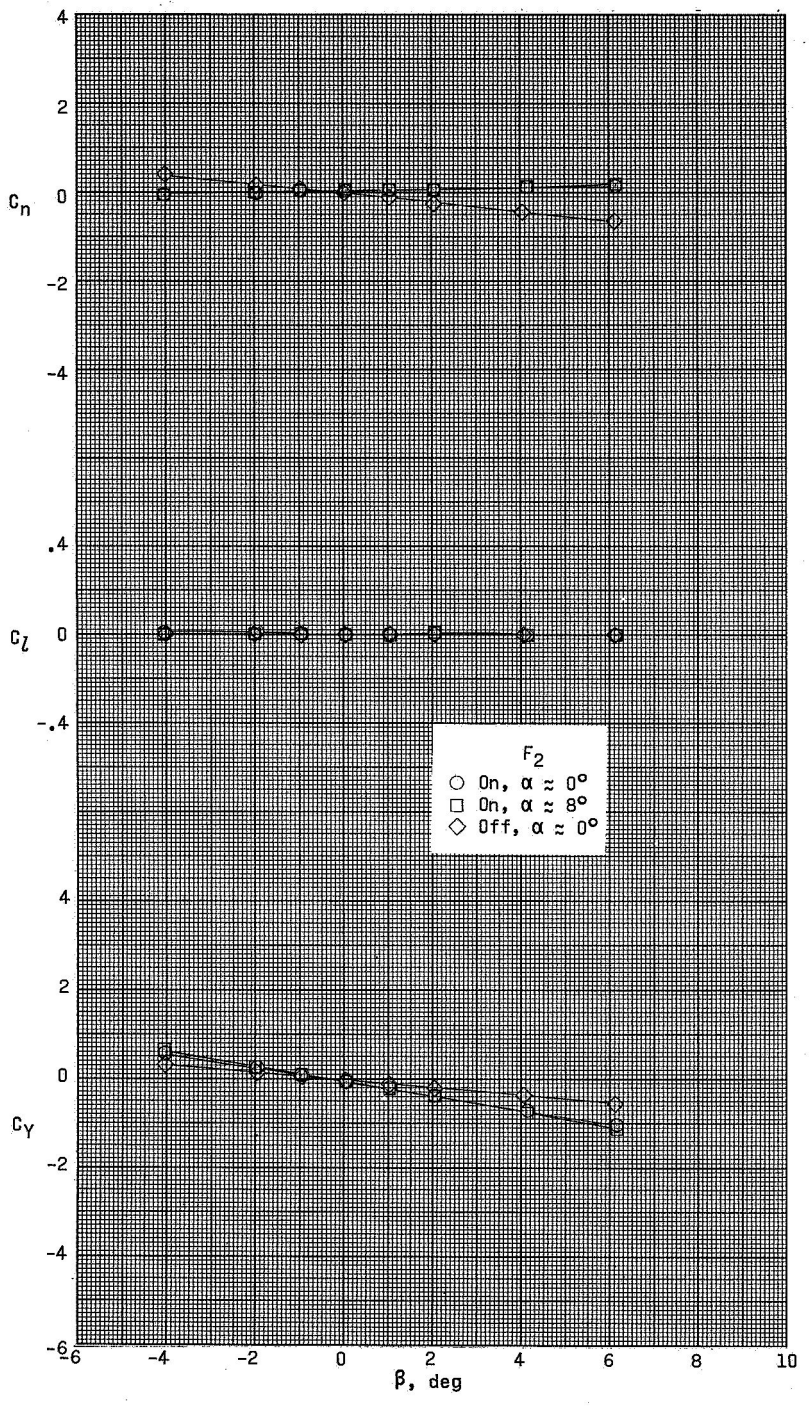

(a) M = 2.30.

Figure 13.- Lateral aerodynamic characteristics of model 4.

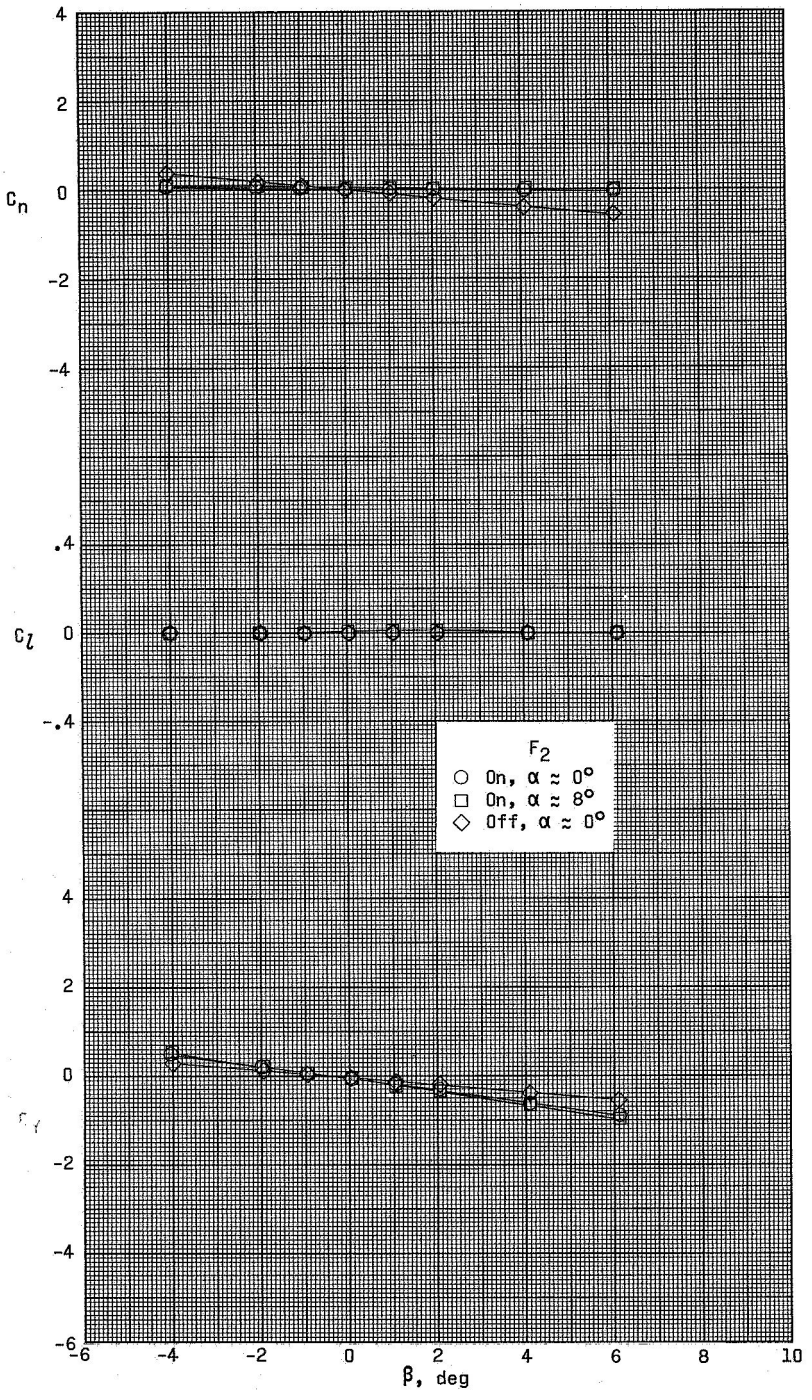

(b) M = 2.96.

Figure 13.- Continued.

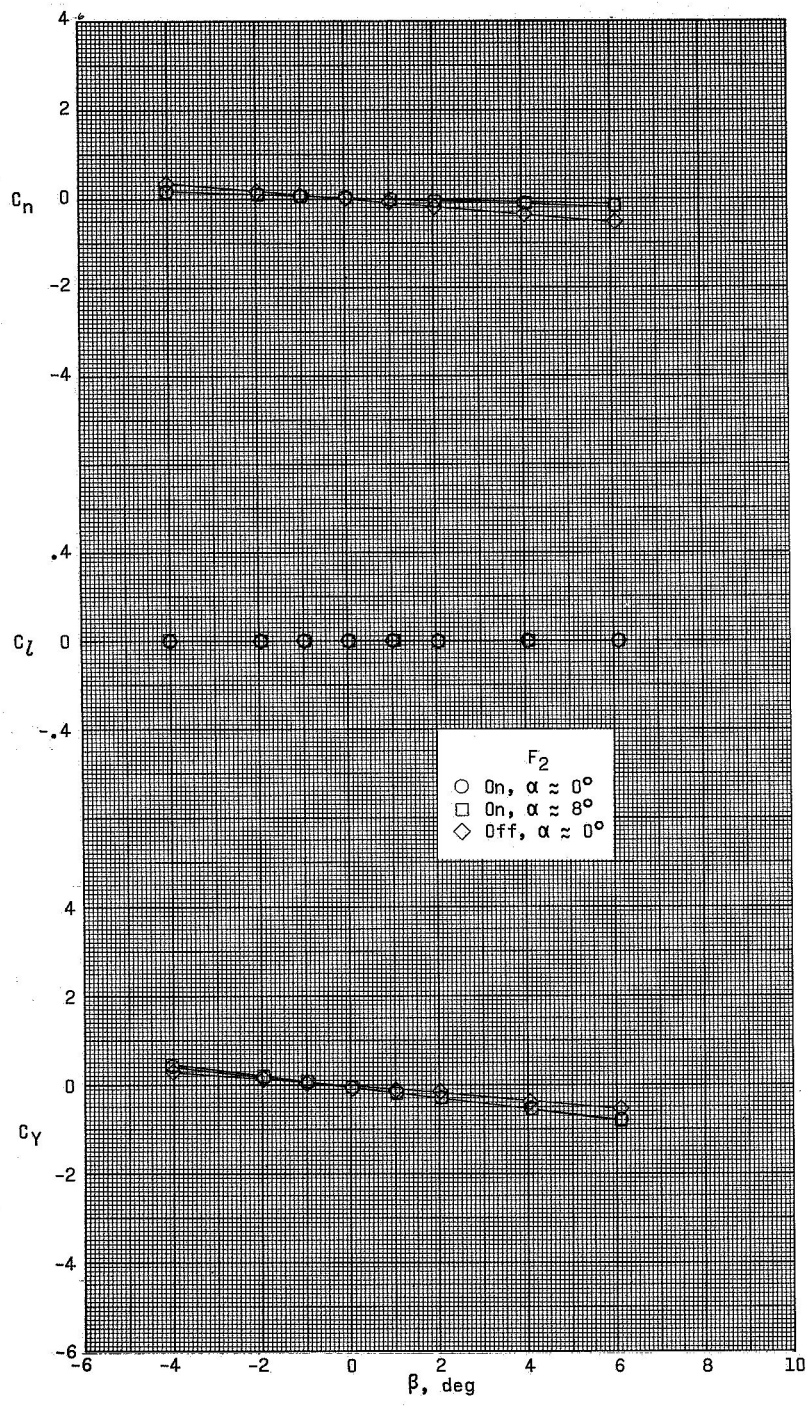

(c) M = 3.95.

Figure 13.- Continued.

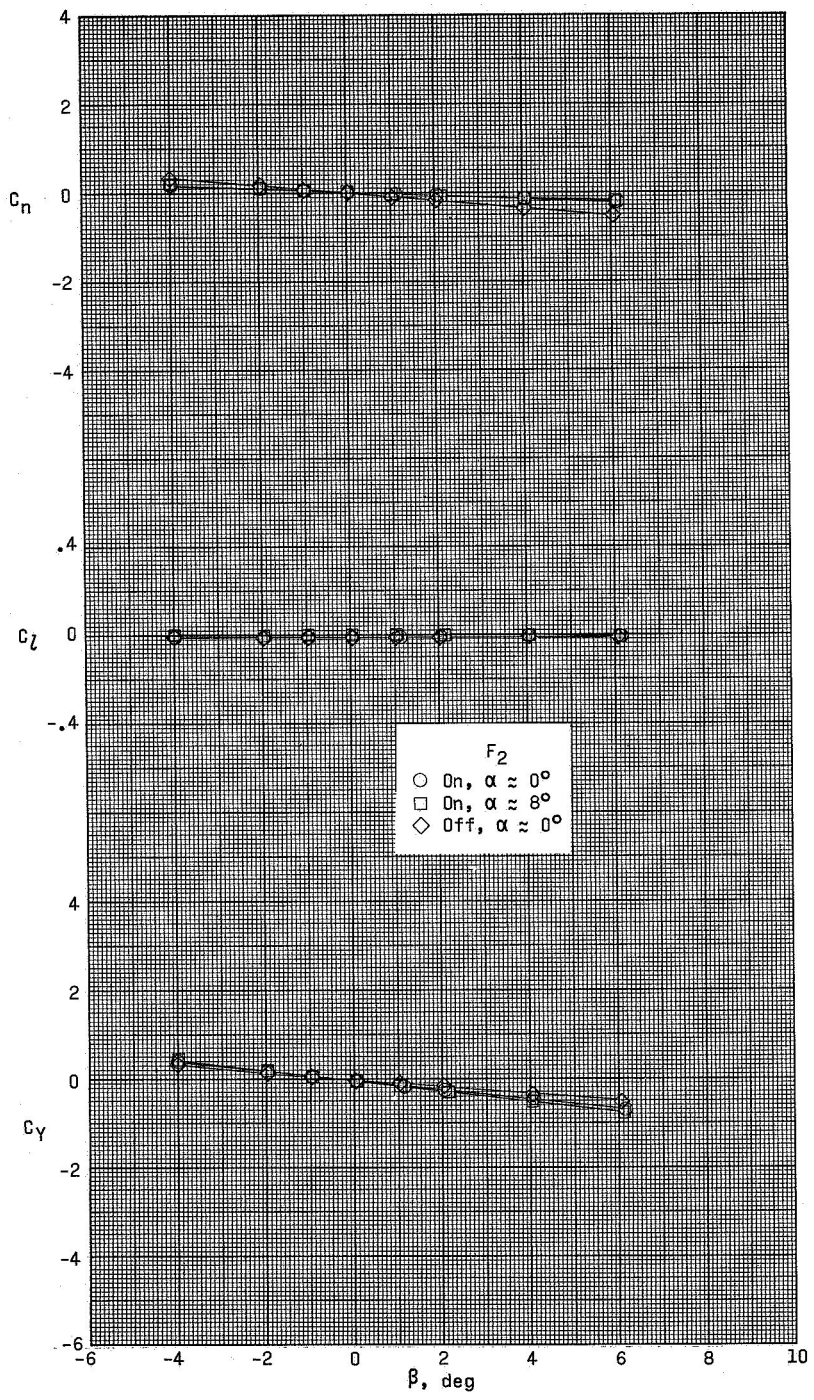

(d) M = 4.63.

Figure 13.- Concluded.

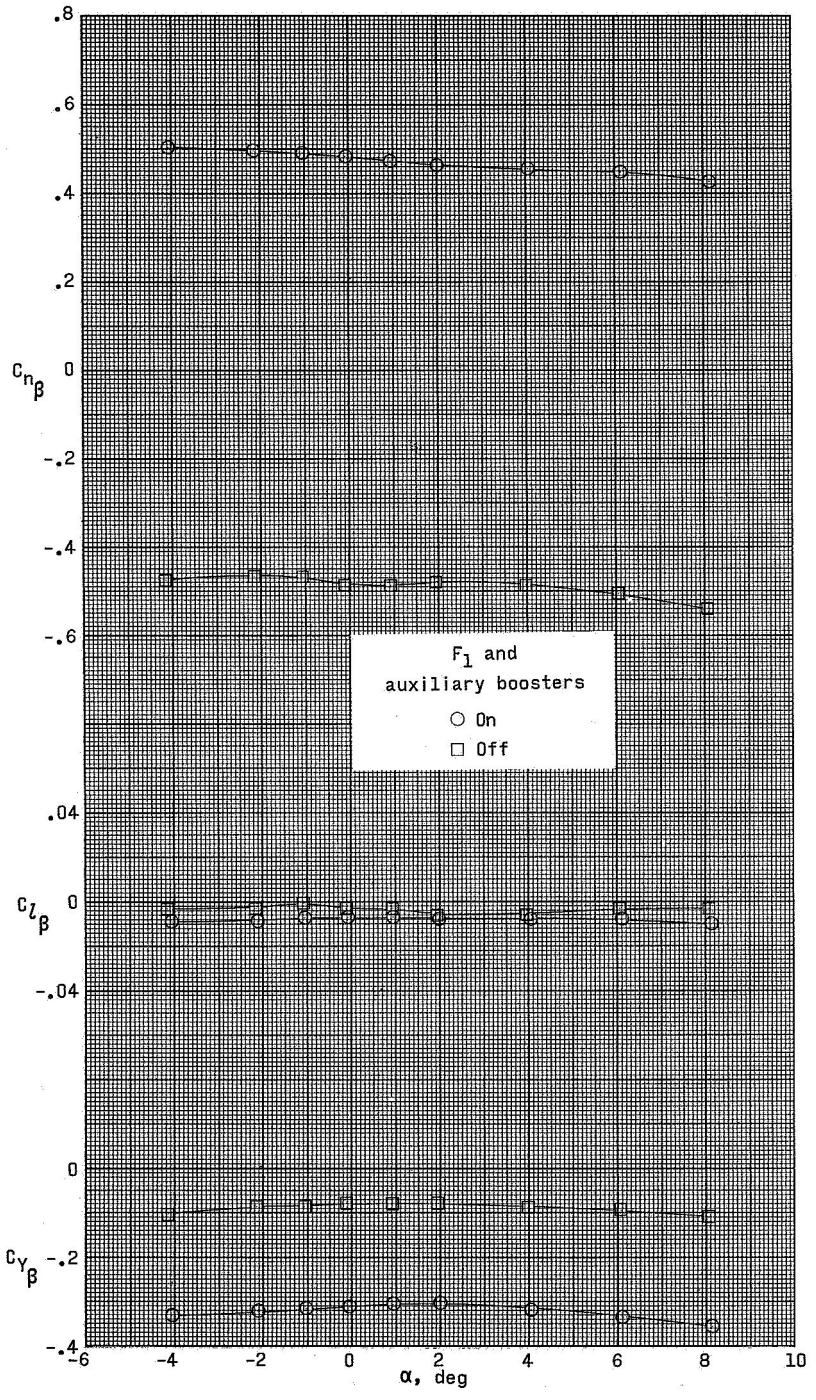

(a) M = 2.30.

Figure 14.- Variation of sideslip derivatives with angle of attack for model 1.

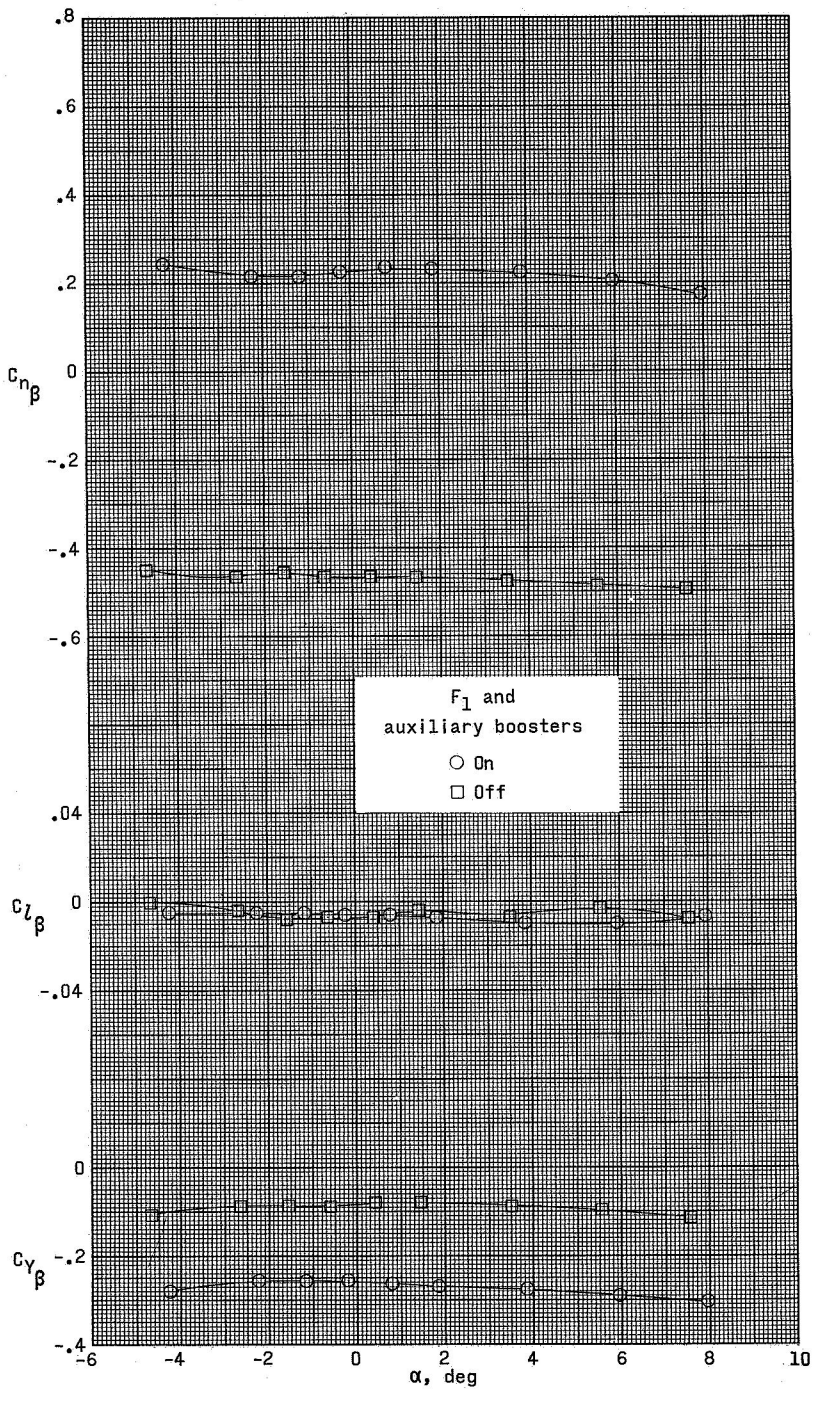

(b) M = 2.96.

Figure 14.- Continued.

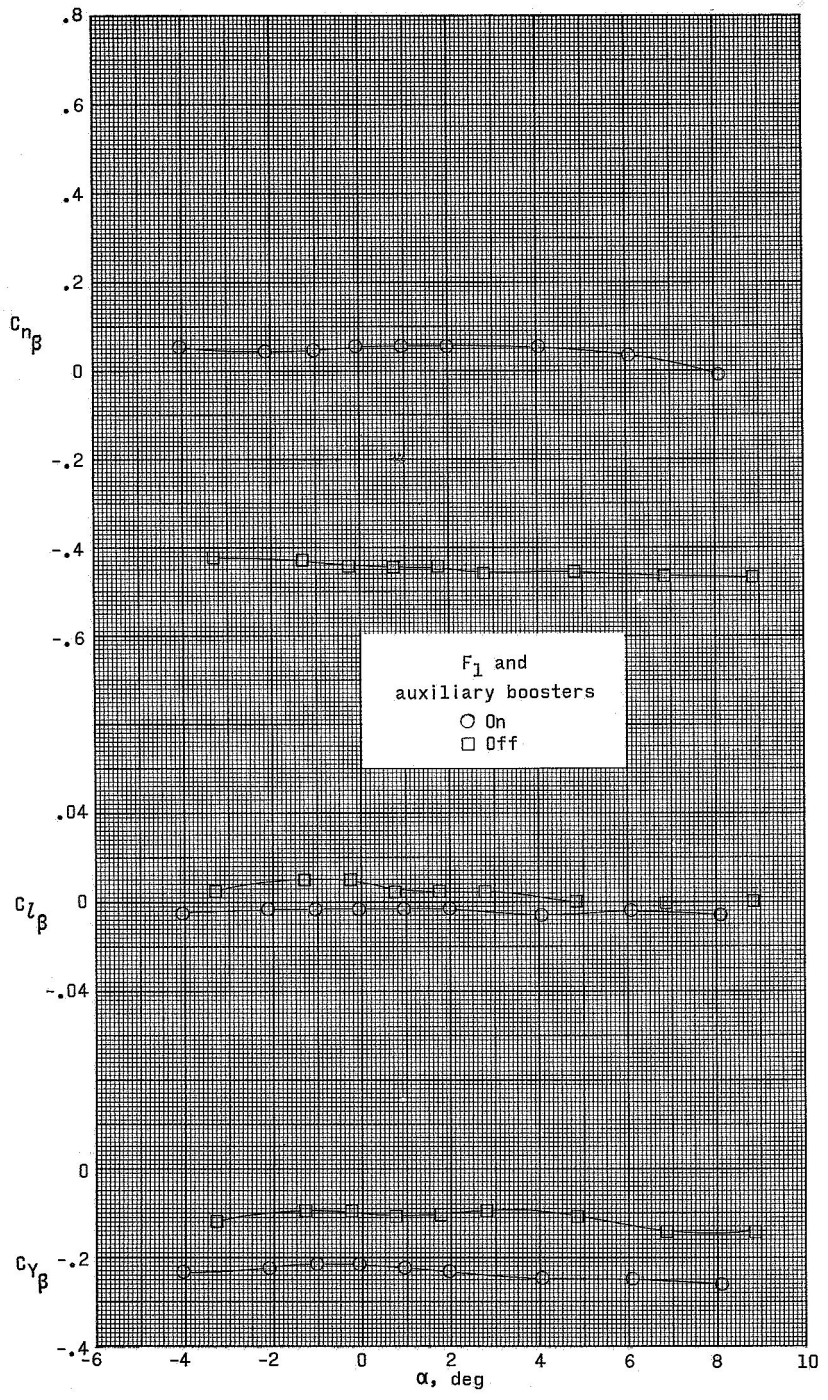

(c) M = 3.95.

Figure 14.- Continued.

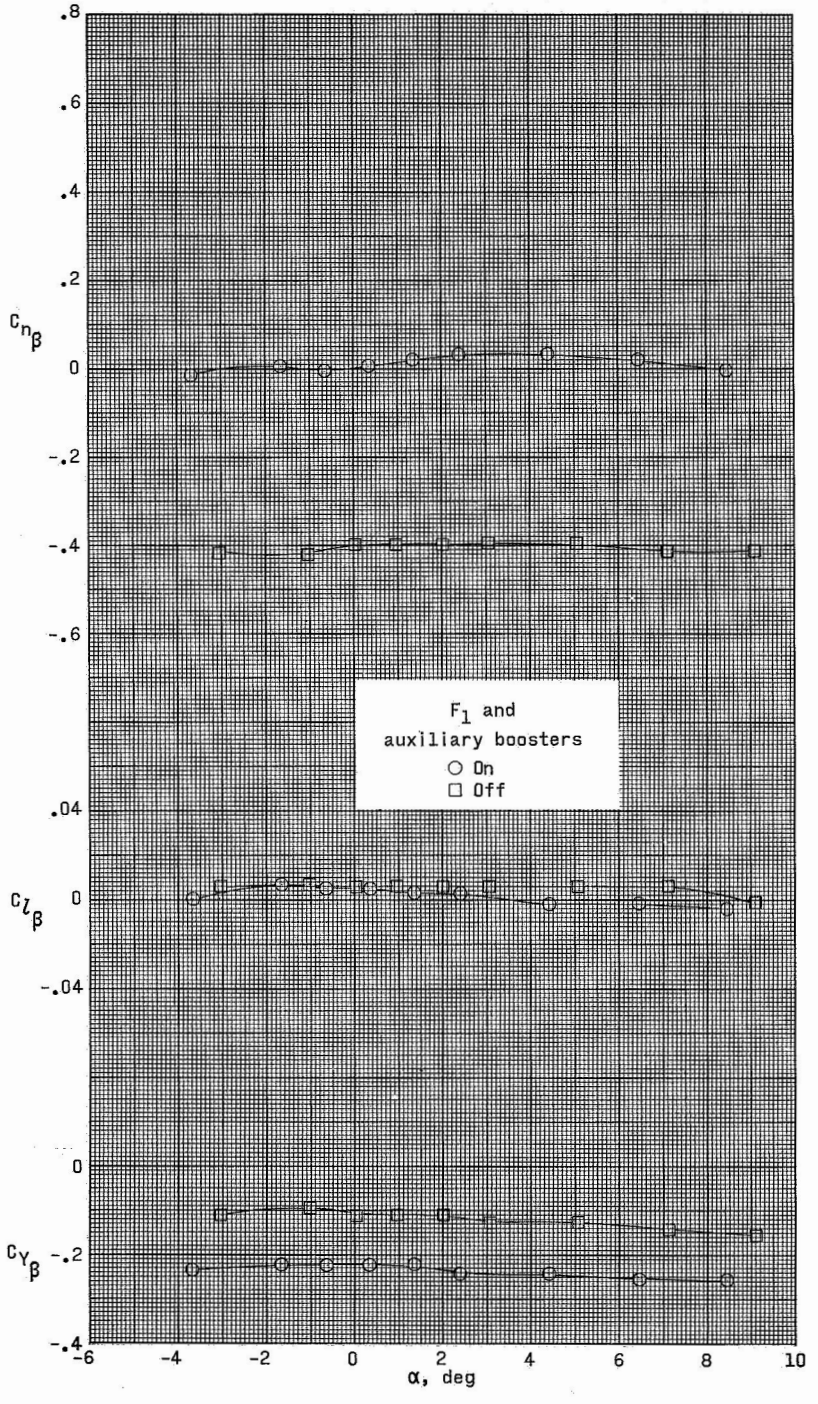

(d) M = 4.63.

Figure 14.- Concluded.

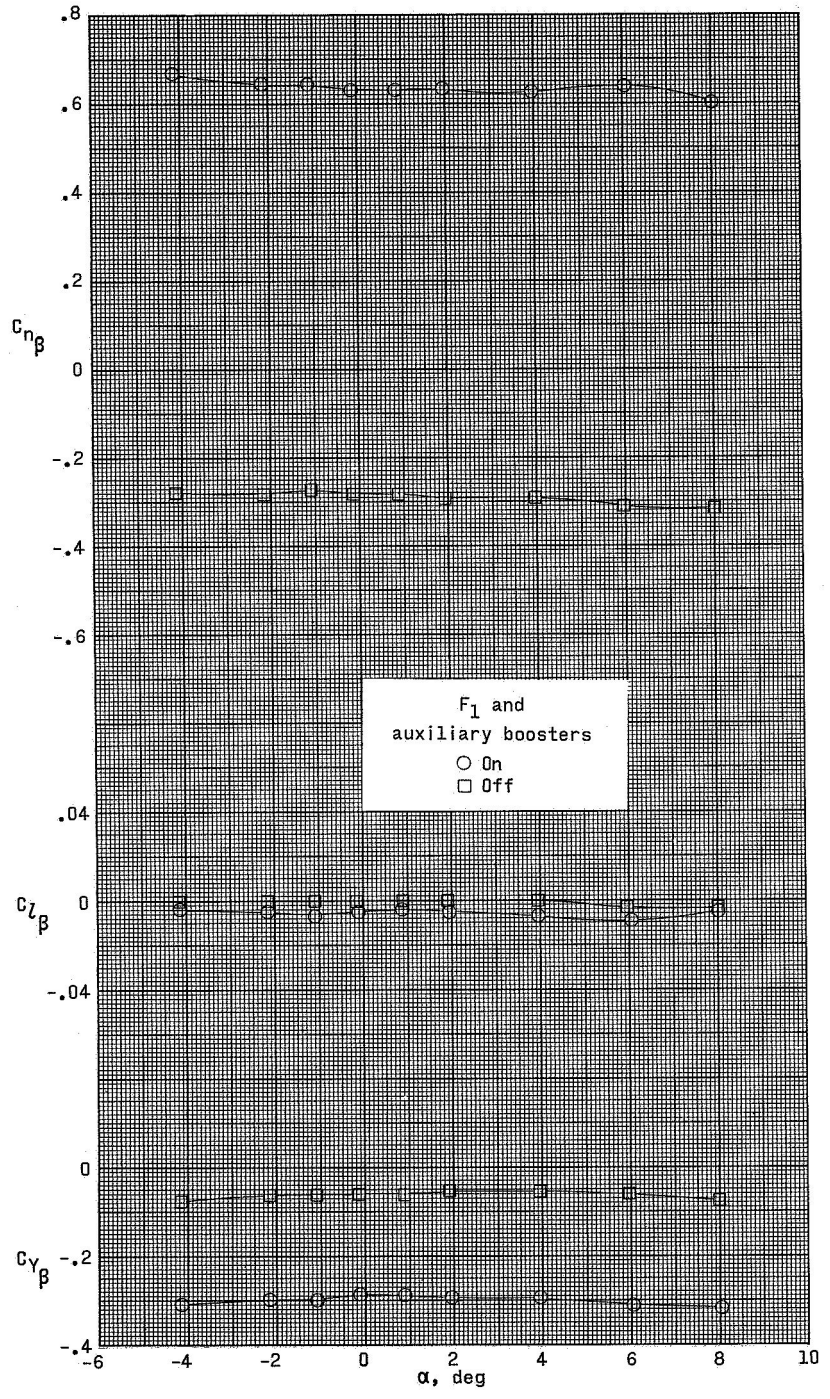

(a) M = 2.30.

Figure 15.- Variation of sideslip derivatives with angle of attack for model 2.

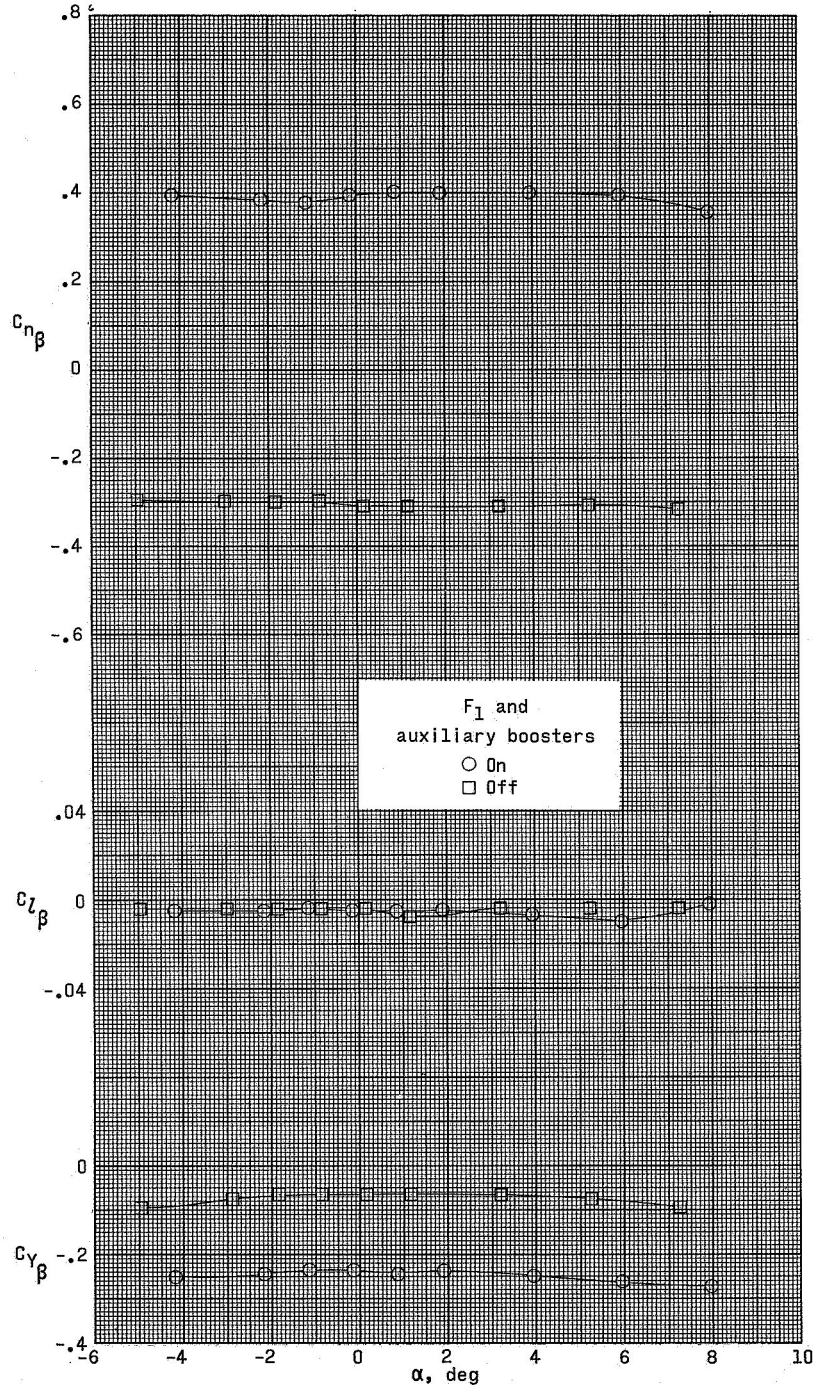

(b) M = 2.96.

Figure 15.- Continued.

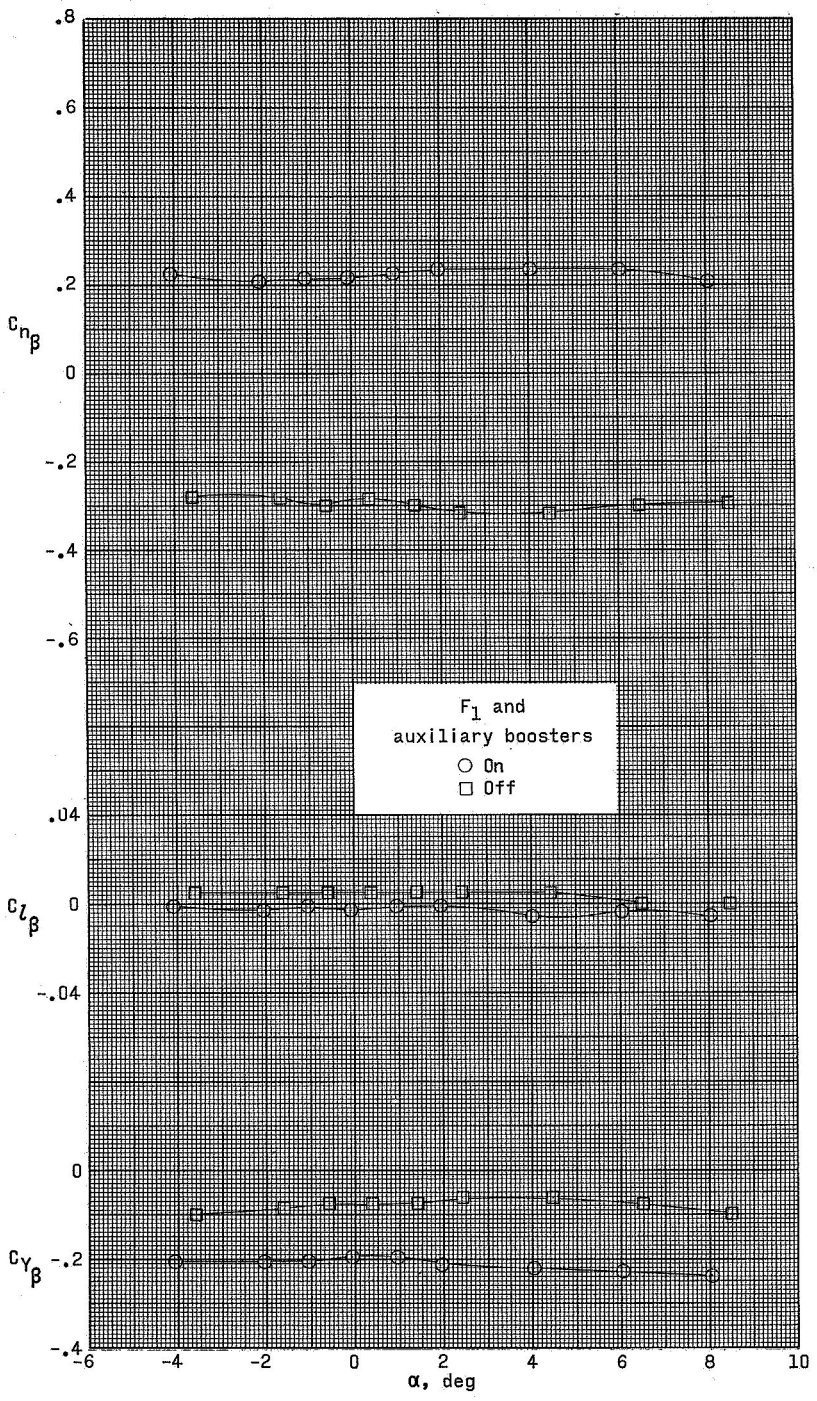

(c) M = 3.95.

Figure 15.- Continued.

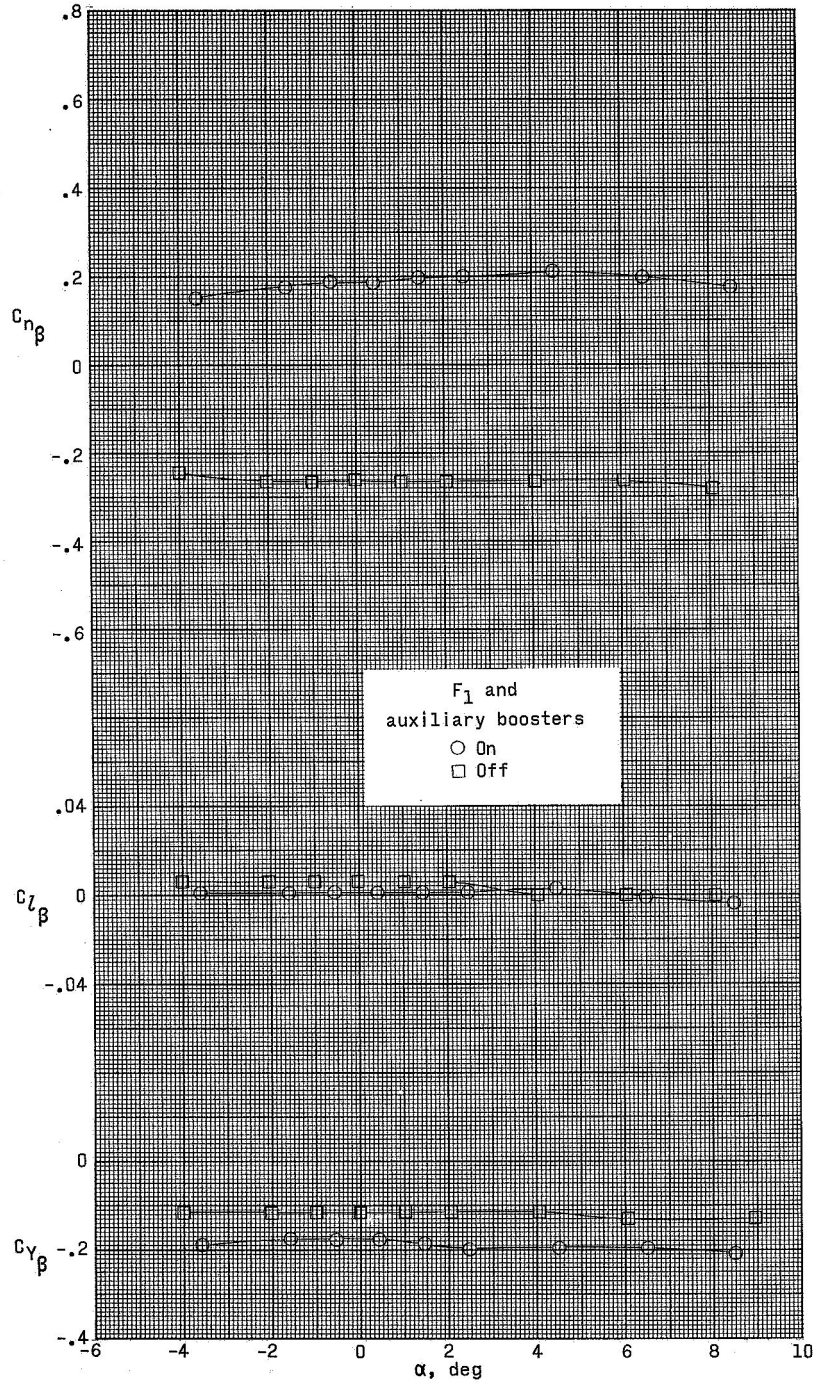

(d) M = 4.63.

Figure 15.- Concluded.

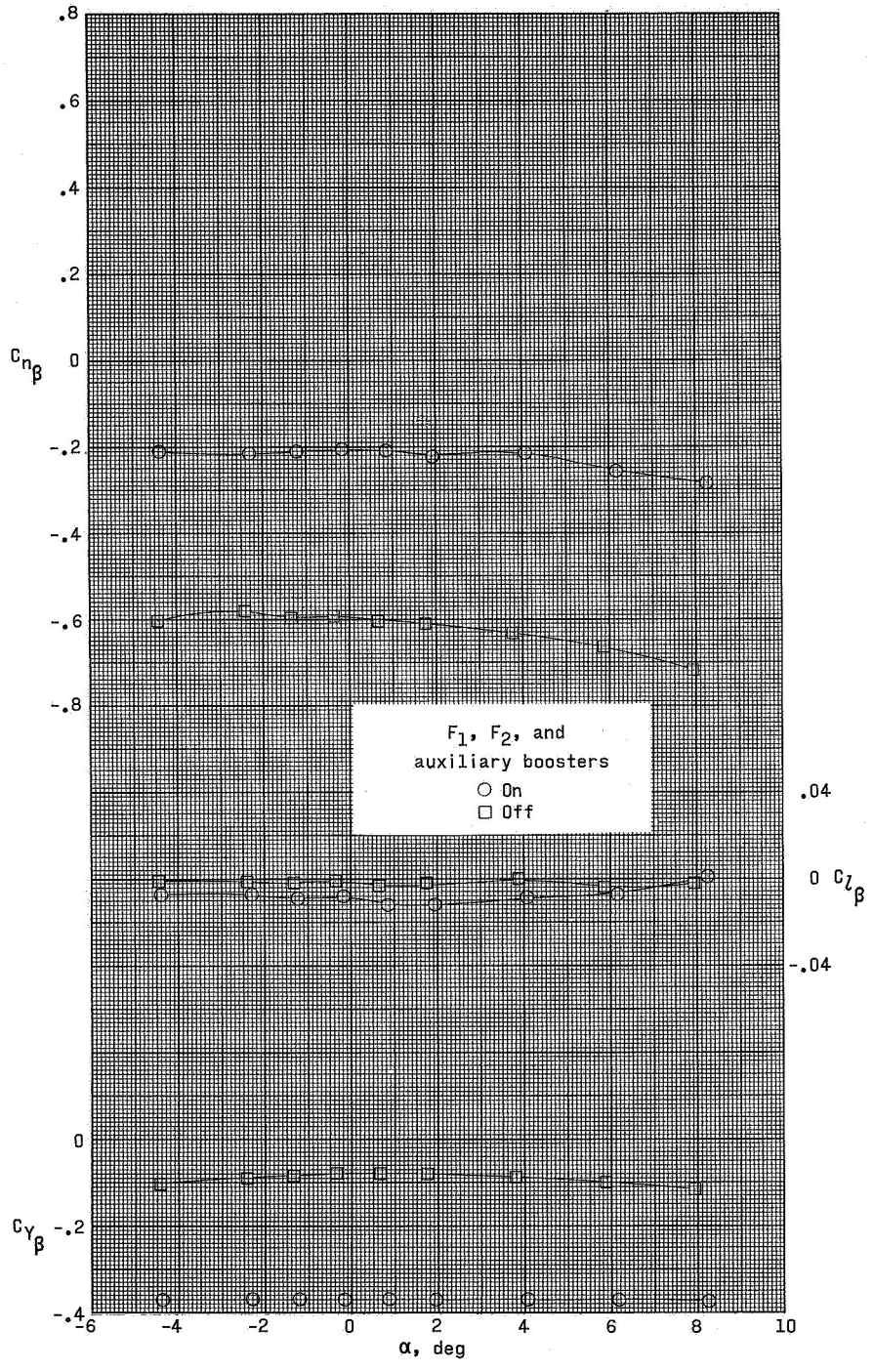

(a) M = 2.30.

Figure 16.- Variation of sideslip derivatives with angle of attack for model 3.

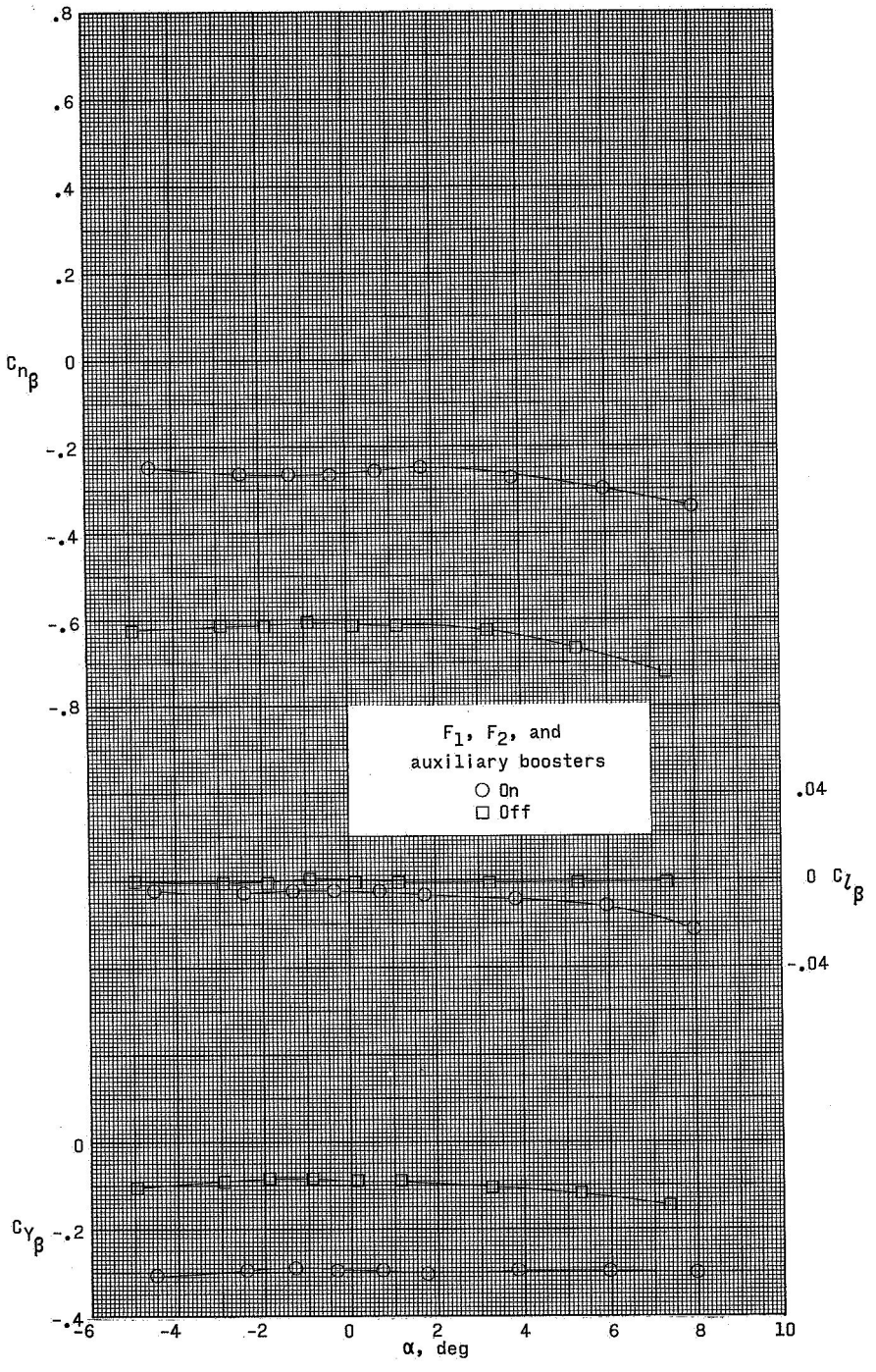

(b) M = 2.96.

Figure 16.- Continued.

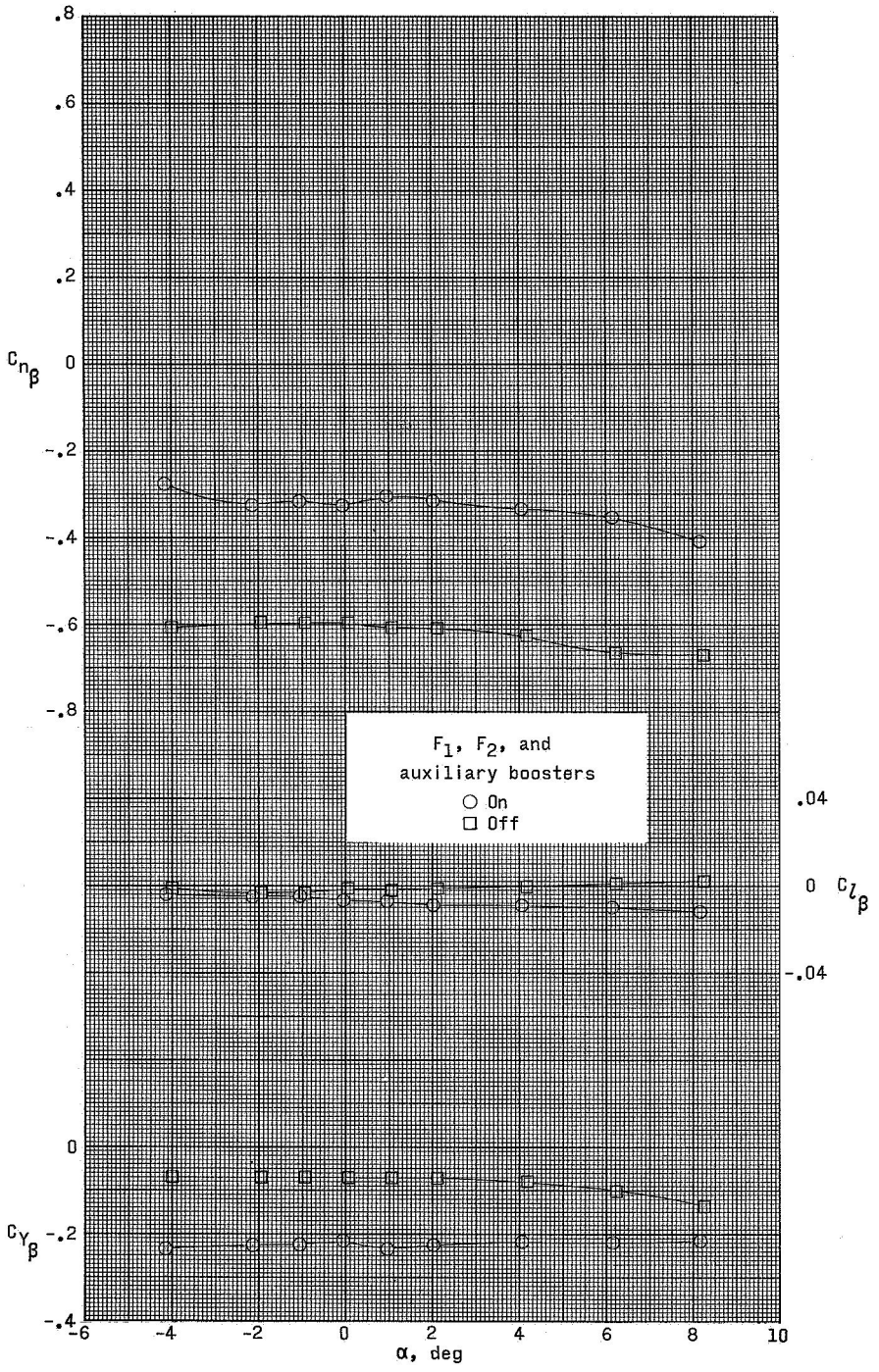

(c) M = 3.95.

Figure 16.- Continued.

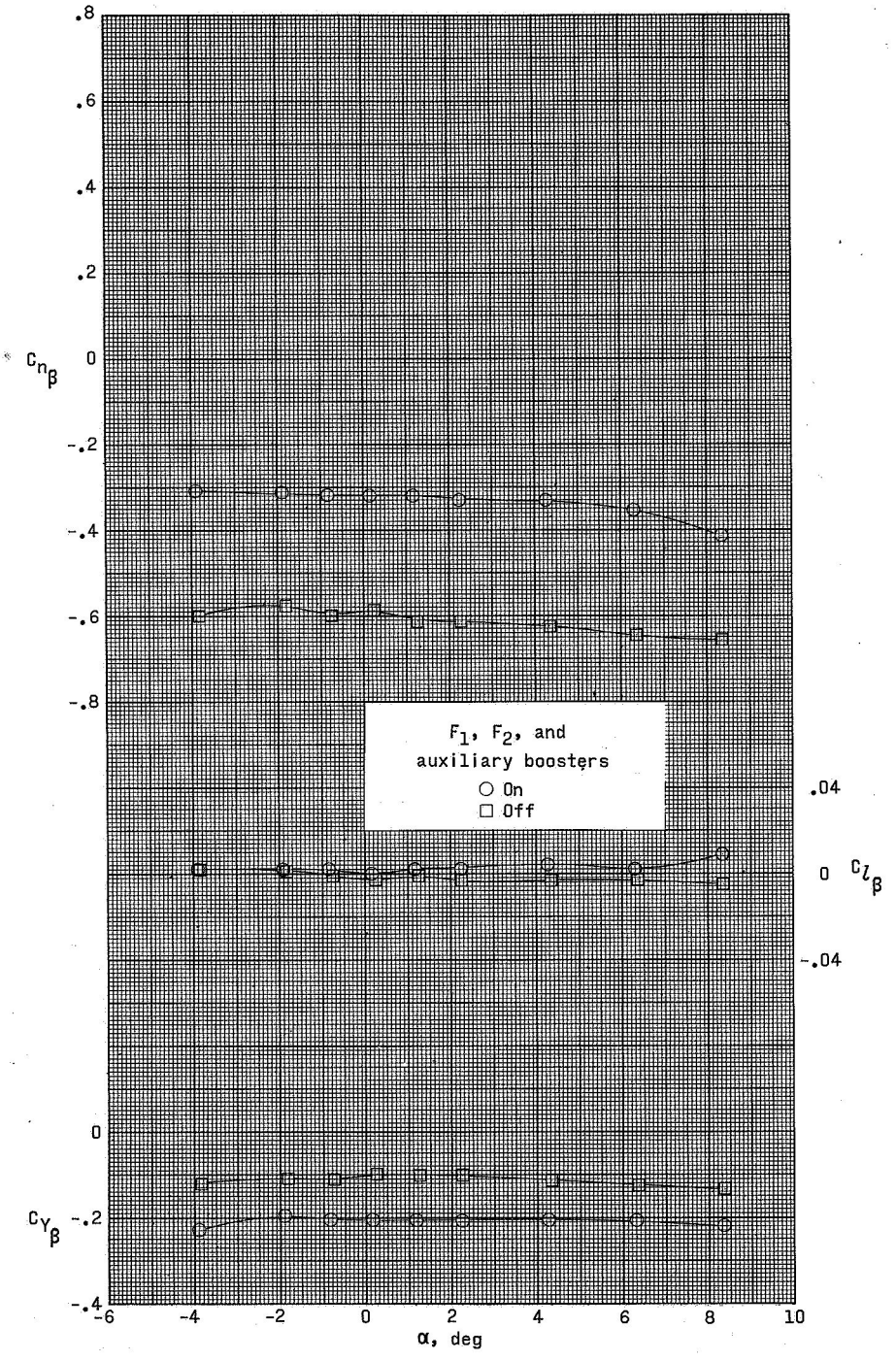

(d) M = 4.63.

Figure 16.- Concluded.

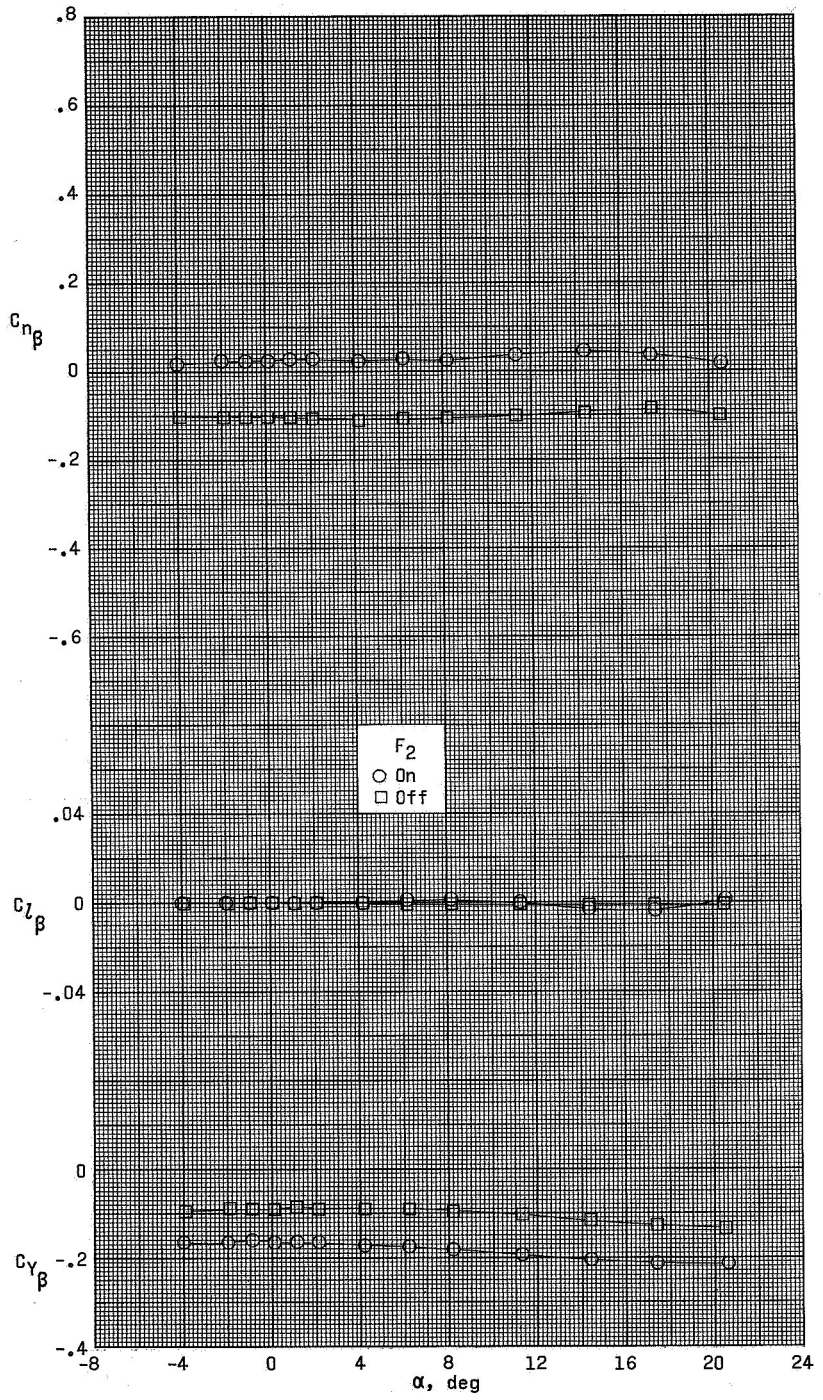

(a) M = 2.30.

Figure 17.- Variation of sideslip derivatives with angle of attack for model 4.

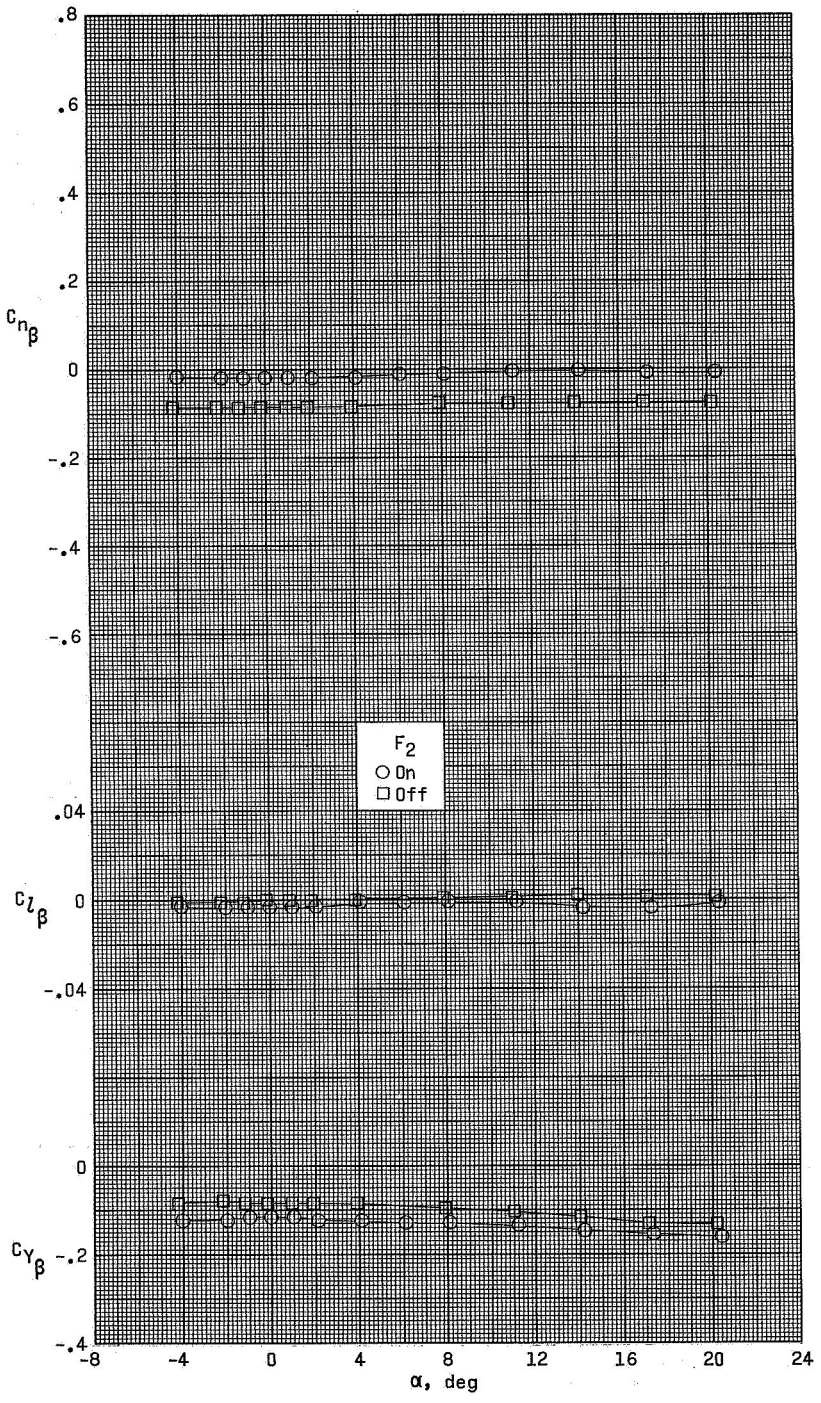

(b) M = 2.96.

Figure 17.- Continued.

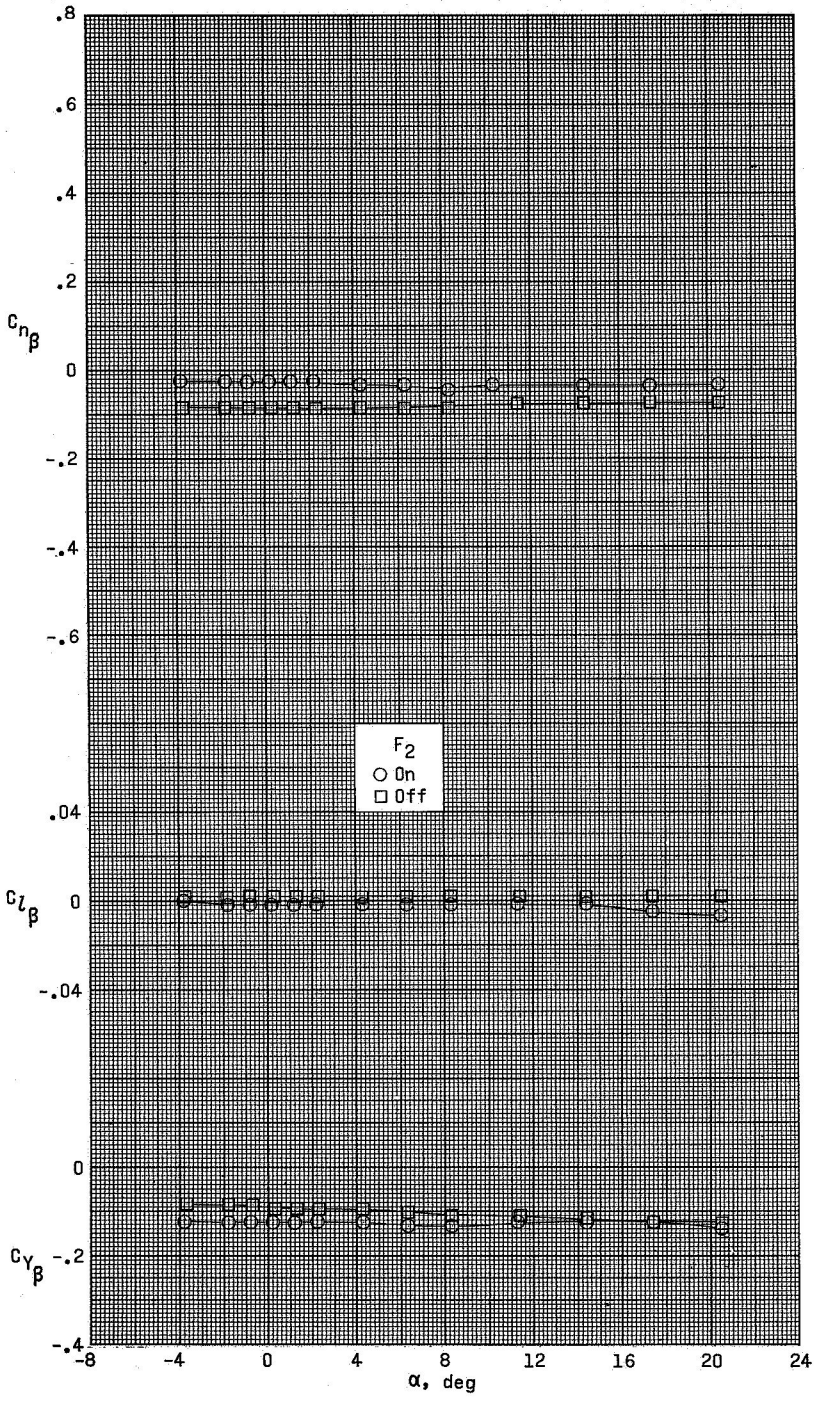

(c) M = 3.95.

Figure 17.- Continued.

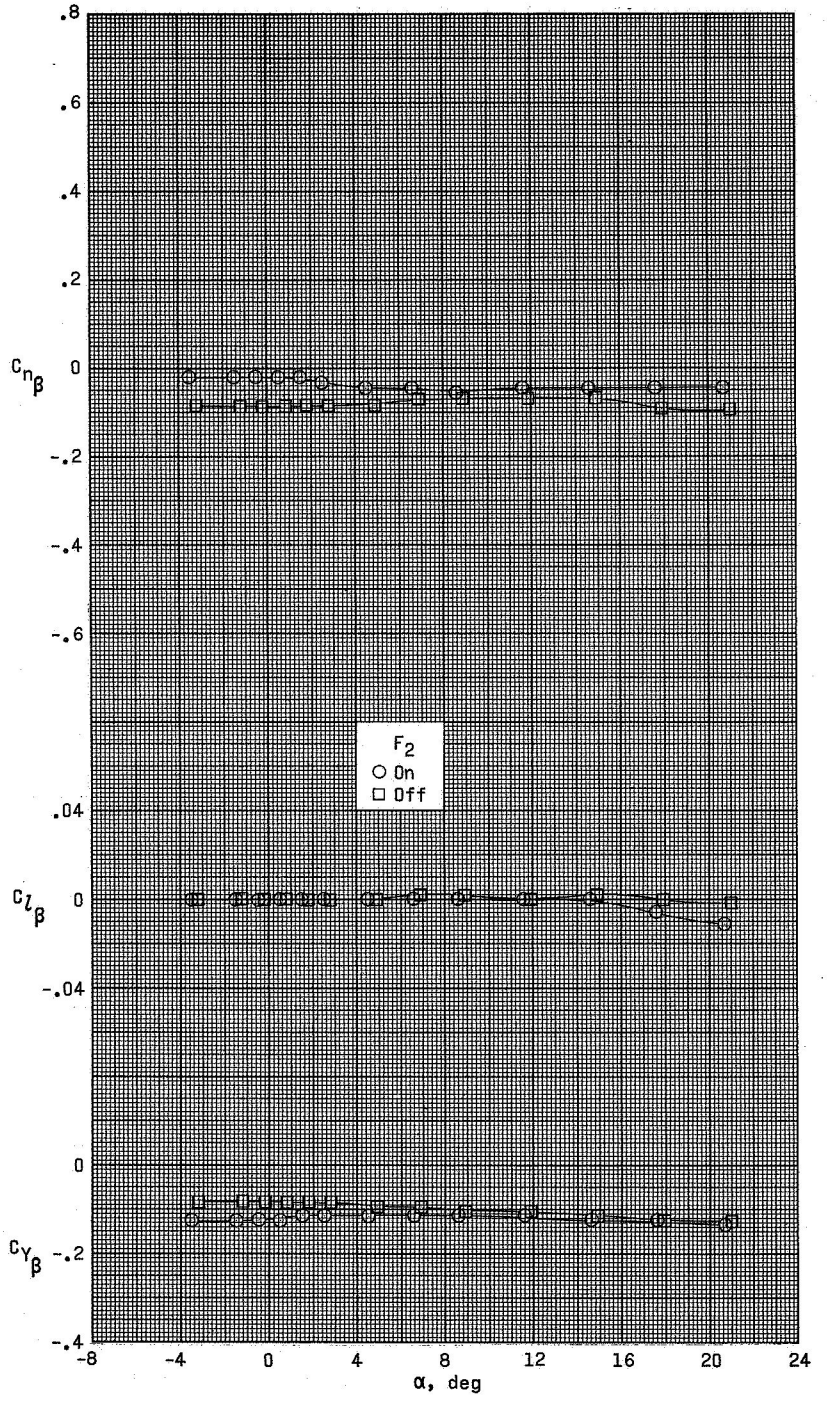

(d) M = 4.63.

Figure 17.- Concluded.

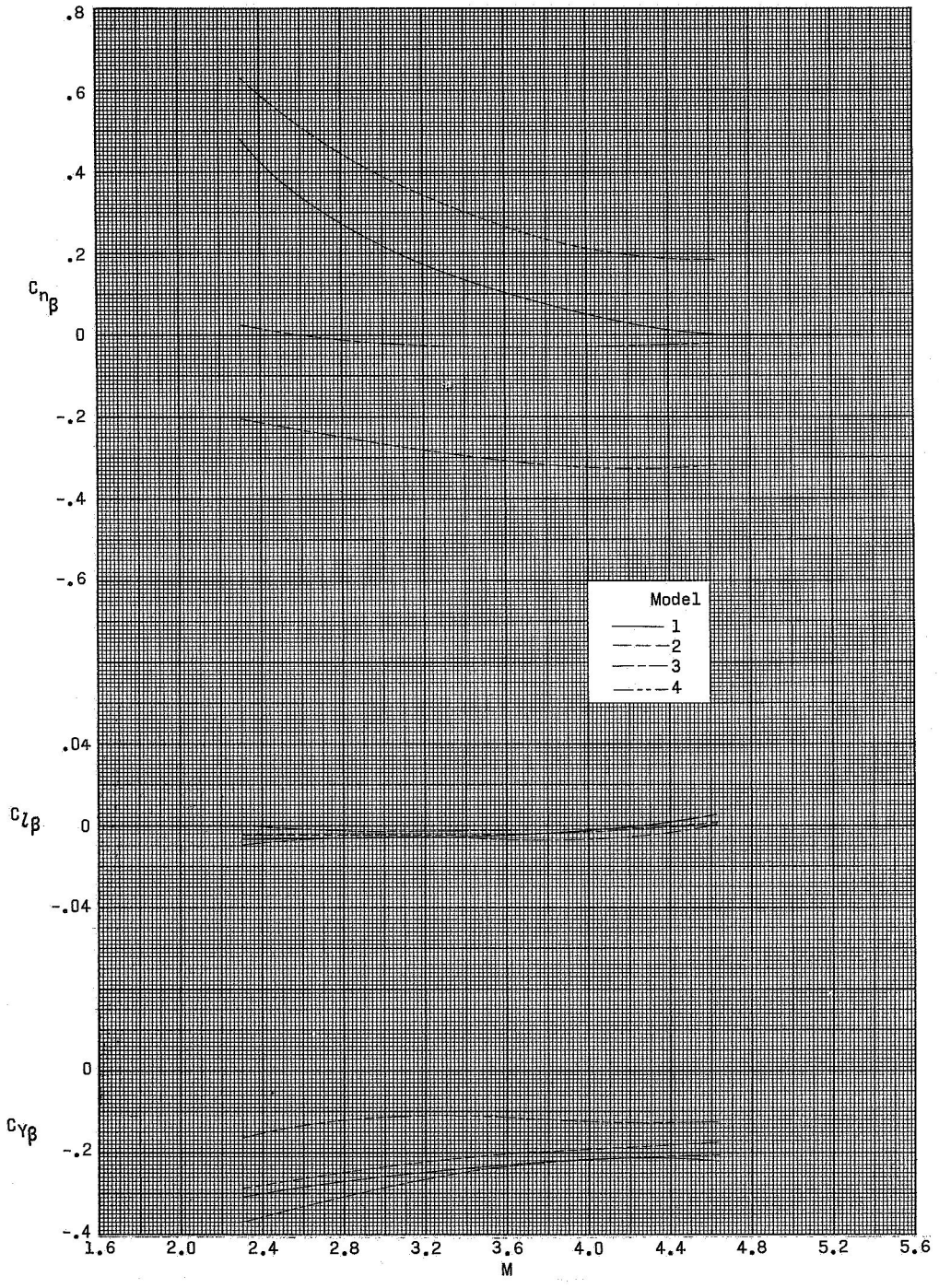

(a) Fins and auxiliary boosters on.

Figure 18.- The effect of Mach number on the lateral stability parameters at $\alpha \approx 0$.

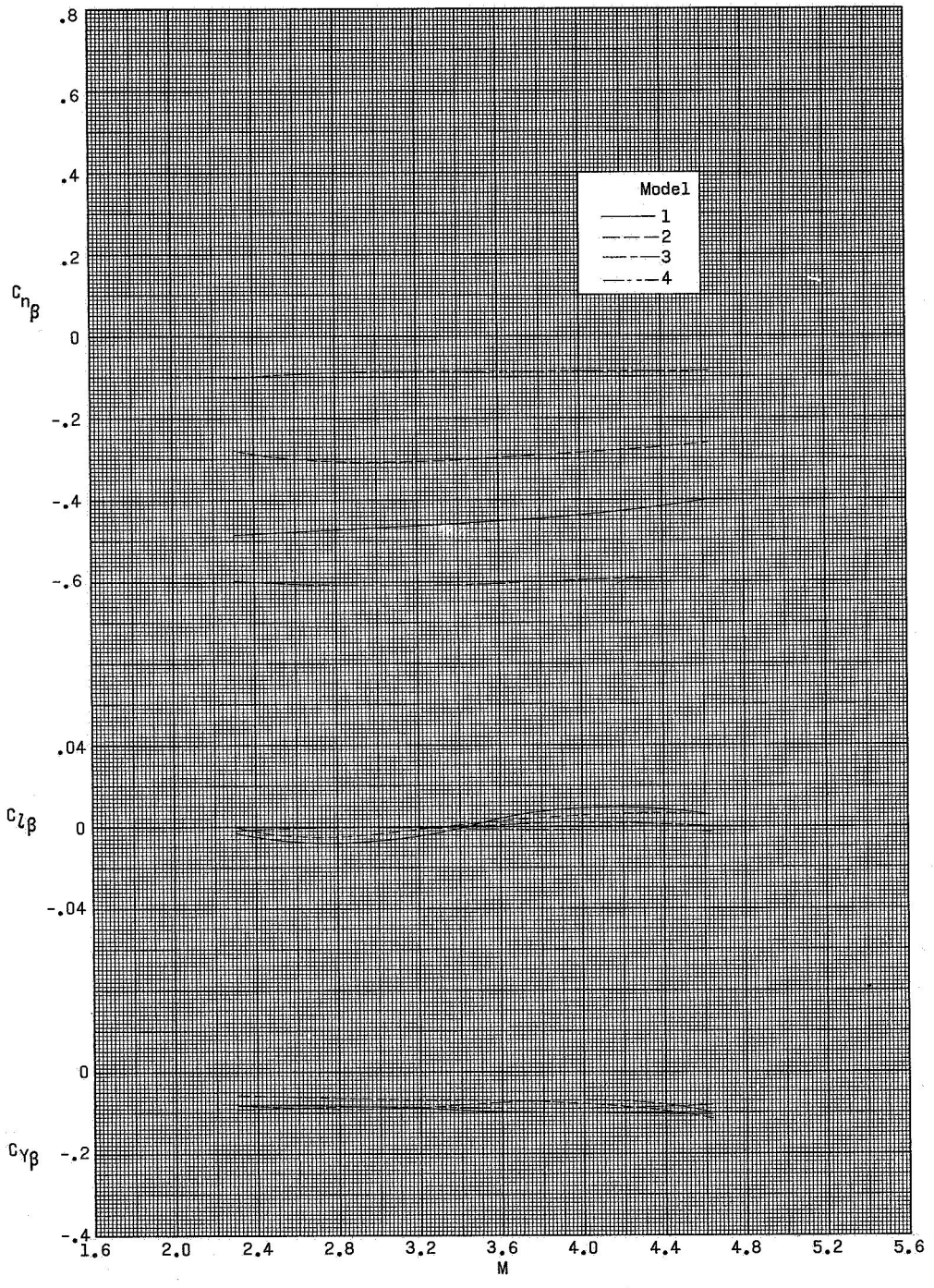

(b) Fins and auxiliary boosters off.

Figure 18.- Concluded.